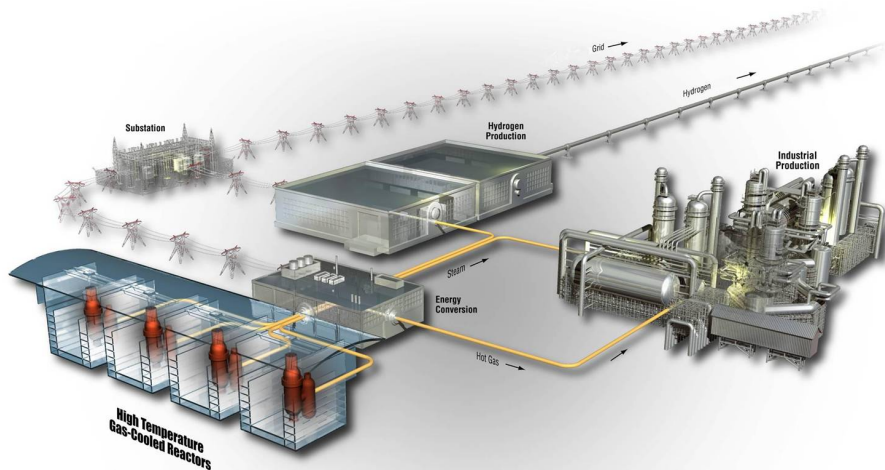# Process Heat Exchanger Options for the Advanced High Temperature Reactor

Piyush Sabharwall
Eung Soo Kim
Michael McKellar
Nolan Anderson
Mike Patterson

June 2011

Idaho National Laboratory

Process Heat Exchanger Options for the Advanced High Temperature Reactor

Piyush Sabharwall
Eung Soo Kim
Michael McKellar
Nolan Anderson
Mike Patterson

June 2011

Idaho National Laboratory
Next Generation Nuclear Plant Project
Idaho Falls, Idaho 83415
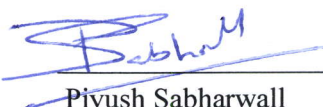
Process Heat Exchanger Options for the Advanced High Temperature Reactor

INL/EXT-11-21584
Revision 1

June 2011

Submitted by:

(signature)

June 8th 2011
Date

Piyush Sabharwall
NGNP Staff Scientist/Engineer
Advanced Nuclear Energy Systems

Approved by:

(signature)

6/10/2011
Date

M. W. Patterson
Project Manager
Hydrogen Process and Heat Transport Systems

(signature)

JUNE 8, 2011
Date

Stephen J Herring
INL Fellow and Deputy Director
Nuclear Science and Engineering

ABSTRACT

This study defines the design options for a secondary heat exchanger that couples the intermediate loop of a molten-salt-cooled nuclear reactor to a power production process. It is the first of several studies needed to select, develop, and demonstrate a secondary heat exchanger. In particular, it identifies design options affecting the functional and operational requirements of the secondary heat exchanger. The reference reactor design and configuration is a 3,400 MW(t) advanced high temperature reactor with three primary heat transfer loops. Multiple power conversion schemes are analyzed for a reactor outlet temperature of approximately 700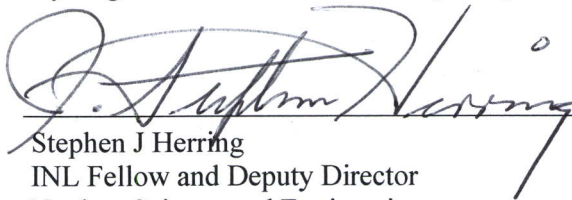°C. The applicability of other high temperature process heat applications that might eventually be coupled to the advanced high temperature reactor is also presented. An evaluation of viable secondary heat exchanger concepts is presented along with the parameters such as materials selection, system configuration, and coolant properties that will affect the secondary heat exchanger design. This study sets the stage for the two evaluations—a comparative analysis study and a feasibility study—that will follow.

SUMMARY

The strategic goal of the Advanced Reactor Concept Program for the advanced high temperature reactor (AHTR) is to broaden the environmental and economic benefits of nuclear energy in the U.S. economy by producing power to meet growing energy demands and demonstrating an AHTR's applicability to market sectors not being served by light water reactors. This study is the first of three that will aid in the development and selection of the secondary heat exchanger (SHX) for power production from the AHTR, supporting large-scale deployment. The study identifies design options that will affect the functional and operational requirements of the SHX, and sets the stage for the comparative analysis and feasibility studies that will follow.

Heat in the AHTR will be transferred from the reactor core by the primary liquid-salt coolant to an intermediate heat-transfer loop through an intermediate heat exchanger. The intermediate heat-transfer loop will circulate intermediate liquid-salt coolant through as many as three SHXs to transfer the heat to the power production process. Electric power generation was the principal process considered, but other processes were also evaluated because the heat transfer characteristics of molten salt coolants offer some advantages compared to high temperature gases produced by certain other reactor types.

A broad comparison of molten salt coolants identified 11 for more detailed analysis, which led to the selection of three as potential intermediate loop coolants: LiF-NaF-KF (FLiNaK), KF-ZrF$_4$, and KCl-MgCl$_2$. Previous studies, which identified LiF-NaF-KF and KF-ZrF$_4$ as promising molten salt coolants, were confirmed. The high neutron cross-sections of KCl-MgCl$_2$ have generally disqualified it from use in the primary loop of thermal reactors, but do not disqualify its use as a coolant in the intermediate loop. Recent evaluations by the University of Wisconsin led to its inclusion as a third intermediate loop coolant with reasonable potential.

The potential power conversion cycles identified are a supercritical Rankine steam cycle, supercritical CO$_2$ cycle, subcritical Rankine steam cycle, and helium Brayton cycle. Each of these cycles achieves different values of thermal efficiency along with diverse operating conditions. The choice of the heat exchanger type and materials of construction will largely depend on the operating conditions of the working fluid required by the power conversion cycle.

Potential industrial applications were evaluated considering a maximum available temperature of 650°C for use by the process heat applications. This assumes the reactor outlet temperature is approximately 700°C and conservatively requires 50°C differential temperature to transfer the reactor's heat through the primary and intermediate loops. The current AHTR design could provide process heat for the following applications in the near term:

- Power production cycles (steam Rankine cycles, helium Brayton cycle, SCO$_2$ cycle)

- Oil shale (in situ)

- Oil shale (ex situ)

- Oil sands.

The basic setup for the selection of the SHX has been established with evaluation goals, alternatives, and criteria. Feasibility studies will be conducted to provide sufficient information for the evaluation and decision making process. Development of the integration methodology is an ongoing task.

CONTENTS

FIGURES

TABLES

ACRONYMS

AHP	analytical hierarchy process
AHTR	advanced high temperature reactor
ASME	American Society of Mechanical Engineers
BPV	Boiler and Pressure Vessel (Code)
FHR	fluoride-salt-cooled high temperature reactor
FOM	figure of merit
IHX	intermediate heat exchanger
LMTD	log mean temperature difference
MCDA	multicriteria decision analysis
MSRE	Molten Salt Reactor Experiment
ORNL	Oak Ridge National Laboratory
PCHE	printed circuit heat exchanger
PHX	primary heat exchanger
ROT	reactor outlet temperature
SHX	secondary heat exchanger

Process Heat Exchanger Options for the Advanced High Temperature Reactor

OBJECTIVE

The work reported herein is a significant early step in reaching the final goal of large-scale deployment and use of molten salt as the heat transport medium for process heat applications. The primary purpose of this study is to aid in the development and selection of the required heat exchanger for power production—the first anticipated process heat application.

1.   INTRODUCTION

The advanced high temperature reactor (AHTR) is part of the fluoride-salt-cooled high temperature reactor (FHR) class of nuclear reactors included in the advanced reactor concept program. AHTRs will produce high outlet temperatures (704°C) using coated particle fuel and can potentially improve upon the attributes of other reactors. An AHTR reactor core consists of coated particle fuel embedded within graphite fuel elements. Graphite reflectors provide additional moderation and core structure. Heat removed from the reactor is transferred to an intermediate salt that, in turn, is transferred to a tertiary side for power production and/or process heat applications. The first FHR is still in the early development stage, but may, of necessity, be a test-scale reactor sized about the same as the Molten Salt Reactor Experiment (MSRE) in order to validate the system attributes before proceeding to larger-scale systems (Holcomb et al. 2009). So far, FHR analyses have focused mainly on power production, but new concepts such as AHTRs are looking into process heat applications, making them more attractive to industry.

A conceptual drawing of a pebble bed AHTR proposed by the University of California at Berkeley is shown in Figure 1-1. This design was the reference for this secondary heat exchanger (SHX) study.
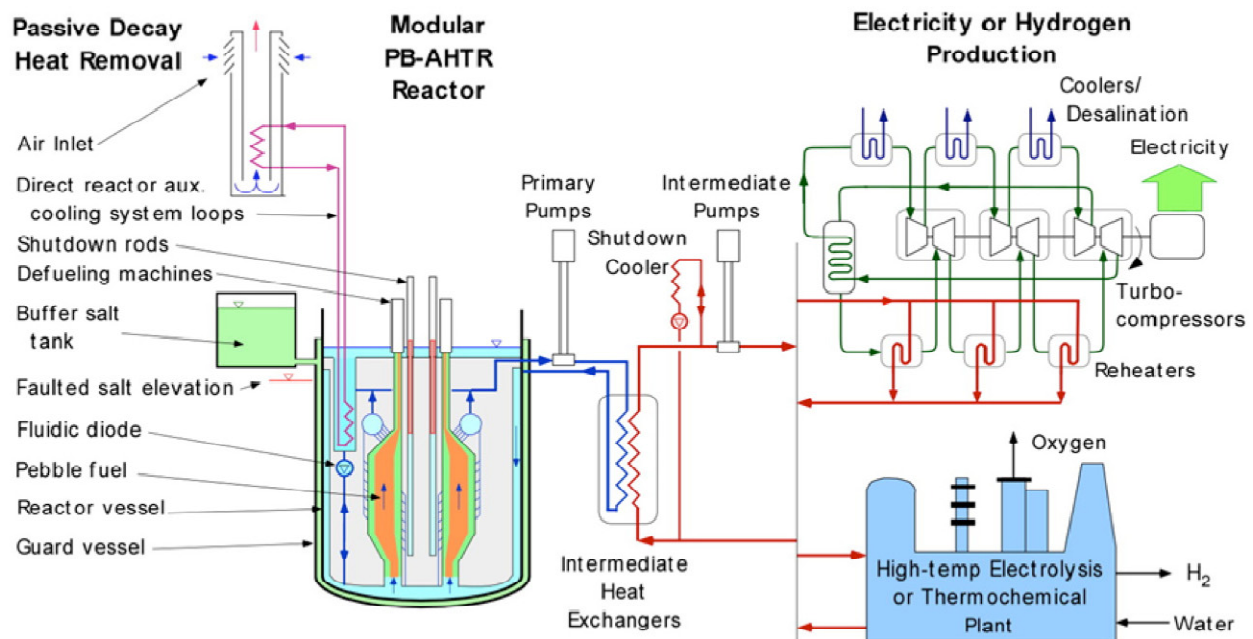
Figure 1-1. Conceptual design of pebble bed AHTR with power generation cycle (Holcomb et al. 2009).

Pebble bed and prismatic type reactor designs have been considered for an AHTR, but a final decision on core type has not been made. Plate-type fuel is currently the leading candidate, but the fuel type used, when compared to other advance reactor concepts, will have higher power density and consequently more rapid fuel burnup. Heat in an AHTR is transferred from the reactor core by the primary liquid-salt coolant to an intermediate heat-transfer loop through intermediate heat exchangers (IHX). The intermediate heat-transfer loop uses an intermediate liquid-salt coolant through an SHX to move the heat to a power conversion system or a process heat industrial application as shown in Figure 1-2. The reactor outlet temperature (ROT) for a first-of-a-kind demonstration will be 704°C. The heat exchangers are considered key components that need to be extensively investigated, because they are operated under a severe environment and their performance is directly related to the overall system efficiency and safety.

An AHTR may use several heat exchangers and/or configurations in order to transfer heat from the reactor primary loop to the power conversion system or industrial plants. Three IHXs are currently planned and will transfer heat from the reactor primary to the intermediate heat transfer loop(s). One, two, or three intermediate loops will be used and the final configuration will depend largely on the power conversion requirements. At this stage of study, it is not expected that assuming a prismatic design would significantly impact this SHX evaluation.

Potential SHX concepts are described with the explanation of evaluation and selection methodology. Development of the integration methodology and feasibility study is an ongoing task that will be covered in the later reports as the work progresses.

2. MOLTEN SALT AS INTERMEDIATE COOLANT

Two main aspects in determining the effectiveness of a coolant are heat transfer and transport capability. Heat transfer capability can be defined by the heat transfer coefficient, while heat transport capability is defined by the ratio of thermal power removed to the pumping power required (Latzko 1970). A coolant could provide good heat transfer capability but have poor heat transport capability. For example, sodium and lithium pose superior heat transfer capability because of larger thermal conductivity, but liquid salts have a much higher value for density compared to both lithium and sodium, and so are better coolants in heat transport (Latzko 1970; Sabharwall et al. 2010b).

Molten salt technology has been used for many decades in industrial heat transfer, thermal storage, heat treatment, high-temperature electrochemical plating, and other materials processing applications. The potential utility of molten salts as heat transfer agents was also demonstrated for nuclear reactors, as the liquid fuel in the Aircraft Reactor Experiment and the MSRE programs. The behavior and material compatibility of various molten salts was studied extensively by Oak Ridge National Laboratory (ORNL) from the 1950s through the 1970s in support of the MSRE and the Molten Salt Breeder Reactor programs (Sohal et al. 2010). Several types of molten salt have been recently investigated by Japanese and U.S. groups in support of fusion reactor and high temperature reactor concepts, respectively. The characteristics essential for a high temperature reactor coolants as defined by Williams (2006) and Sabharwall et al. (2010a) are:

- Chemical stability at high temperatures (500 to 800°C)

- Freezing (melting) temperature as low as possible, preferably lower than 525°C

- Large specific heat and thermal conductivity

- Low vapor pressures that are substantially less than one atmosphere at operating temperatures and are thus not volatile

- Compatible with high-temperature materials, alloys, graphite, and ceramics.

Molten salts are excellent candidates for meeting most of these requirements because they can be heated up to 1000°C and still maintain thermal stability. This allows high energy steam generation at utility-standard temperatures of 11.4 MPa and 550°C, thus achieving high thermodynamic cycle efficiencies of approximately 40% in modern steam turbine systems. However, no single-component salt meets the requirement of low melting temperature. Hence, multicomponent eutectic mixtures are needed to reduce the melting temperature to less than 500°C and are characterized by a single melting point. Combining multiple salts to form a eutectic composition provides compositional and phase stability, and therefore, uniform thermophysical properties in the operating temperature range (Grimes et al. 1972; Ingersoll et al. 2007).

Molten salts are excellent coolants, with a 25% higher volumetric heat capacity than pressurized water and nearly five times that of liquid sodium as indicated by LeBlanc 2010b. The greater heat capacity of molten salts results in more compact components, such as pumps and heat exchangers, because of the higher volumetric heat capacity. It also eliminates gross chemical exothermal reactions between the reactor, intermediate loop, and power cycle coolants as explained by Renault et al. (2009). Since liquid salts are essentially unpressurized in the system (loop), a leak in the system would not cause an extreme pressure difference in the plant. However, salt mixtures do not have much experimental data available for the determination of density, viscosity, and thermal conductivity as shown by Sohal et al. (2010).

A broad comparison of molten salts identified 11 potential coolants that were evaluated in more detail before identifying three for further analysis as the intermediate loop coolant affecting the SHX design. Previous studies of individual molten salt mixtures resulted in chlorides and fluorides receiving the most

serious consideration. The neutron cross section of molten chlorides eliminates their use in the primary loop of thermal spectrum reactors, but does not automatically eliminate their use in an intermediate loop. Since the University of Wisconsin is presently considering them for use as potential heat transport fluids (Anderson et al. 2010), their properties were included for evaluation as potential design input for the SHX. The three heat transfer molten salts identified as the most likely possible candidates for use in the intermediate loop side of the SHX are LiF-NaF-KF (FLiNaK), KCl-MgCl$_2$, and KF-ZrF$_4$. Their physical properties are shown in Table 2-1.

Table 2-1. Basic physical properties of molten salts (Williams 2006).

Salt	Composition (mol %)	Molecular Weight (g/mol)	Melting Point (°C)	Boiling Point (°C)
LiF-NaF-KF	(46.5-11.5-42)	41.3	454	1570
KF-ZrF$_4$	(58-42)	103.9	390	~1450
KCl-MgCl$_2$	(68-32)	81.4	426	>1418

The characteristics of the 11 candidate coolants in this study were extensively investigated in three different aspects—coolant thermal performance, coolant cost, and coolant chemistry (corrosion and corrosion-resistant materials)—to select the three salts shown. The detailed comparison methods and evaluation results for these aspects are described in Appendixes A and B.

3.   POWER CONVERSION SCHEMES

3.1   Introduction

This section compares potential power cycles and their effect on intermediate heat loops using a variety of salts. The salts analyzed for this study are FLiNaK (a tertiary salt), KCl-MgCl$_2$, and KF-ZrF$_4$ (two binary salts). The primary reactor loop fluid is FLiBe (a binary salt). The power cycles analyzed are supercritical and subcritical Rankine steam cycles, supercritical carbon dioxide, CO$_2$, modified Brayton cycle, and a standard helium Brayton cycle.

Power cycles are the first likely application of the AHTR, and as such, determine many of the functional requirements for the primary heat exchanger (PHX). They are analyzed in considerable detail because accurate comparisons of the trade-offs in efficiencies versus cost and risk of specific PHX designs are required. Relatively small improvements in efficiency may justify the expense of a PHX that will withstand very large differential pressures and other extreme fluid conditions, but the impact of designing a revolutionary heat exchanger that doesn't work is severe. Therefore, analysis and comparison of power cycles is presented in sufficient detail to support informed decision-making.

3.2   General Considerations of Power Cycles

Several power cycles are used to generate electricity. The major difference between nuclear and non-nuclear power cycles is the heat source. Fossil fuels are the heat source for conventional plants, whereas nuclear fission is the heat source for a nuclear plant. A secondary difference is the type of cycle. Some fossil fuel power cycles are open cycles in which the reacted gases are exhausted to the atmosphere. Nuclear power cycles are closed cycles.

One of the primary functions of a nuclear reactor is to produce electricity. A power cycle generally consists of four stages: heat addition, power generation through expansion, heat rejection, and compression. When the working fluid of the power cycle directly cools the core of the nuclear plant, it is called a direct cycle. If the working fluid of the power cycle and the primary cooling loop of the reactor core are separate, it is called an indirect cycle. In an indirect cycle, heat from the core is provided to the power cycle by means of a steam generator or IHX. Direct power cycles can provide more electrical power from heat generated by the core but the power cycle components are contaminated with radioactive materials.

Optimal thermodynamic performance of a cycle is measured by its thermal efficiency. The thermal efficiency is defined as the electrical power output divided by the heat input, or

$$\eta_{th} = \frac{\dot{W}_{elec}}{\dot{Q}_{in}}.$$
(1)

A power cycle is thus based on the thermodynamic concept of a heat engine. Power may be produced from a heat engine that is placed between a high-temperature source and a low-temperature sink as shown in Figure 3-1. The work of the heat engine is defined as

$$\dot{W} = \dot{Q}_H - \dot{Q}_L.$$
(2)
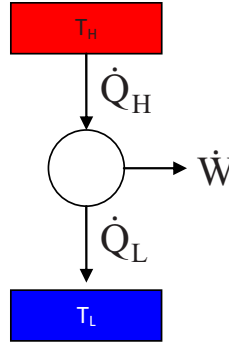
Figure 3-1. Heat engine between hot source and cold sink.

Heat is transferred from the high-temperature source to the heat engine and heat is rejected from the heat engine to the low temperature sink. The thermal efficiency of a heat engine can be shown as

$$\eta_{th} = \frac{\dot{Q}_H - \dot{Q}_L}{\dot{Q}_H} \quad . \tag{3}$$

In real situations, a temperature difference is needed to transfer the heat from the source to the heat engine and from the heat engine to the heat sink. However, if those differences were made to go to zero, an ideal or maximum efficiency could be determined. The maximum efficiency is called the Carnot efficiency and is a function of source and sink temperatures only, as in

$$\eta_{Carnot} = \frac{T_H - T_L}{T_H} \quad . \tag{4}$$

This report analyzes four power cycles: Rankine supercritical and subcritical steam cycles, helium Brayton gas cycle, and a modified supercritical carbon dioxide Brayton cycle. The following assumptions were made for all of the cycles analyzed:

- Reactor heat output is 3,400 MW(t)

- Outlet temperature of the reactor is 704°C

- Inlet temperature of the reactor is 600°C

- Turbines and compressors of the Brayton cycles have 90% isentropic efficiencies

- Circulators and pumps have 75% isentropic efficiencies

- IHX and steam generators have minimum approach temperatures of 25°C

- All other heat exchangers in the Brayton cycles have minimum approach temperatures of 20°C

- The feedwater heaters in the Rankine cycles have minimum approach temperatures of 5.6°C

- Pressure drops across the components are 2% of the inlet pressure to the component.

The assumptions for the reactor are based on a fluoride salt cooled reactor concept developed at ORNL (Holcomb et al. 2009).

3.2.1 Rankine Steam Cycle

The Rankine steam cycle is the most basic thermodynamic power cycle. The simplest cycle consists of a steam generator, a turbine, a condenser, and a pump as shown in Figure 3-2. The working fluid is

water. Low-pressure water is pumped to a high pressure. Heat is transferred to the water through a steam generator to produce high-pressure steam. The steam expands through the turbine to produce flow work or power, which is then converted to electricity in a generator. The low-pressure saturated steam/water is condensed to liquid water in the condenser (Van Wylen and Sonntag 1973).

The efficiency for this cycle is defined as the power difference between the turbine and the pump divided by the heat input from the steam generator as in

$$\eta_{th} = \frac{\dot{W}_{Turbine} - \dot{W}_{Pump}}{\dot{Q}_{SteamGenerator}} \; . \tag{5}$$
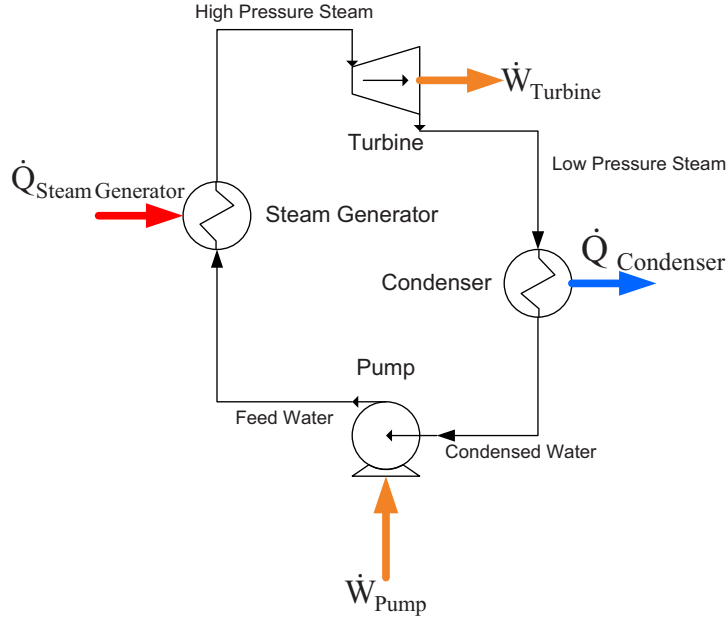
Figure 3-2. Basic Rankine steam cycle.

The cycle efficiency can be improved through heat recuperation in which partially expanded streams from the turbine exchange heat with the stream exiting the pump or feedwater stream using exchangers labeled as feedwater heaters. The efficiency can also be improved by reheating the partially expanded stream in the steam generator before it is further expanded in the turbine. Figure 3-3 shows a Rankine steam cycle with feedwater heaters and a set of turbines. The partially expanded streams are split from the primary turbine stream to supply heat to the steam generator's feedwater. These streams are mixed with the exit stream of the low-pressure turbine before the condenser. The power cycle is separated from the heat of the reactor through one circulation loop—the intermediate salt loop. The purpose of the separation is to prevent tritium migration to the components of the power cycle. The thermal efficiency of the Rankine cycle for this work is defined as

$$\eta_{th} = \frac{\sum \dot{W}_{turbines} - \sum \dot{W}_{pumps}}{\dot{Q}_{reactor}} \; . \tag{6}$$
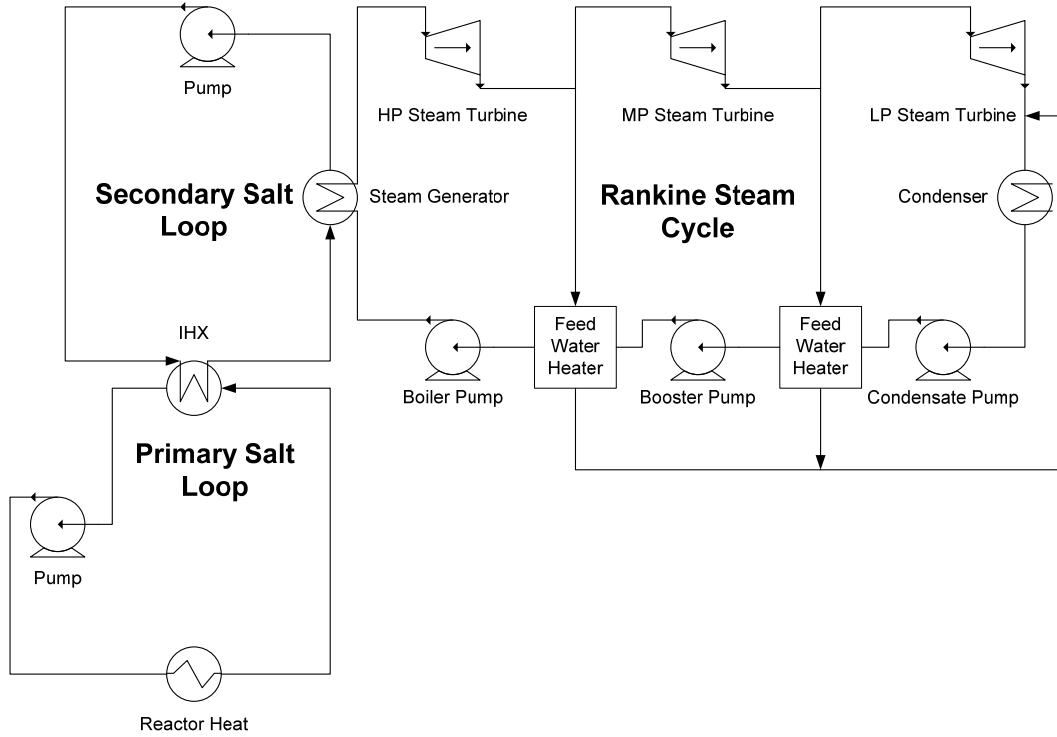
Figure 3-3. Rankine steam cycle with feedwater heaters.

3.2.2 Brayton Gas Cycle

The basic Brayton gas cycle is shown in Figure 3-4. The high-pressure working gas is expanded in a turbine to produce power. The low-pressure warm gas is cooled in an ambient cooler, which reduces the power of compression. The low-pressure cold gas is compressed to the high-pressure of the system. Often the turbine and the compressor are mechanically connected through a single shaft. The thermal efficiency of the cycle is presented as

$$\eta_{th} = \frac{\dot{W}_{Turbine} - \dot{W}_{Compressor}}{\dot{Q}_{Gas\,Heater}}.$$
(7)

As with the Rankine steam cycle, the thermal efficiency may be improved through partial expansion with reheat and recuperation. For an indirect cycle, the gas heater is the heat from the reactor, and not only is the compression in the Brayton cycle considered, but also the compression of the pump within the primary and intermediate salt loops. Figure 3-5 shows the cycle analyzed for this report, which includes both reheat and recuperation (Van Wylen and Sonntag 1973). The reactor outlet flow is split into two streams, one going into a heater and the other into a reheater. Both gas turbines have the same high inlet temperature. The thermal efficiency for the Brayton cycle as shown in Figure 3-5:

$$\eta_{th} = \frac{\sum \dot{W}_{Turbines} - \sum \dot{W}_{Pumps}}{\dot{Q}_{Reactor}}$$
(8)

8
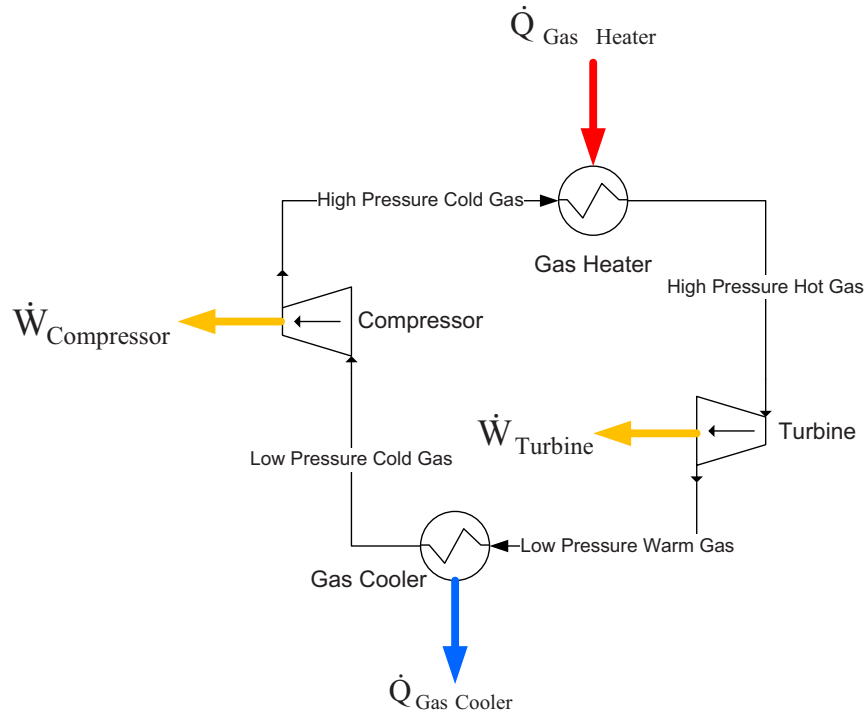
Figure 3-4. Simple Brayton cycle.
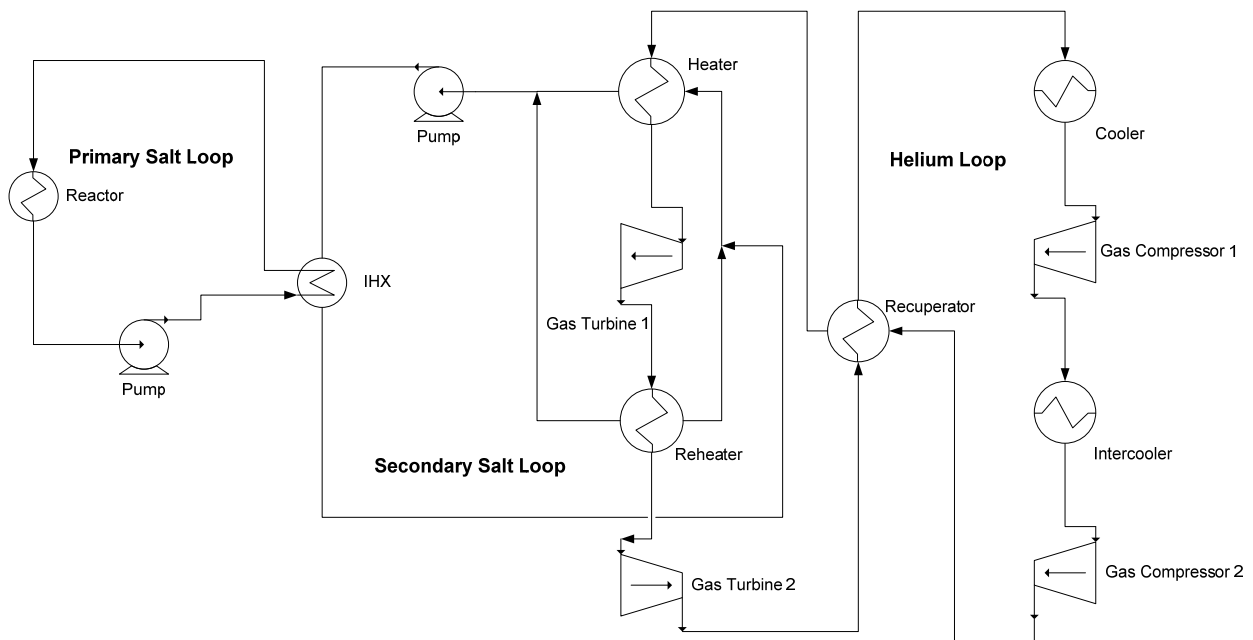
Figure 3-5. Helium Brayton cycle with reheat and recuperation.

3.2.3   Supercritical Carbon Dioxide Recompression Brayton Cycle

The supercritical carbon dioxide recompression Brayton cycle is a cycle developed at the Massachusetts Institute of Technology (Dostal, Driscoll, and Heizlar 2004). Figure 3-6 shows a simplified

process flow diagram of the cycle. The supercritical CO_2 coolant is heated by the intermediate salt loop and expanded through the turbine to produce electric power. The coolant, at a lower temperature and pressure, then passes through high-temperature and low-temperature recuperators where it is further cooled. The coolant flow is then split into two streams (right side of Figure 3-6). One stream passes through a precooler that provides additional cooling to the working fluid before it enters Compressor 1. Compressor 1 provides the driving force to circulate the fluid back through the two recuperators where heat is recovered before the working fluid is returned to the reactor inlet to complete the cycle. The second split stream passes directly to Compressor 2 (the recompressor) without any additional cooling, where it is compressed and joined with the first split stream before it passes through the high temperature recuperator and returns to the reactor inlet to complete the cycle.

The calculated power conversion cycle thermal efficiency (η_{pcs}) is defined as

$$\eta_{pcs} = (P_{turbine} - P_{compressors})/P_{reactor} \quad\quad\quad (9)$$

where:

$P_{turbine}$ = Power of the primary side turbine

$P_{compressors}$ = Power of high and low pressure compressors

$P_{reactor}$ = Reactor heat.
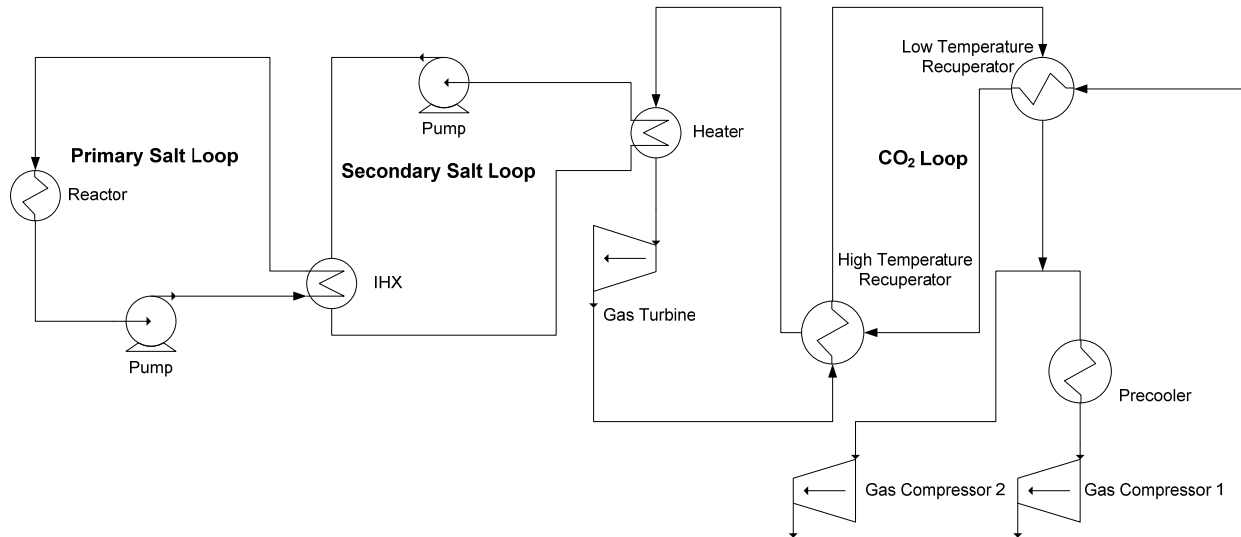
Figure 3-6. Supercritical CO_2 recompression Brayton cycle.

3.3   Process Models

The process models for this mathematical analysis were developed using Honeywell's UniSim Design R390.1 (Build 15107) process modeling software. UniSim Design software, which includes thermodynamic data for all chemical species, inherently ensures mass and energy balances across all components. The software realistically models components such as pumps, compressors, turbines, and heat exchangers. It also models chemical equilibrium reactions. The models described in this report were developed assuming steady-state operation.

3.3.1 Primary and Intermediate Salt Loops

Four salts were used in the process models of this study. The salt in the primary loop is a binary salt composed of FLiBe. Three salts were considered for the intermediate heat transfer loop: a tertiary salt made of lithium fluoride, sodium fluoride, and potassium fluoride (or FLiNaK) and two binary salts: potassium chloride-magnesium chloride $KCl-MgCl_2$, and potassium fluoride-zirconium fluoride $KF-ZrF_4$. These salts are not part of the properties found within the UniSim design software and were therefore incorporated into the software as UniSim's hypothetical fluids routines. The properties of the salts used in the analyses are found in Sohal et al. (2010) and Anderson and Sabharwall (2010).

The process model of the salt loops is found in Figure 3-7. The pressure of the loop is near atmosphere (0.156 MPa). The temperature into and out of the reactor is 600°C and 704°C respectively. The intermediate loop provides heat to the power cycle.
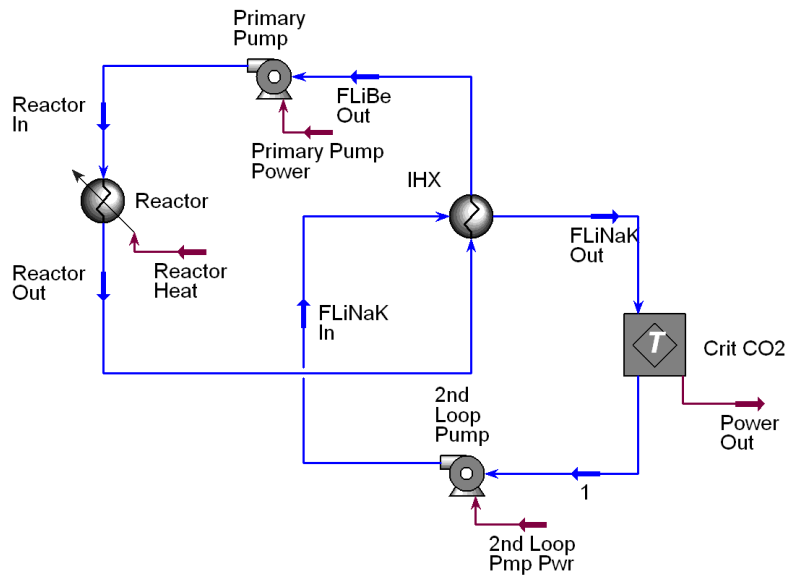
Figure 3-7. Primary and intermediate salt loops.

3.3.2 Rankine Cycles

The Rankine cycle process model developed for this study is based on a supercritical steam cycle developed by Babcock and Wilcox (Kitto and Stultz 2005). The cycle has seven feedwater heaters and a steam generator with reheating as shown in Figure 3-8. This same model is also used for the subcritical steam cycle. The high pressure turbine has an efficiency of 85%, the two-stage intermediate pressure turbine has an efficiency of 90%, and the five-stage low pressure turbine has an efficiency of 80%. Each flow from the turbines to the feedwaters is 5% of the total flow. The turbine outlet pressures of the flows to the feedwater heaters are adjusted to ensure that the flows are condensed as they heat the water returning to the steam generator. The mass flow of the returning water is adjusted until the fluid entering the condensing pump is a saturated liquid. The pressure at the condenser is 10 kPa (1.5 psia), giving a condensing temperature of 46°C, which should be suitable for water or air cooled condensing. This model does not account for the condensed water or air.
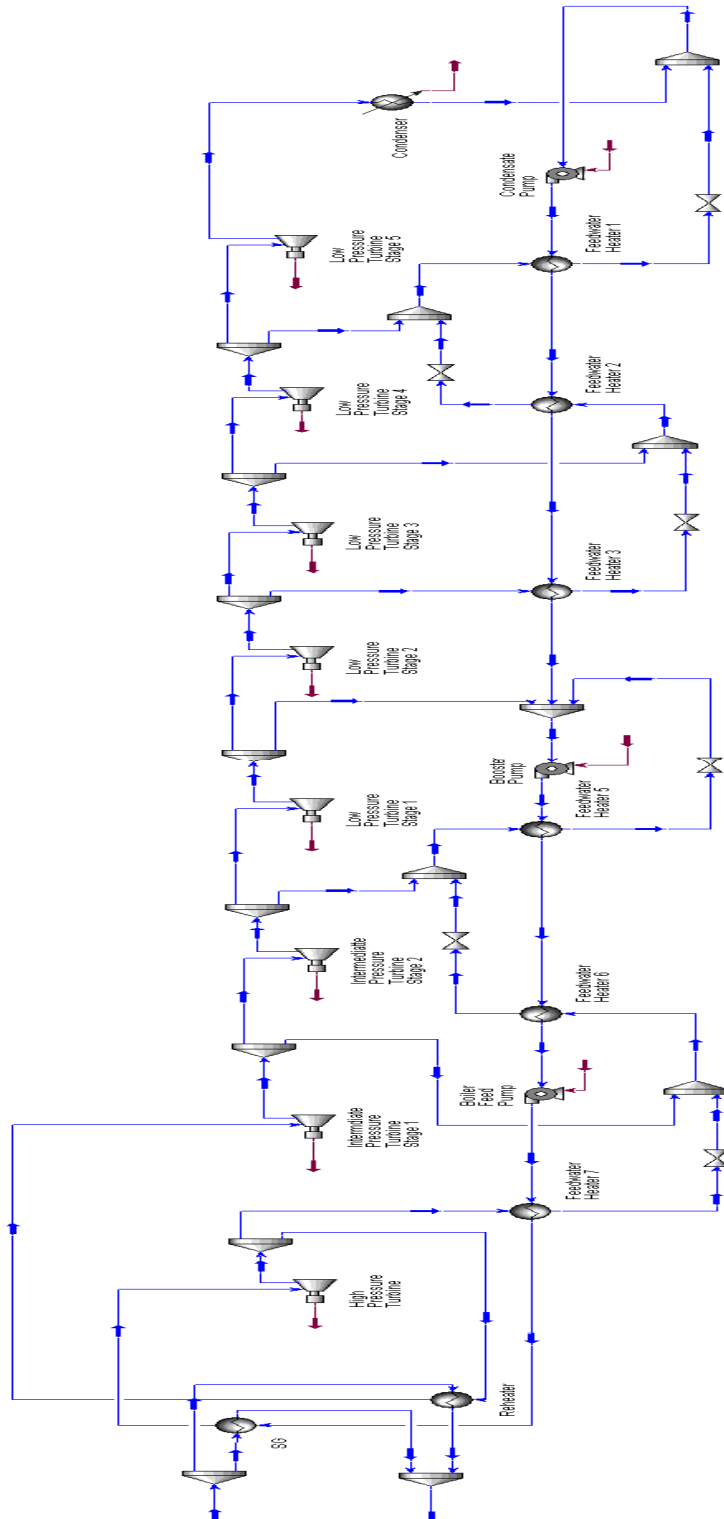
Figure 3-8. Process flow diagram of Rankine steam cycle.

3.3.3   Brayton Helium Cycle

The Brayton cycle has a heater and a reheater that uses the heat from the salt to raise the temperature of the helium to the same high temperature for both turbines as shown in Figure 3-9. The incoming salt flow is split 50% each. The helium mass flow rate is determined by the temperature difference and flow of the incoming salt and by setting the heater and reheater to have 25°C minimum approach temperatures. The recuperative heat exchanger has a minimum approach temperature of 20°C. Before each compressor, the helium gas is cooled to 36°C. The compressors and turbines have isentropic efficiencies of 90%. Outlet pressures of the compressors and turbines were adjusted until maximum thermal efficiency was achieved.
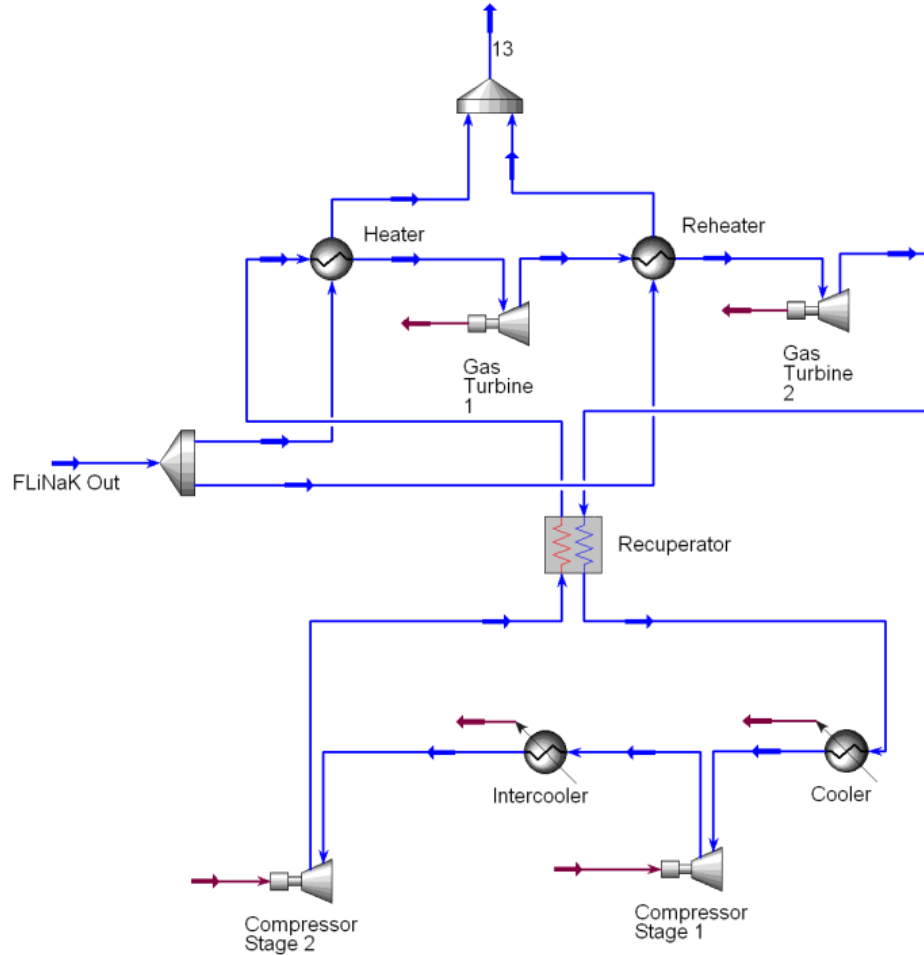
Figure 3-9. Process flow diagram of Brayton cycle.

3.3.4   Supercritical Carbon Dioxide Recompression Brayton Cycle

The supercritical CO_2 uses the same conditions as the helium Brayton cycle except for pressures. The lower pressure of the cycle was adjusted near the critical point of carbon dioxide. The upper pressure, the pressure out of gas turbine 1, the outlet compressor pressure, and the temperature of the carbon dioxide entering the heater were adjusted to maximize the thermal efficiency of the cycle. The split between the compressors shown in Figure 3-10 was adjusted to ensure that the isentropic efficiency of compressor 2 was 90%.

13
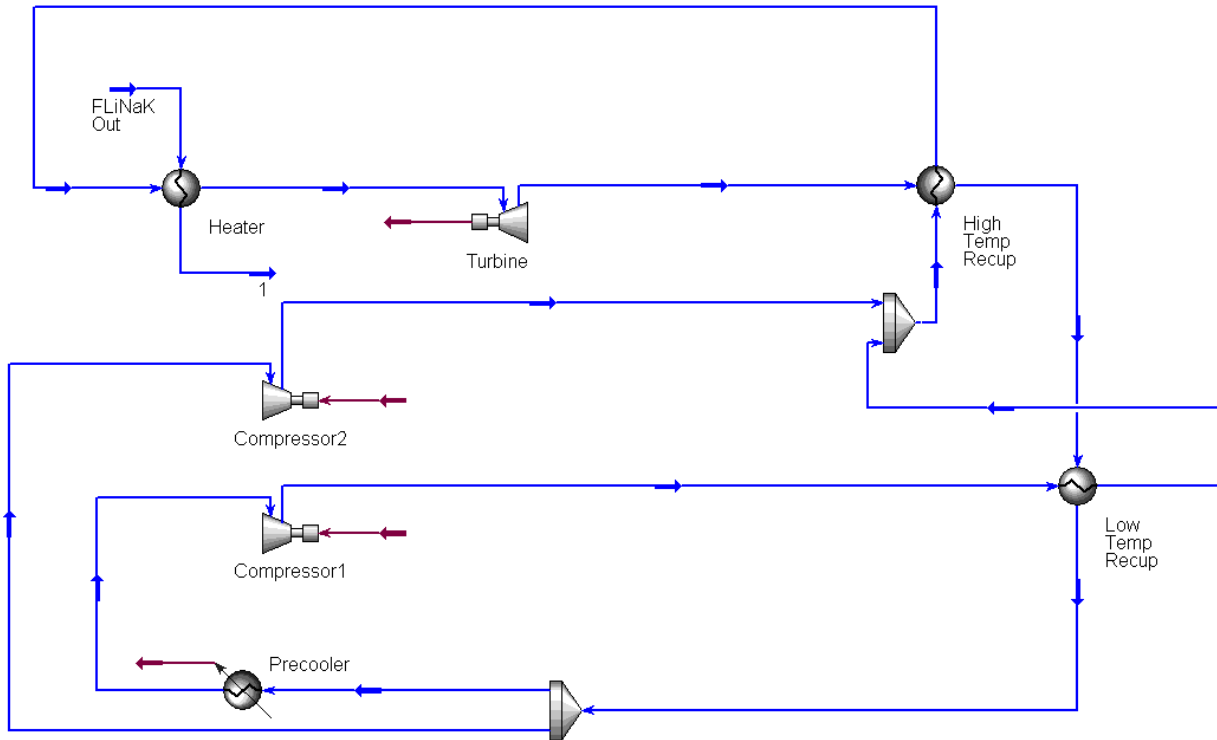
Figure 3-10. Process flow diagram of supercritical CO$_2$ modified Brayton cycle.

3.4   Results

3.4.1   Primary and Intermediate Salt Loops

The primary salt loop conditions did not change for all the cases studied. The mass flow rate of the salt loop is established by the inlet and outlet reactor temperatures of 600°C and 704°C, respectively, and the reactor heat of 3,400 MW(t). A nearly constant 25°C temperature difference was set for the IHX, between the primary and intermediate salt loops. This difference established the mass flow rates of each of the salts in the intermediate loop. The power cycles did not influence the IHX so the results are presented for the different salts without regarding the power cycle used. Table 3-1 presents the mass flow rates and inlet and outlet temperatures for the IHX. Table 3-2 presents the design conditions for the IHX between the salt loops. The UA is the product of the overall heat transfer coefficient and heat transfer area. The magnitude of the UA indicates a relative size. The log mean temperature difference (LMTD) is a measure of the average temperature between the hot and cold sides of the heat exchanger. The product of the UA and LMTD is the duty of the heat exchanger. The duty is the amount of heat transferred from the hot side to the cold side of the heat exchanger. As can be seen in Tables 3-1 and 3-2, the intermediate heat exchangers for the binary salts are identical. The FLiNaK salt has a slightly smaller heat exchanger. The mass flow rate of the FLiNaK salt is the smallest as well. Based on the heat transfer and thermodynamic results, the FLiNaK salt has the best performance. However the difference is not enough to make a final conclusion. The corrosive and economic aspects (the cost of ^{7}Li enrichment for FLiBe in the primary loop) of each salt needs to be accounted for, which may favor a salt different than FLiNaK.

Table 3-1. Mass flow rates and IHX temperatures for the primary and intermediate salt loops.

Salt	Inlet IHX Temperature (°C)	Outlet IHX Temperature (°C)	Pressure (MPa)	Mass Flow Rate (kg/s)
FLiBe	704.0	600.0	0.156	79.6
FLiNaK	575.0	676.2	0.156	102.2
KCl-MgCl$_2$	575.0	679.0	0.156	166.4
KF-ZrF$_4$	575.0	679.0	0.156	183.0

Table 3-2. Design data for IHX between primary and intermediate salt loops.

Salt	Duty (MW)	UA (MW/°C)	LMTD (°C)
FLiNaK	20.0	0.773	25.9
KCl-MgCl$_2$	20.0	0.800	25.0
KF-ZrF$_4$	20.0	0.800	25.0

3.4.2   Power Cycles

The overall thermal efficiencies of the power cycles are presented in Table 3-3. The maximum and minimum pressures of each cycle are presented in Table 3-4 and Table 3-5. The mass flow rates of the power cycles are shown in Table 3-6. The supercritical steam Rankine cycle has the highest thermal efficiency followed by the supercritical CO_2. These cycles also have the highest pressures of 24.99 and 21.66 MPa, respectively. The subcritical steam Rankine has an efficiency of 42% with a high pressure of 17.7 MPa. A case with supercritical steam Rankine cycle was run by removing reheat, the efficiency remains about the same but the last stages of the low pressure turbine have more water in them. Based on industry examples, it appears that reheat is used for the proposed scaled system. Currently existing coal fired and natural gas power plants do have the same pressure difference across the heat exchanger, a high level cost analysis should reveal which power cycle is optimal. The analysis can determine if the extra 2% in cycle efficiency warrants the higher pressure difference across the heat exchanger.

Table 3-3. Thermal efficiencies of the power cycles.

Salt/Power Cycle	Helium Brayton	Critical CO$_2$ Modified Brayton	Super Critical Steam Rankine	Sub-Critical Steam Rankine
FLiNaK	40.3 %	43.7 %	44.0%	41.9%
KCl-MgCl$_2$	40.4 %	43.9%	44.0%	42.0%
KF-ZrF$_4$	40.4 %	43.9%	44.0%	42.0%

Table 3-4. Maximum pressure for each power cycle.

Salt/Power Cycle	Helium Brayton	Critical CO$_2$ Modified Brayton	Super Critical Steam Rankine	Sub-Critical Steam Rankine
FLiNaK	7.11	21.66	24.99	17.7
KCl-MgCl$_2$	7.35	21.66	24.99	17.7
KF-ZrF$_4$	7.49	21.66	24.99	17.7

Table 3-5. Minimum pressure of each power cycle.

Salt/Power Cycle	Helium Brayton	Critical CO$_2$ Modified Brayton	Super Critical Steam Rankine	Sub-Critical Steam Rankine
FLiNaK	2.69	8.27	0.01014	0.01014
KCl-MgCl$_2$	2.79	8.38	0.01014	0.01014
KF-ZrF$_4$	2.79	8.38	0.01014	0.01014

Table 3-6. Mass flow rates of power cycles.

Salt/Power Cycle	Helium Brayton	Critical CO$_2$ Modified Brayton	Super Critical Steam Rankine	Sub-Critical Steam Rankine
FLiNaK	13.43	102.2	6.96	7.09
KCl-MgCl$_2$	13.42	102.3	6.96	7.11
KF-ZrF$_4$	13.22	102.3	6.95	7.10

The helium Brayton cycle has the lowest efficiency with the lowest pressure. The power cycle efficiencies do not vary much with respect to the intermediate loop salt used. The pressures and flows do not vary much when considering salt type. There is some variation in salt type when considering the helium Brayton cycle. The pressures of the cycles are set to get their specific performance except for the Brayton cycle. Helium is nearly an ideal gas. Assuming the ideal gas law and considering the first law of thermodynamics for the turbines and compressors, the turbine power can be equated as

$$\dot{W} = P_{in} v_{in} \ A_{in} \eta_{turbine} \frac{\gamma}{\gamma-1} \left[\left(\frac{P_{out}}{P_{in}} \right)^{\frac{\gamma-1}{\gamma}} - 1 \right] \tag{10}$$

where:

$\dot{W}$ = power of the turbine

P_{in} = pressure into the turbine

P_{out} = pressure out of the turbine

A_{in} = cross sectional area into the turbine

v_{in} = velocity into the turbine

$\eta_{turbine}$ = the isentropic efficiency of the turbine

γ = the specific heat ratio.

The power of the compressor has an identical form except the left hand terms are divided by the efficiency instead of multiplied. The specific heat ratio is constant for an ideal gas. For a specific design point, the turbine and compressor efficiencies and areas are constant. Therefore the turbine and compressor powers are a function of inlet pressure, pressure ratio, and velocity. Equation (10) implies that the same power cycle efficiency may be found at lower pressures. With that in mind, another case was modeled in which the lowest pressure of the Brayton cycle were set at 20 psia (0.137 MPa), the same pressure as the salt loops. In this analysis FLiNaK was used as the intermediate salt. The thermal efficiency of this Brayton cycle in this analysis is 40.3%, with a high pressure of 0.341 MPa and a low pressure of 0.135 MPa. The mass flow rate through the power cycle is 13.8 kg/s. The helium Brayton

cycle has the advantage over the other cycles in that the absolute pressures within the cycle may be adjusted and still produce the same power cycle efficiency.

However, there are consequences for running at the lower pressure: the equipment size must increase as the pressure goes down. The data from the FLiNaK cases were used to create Table 3-7 in which the largest pipe size was calculated for each cycle. The largest flows are found at the highest volume flow rates and lowest fluid densities of the power cycles. In each case, this location is at the outlet of the last turbine. The velocity was assumed to be 30.5 m/s (100 ft/s) for each case and the density at those locations were used. Table 3-7 shows the results of this analysis. The low pressure helium gas has a pipe diameter that is 4.6 times greater than the higher pressure gas. The super critical CO_2 cycle has the smallest pipe size because of the high density of the carbon dioxide near the critical point. The large pipe sizes of the Rankine cycles are because of the very low pressures in the condenser resulting in very low steam densities. The low pressure of the Brayton cycle may be adjusted to find an optimal pipe size and pressure ratio across the IHX. The mass flow rates of the Rankine cycles shown in Table 3-8 are different than those found in Table 3-6 because of the flows diverted for the feedwater heaters. The flows in Table 3-8 are the flows through the steam generator.

Table 3-7. Maximum pipe size for each power cycle.

	High Pressure Helium Brayton	Low Pressure Helium Brayton	Critical CO_2 Modified Brayton	Super Critical Steam Rankine	Subcritical Steam Rankine
Pressure (MPa)	2.8	0.1379	8.79	.0103	.0103
Temperature (°C)	519.3	522.8	542.8	46.48	46.48
Mass Flow Rate (kg/s)	13.4	13.8	102.2	4.92	5.01
Density (kg/m)	1.699	0.0834	0.562	0.0744	0.0744
Diameter (m)	0.575	2.631	0.2756	1.662	1.676
Diameter (inches)	22.62	103.6	10.85	65.43	65.98

Table 3-8. Temperatures, mass flows, and pressures of heat exchangers between intermediate loops and power cycles.

	Inlet IHX Temperature (°C)	Outlet IHX Temperature (°C)	Pressure (MPa)	Mass Flow Rate (kg/s)
Subcritical Rankine				
Steam Generator				
FLiNaK	676.2	585.6	0.153	96.5
Water	239.5	550.0	17.346	7.09
Reheater				
FLiNaK	676.2	384.3	0.153	5.72
Water	359.3	550.0	4.62	6.74
Steam Generator				
KCl-MgCl$_2$	679.0	586.0	0.153	157.4
Water	241.6	550.0	17.346	7.11
Reheater				
KCl-MgCl$_2$	679.0	383.5	0.153	9.00
Water	358.5	550.0	4.59	6.75
Steam Generator				
KF-ZrF$_4$	679.0	586.1	0.153	173.1
Water	241.7	550.0	17.346	7.10
Reheater				
KF-ZrF$_4$	679.0	381.3	0.153	9.91
Water	356.3	550.0	4.51	6.75
Supercritical Rankine				
Steam Generator				
FLiNaK	676.2	586.5	0.153	95.4
Water	251.6	593.0	24.49	6.96
Reheater				
FLiNaK	676.2	406.7	0.153	6.85
Water	381.7	593.0	6.09	6.612
Steam Generator				
KCl-MgCl$_2$	679.0	586.7	0.153	155.5
Water	251.6	593.0	24.49	6.96
Reheater				
KCl-MgCl$_2$	679.0	406.7	0.153	10.8
Water	381.7	593.0	6.09	6.612
Steam Generator				
KF-ZrF$_4$	679.0	586.8	0.153	171.1
Water	251.4	593.0	24.49	6.95
Reheater				
KF-ZrF$_4$	679.0	405.0	0.153	11.9
Water	380.0	593.0	6.01	6.6025

	Inlet IHX Temperature (°C)	Outlet IHX Temperature (°C)	Pressure (MPa)	Mass Flow Rate (kg/s)
Helium Brayton				
Heater				
FLiNaK	676.2	568.3	0.153	51.1
Helium	498.9	651.2	6.97	13.4
Reheater				
FLiNaK	676.2	581.6	0.153	51.1
Helium	517.2	651.2	4.40	13.4
Heater				
KCl-MgCl$_2$	679.0	568.9	0.153	83.2
Helium	502.3	654.0	7.203	13.4
Reheater				
KCl-MgCl$_2$	679.0	581.1	0.153	83.2
Helium	519.0	654.0	4.54	13.4
Heater				
KF-ZrF$_4$	679.0	568.2	0.153	91.5
Helium	499.0	654.0	7.3402	13.2
Reheater				
KF-ZrF$_4$	679.0	581.8	0.153	91.5
Helium	518.0	654.0	4.61	13.2
Super-critical CO$_2$ Brayton				
Heater				
FLiNaK	676.2	575.0	0.153	102.2
CO$_2$	494.0	651.2	20.8	102.2
Heater				
KCl-MgCl$_2$	679.0	575.0	0.153	166.4
CO$_2$	497.0	654.0	20.8	102.3
Heater				
KF-ZrF$_4$	679.0	575.0	0.153	183.0
CO$_2$	497.0	654.0	20.8	102.3

3.5   Conclusions and Recommendations

The following conclusions were drawn:

- Use of FLiNaK results in the smallest heat exchanger size, but the difference is not large enough to justify a conclusive decision based on size alone.

- The binary salts have identical results with respect to the IHX design.

- The supercritical Rankine steam cycle has the highest power cycle efficiency and the advantage of being a current commercial technology, but the disadvantage of the highest turbine inlet pressure.

- The supercritical power cycle has the highest efficiency but the highest pressure difference (23.9 MPa); supercritical cycles heated by coal and natural gas have the same problem. The subcritical

Rankine cycle should be considered because it has a pressure difference of 16.9 MPa, which would reduce the stress on the heat exchanger with only a shift from 44% to 42% efficiency.

- The supercritical CO_2 cycle has a power cycle efficiency that is nearly the same as the supercritical Rankine steam cycle. It also has a maximum pipe diameter that is less than the other power cycles and the advantage of very few components. The disadvantage is high turbine inlet pressure, and the cycle is in small-scale testing so not available commercially.

- The subcritical Rankine steam cycle is currently used in commercial power plants. The power cycle efficiency is reasonable.

- The helium Brayton cycle has the advantage of adjustable pressures to reduce the pressure difference across the IHX. Brayton cycles have been developed for future gas reactors, but commercial cycles are not available.

The following recommendations should be considered:

- The corrosive nature of the salts needs to be considered for a final selection.

- The cost of each salt needs to be considered.

- The economics and technology development of the power cycles need to be developed and considered.

4. APPLICABILITY OF HEAT EXCHANGER TO PROCESS HEAT APPLICATIONS

The strategic goal of the Advanced Reactor Concept Program is to broaden the environmental and economic benefits of nuclear energy in the U.S. economy from power production to meet the energy needs and also demonstrate applicability to market sectors not being served by light water reactors. The AHTR offers unique advantages for a variety of markets beyond power production because of the high ROT and because superior heat transport characteristics of molten salt. Increased ROT would expand the AHTR's applicability to many other applications so a brief descriptions of each are provided.

This section also presents the integration of AHTR technology with conventional chemical industrial processes. The process heat industrial applications being considered are: hydrogen production via steam methane reforming of natural gas and high temperature steam electrolysis, substitute natural gas production, oil sands recovery via steam assisted gravity drainage, coal-to-liquid production, natural gas-to-liquids production, methanol-to-gasoline production, ammonia production, ex situ oil shale, and in situ oil shale. The temperature ranges of applications that could be coupled to the AHTR with the current ROT (green band) and others that could potentially be coupled if the ROT was raised (red band) are shown in Figure 4-1. These are representative and should not be considered inclusive of all potential applications.
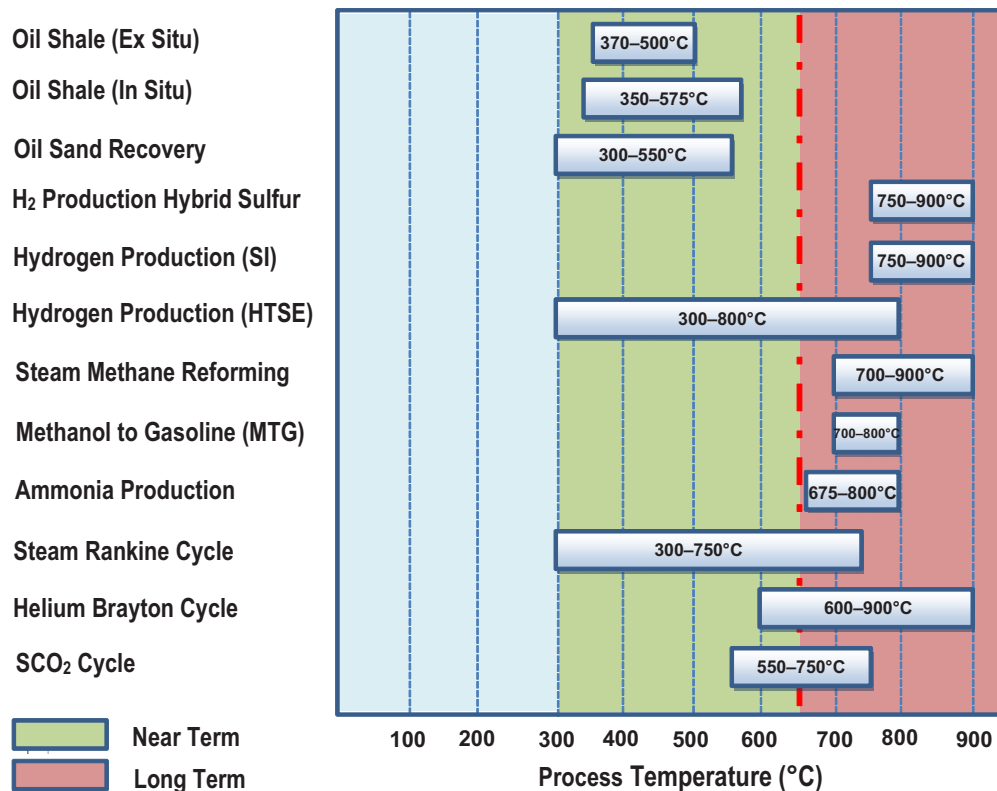
Figure 4-1. Process applications for AHTR versus process required temperature range.

21

In these analyses, heat from an AHTR is transferred from the reactor core by the primary liquid-salt coolant to an intermediate heat-transfer loop through an IHX. The intermediate heat-transfer loop circulates intermediate liquid-salt coolant through a SHX to move the heat to a power conversion system or for process industrial application as shown in Figure 4-2.

The ROT is currently 704°C, but will possibly increase to 900 to 1000°C for the nth-of-a-kind. With its ability to provide higher ROT, the process heat application becomes an attractive option. Even though the ROT for the AHTR is 700°C (~704°C), the maximum available temperature for any process application is 650°C as shown by the dashed line in Figure 4-1. Process heat applications are mentioned in this section, but details are given in TEV-1160, "AHTR Technical Evaluation" (Sabharwall and Kim 2011).
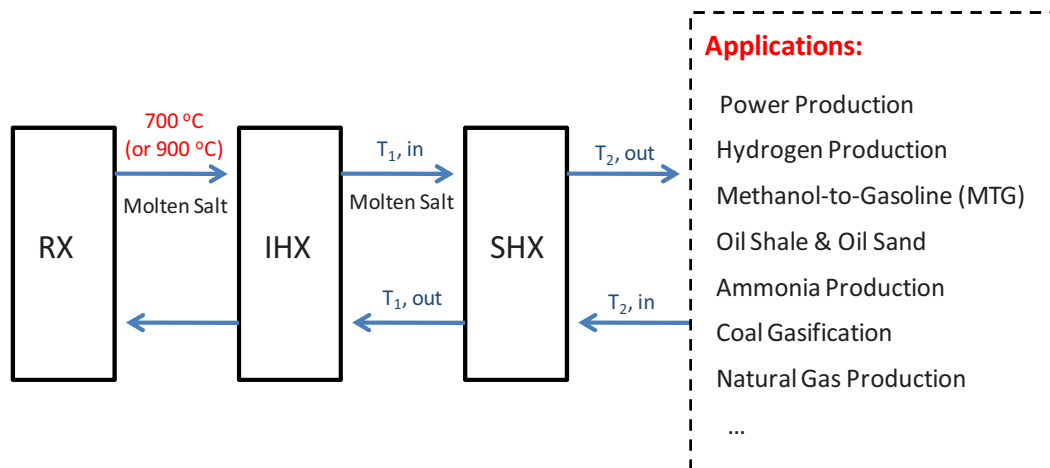
Figure 4-2. Thermal energy transfer in AHTR for power or process application.

The following assumptions were made to carry out the analysis:

- The reactor outlet temperature for AHTR is assumed to be 700°C

- An AHTR ROT should be sufficiently larger (~50°C) than the process application temperature requirement

- Any power production/industrial application requiring greater than 650°C is referred to as long term objective

- The minimum AHTR heat exchanger temperature should be maintained high enough to avoid molten salt freezing (>500°C), which will provide about 50 and 65°C temperature threshold before fluoride salts such as LiF-NaF-KF (FLiNaK) and chloride salts such as $KCl-MgCl_2$ freeze

- Heat exchanger tube material should have sufficient mechanical integrity to sustain pressure difference across the tube wall (will depend on application).

The process heat applications mentioned briefly in this section are discussed in greater detail in TEV-1160, "AHTR Technical Evaluation" (Sabharwall and Kim 2011). With the ROT of 704°C and the maximum available temperature of 650°C for process heat applications, the current AHTR could provide process heat for the following applications:

- Near-term integration (<650°C):

  - Power production cycles (Steam Rankine Cycle, Helium Brayton Cycle, SCO_2 cycle)

  - Oil shale (in situ)

- Oil shale (ex situ)
- Oil sands.

- Long-term integration (>650°C):
    - Hydrogen production via steam methane reforming
    - Substitute natural gas production
    - Coal-to-liquid production
    - Natural gas-to-liquid production
    - Methanol-to-gasoline production
    - Ammonia production.

An AHTR, when compared to gas-cooled reactors for process heat applications, benefits from a higher reactor inlet temperature because the molten salt is a more efficient heat transport medium and can transfer all of the reactor's heat with less temperature drop. This allows smaller and more efficient heat exchange equipment and produces smaller thermal stresses on those components.

5.   SHX

5.1   Introduction

The fundamental objective of this project was to identify and evaluate heat exchanger concepts for use as the SHX for the AHTR. The SHX provides the interface between the intermediate coolant and the power conversion system or process application. The identification of a viable SHX concept is based on the options for the power conversion scheme or the process heat application design needs.

The SHX serves as the coolant boundary and must be constructed to maintain system integrity under normal, off-normal, and accident conditions. To maintain high cycle efficiencies, it must also minimize temperature differences between the intermediate molten salt and the process working fluid while minimizing the pressure drop. The difference in pressure required in the power conversion system and process heat applications imposes stringent requirements on the heat exchanger design.

Candidate materials of construction include Alloys N, 800H, and 617, which exhibit (in varying degrees) high temperature tensile and creep strength and resistance to environmental degradation in molten salts. Longer-term research and development programs will evaluate ceramic and composite designs. Issues that must be addressed during the design process include materials compatibility with both the intermediate salt and the working fluid used in the power conversion system, high temperature strength, creep and creep-fatigue resistance, and the fabrication processes needed to manufacture an acceptable design (Holcomb et al. 2009).

5.2   Heat Exchanger Concepts

Some concepts identified as potential options for the SHX are: shell and tube, plate, plate and fin, printed circuit, helical coil, and ceramic. Each of these heat exchanger concepts are addressed below.

5.2.1   Shell and Tube Heat Exchanger

The shell and tube heat exchanger is the most common type found in industry. This exchanger is generally built of a bundle of round tubes mounted in a cylindrical shell with the tube axis parallel to that of the shell. One fluid flows inside the tubes and the other fluid flows across and along the tubes. The major components of this heat exchanger are the shell, tubes (or tube bundles), front-end head, rear-end head, baffles, and tube sheets (Shah and Sekulic 2003). In a shell and tube heat exchanger, the diameter of the outer shell is greatly increased, and a bank of tubes rather than a single central tube is used, as shown in Figure 5-1 (Sherman and Chen 2008). Fluid is distributed to the tubes through a manifold and tube sheet. To increase heat transfer efficiency, further modifications to the flow paths of the outer and inner fluids can be accomplished by adding baffles to the shell to increase fluid contact with the tubes, and by creating multiple flow paths or passes for the fluid flowing through the tubes (Sherman and Chen 2008). These heat exchangers are used for gas-liquid heat transfer applications primarily when the operating temperature and/or pressure are very high (Shah and Sekulic 2003).
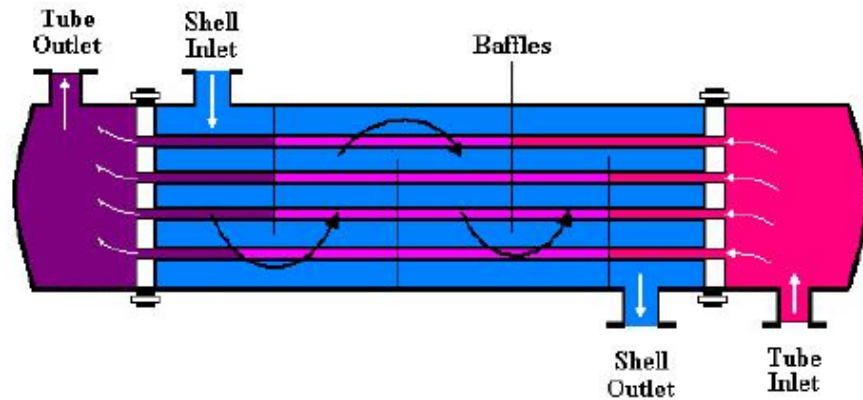
Figure 5-1. Shell and tube heat exchanger with baffles (Sherman and Chen 2008).

5.2.2 Plate Heat Exchanger

In a plate type heat exchanger, plate or planar surfaces are the fundamental heat transfer surfaces rather than tubes. Common plate heat exchangers deploy metal plates arranged in a stack-wise fashion and sealed with gaskets, welds, brazing, or diffusion welding as shown in Figure 5-2. Counter flow, cross flow, and co-current flow can be arranged by altering the design of the supply manifolds to the heat exchanger (Sherman and Chen 2008). Plate type heat exchangers consists of a series of thin, corrugated alloy plates sealed and compressed together inside a carbon steel frame. Once compressed, the plate pack forms an arrangement of parallel flow channels. Each plate has a contoured surface that provides additional surface area, tortuous flow paths, and contact points with adjacent plates (Shah and Sekulic 2003). The two fluids (hot and cold) flow countercurrent to each other in alternate channels, as shown in Figure 5-2. Each plate is fitted with a gasket to direct the flow, seal the unit, and prevent fluid intermixing. The choice of gasket material is based on the application of the heat exchanger (Shah and Sekulic 2003). These plates act as primary heat transfer surfaces by conducting heat directly through metal plates from one fluid to another.
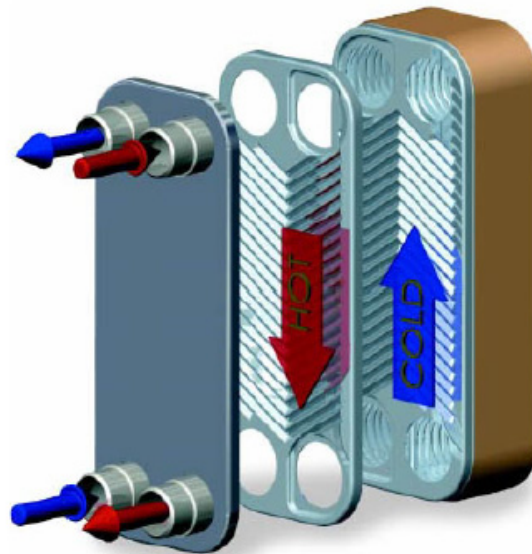
Figure 5-2. Flat plate compact heat exchanger (Sherman and Chen 2008).

The hybrid welded-plate heat exchanger (Bavex heat exchanger) shown in Figure 5-3 is reported to be capable of operating at 900°C and pressures up to 6 MPa on the plate side. It is called a hybrid because one fluid is contained inside the plates while the other flows between the plates from baffled plenums inside a pressure boundary (Fisher and Sindelar 2008). It is reminiscent of a shell and tube arrangement with substantially greater surface area. Plates can be produced up to 0.35 m wide and 16 m long (Fisher and Sindelar 2008). Other variants of the welded plate type heat exchanger are produced, some of which do not require external shells. Service conditions range up to 700°C and 30 MPa (in an external shell).
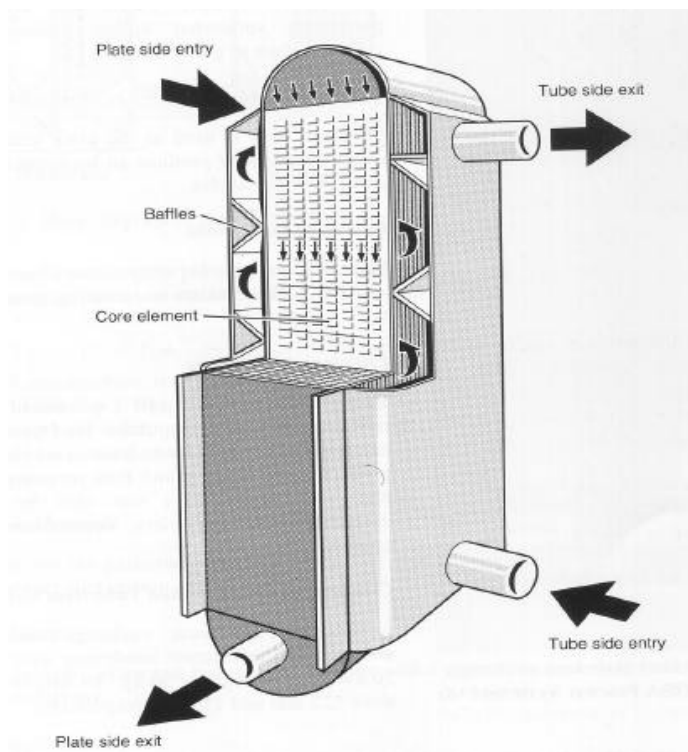
Figure 5-3. Bavex welded plate heat exchanger (Fisher and Sindelar 2008).

5.2.3   Plate and Fin Heat Exchanger

Plate and fin heat exchangers are formed by stacking flat metal plates alternately with corrugated metal plates (fins). Metal bars are placed around the perimeters between pairs of plates to support the stack and seal the edges, except for inlet and outlet passages (Sherman and Chen 2008). Heat transfer occurs as hot and cold fluids flow through the fins between alternate flat plates. Corrugated plates are secondary heat transfer surfaces, adding surface area and turbulence to the fluid flow (dependent on configuration) for greater heat transfer to the plates. Large numbers of plate and fin heat exchangers have been joined by brazing since the 1940s. More recently, manufacturers have also used diffusion welding for plate and fin models, as can be seen in Figure 5-4 (Fisher and Sindelar 2008). Both stainless steel and titanium plate and fin heat

Figure 5-4. Elements of diffusion-bonded plate and fin heat exchanger (Fisher and Sindelar 2008).

exchangers have been produced for service where conditions of higher temperature and/or pressure exist. A plate and fin heat exchanger with the arrangement of flat plates separated by corrugated spacers in order to increase the contact surface area between the plates is shown in Figure 5-5.
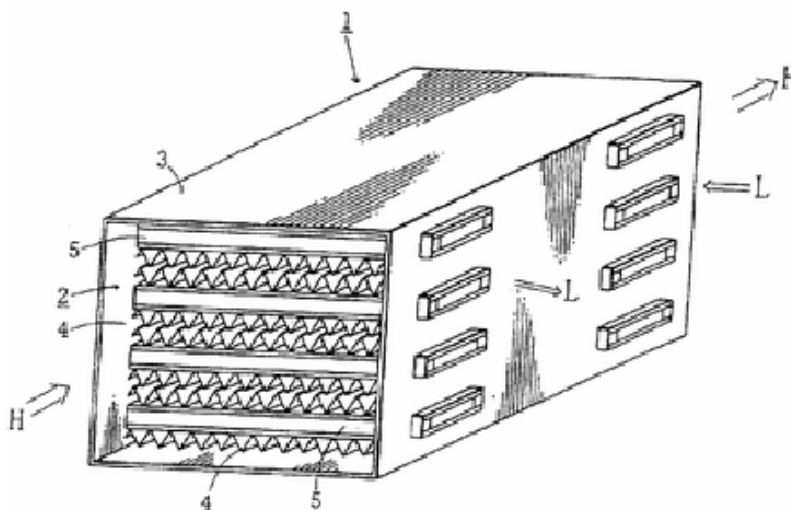
Figure 5-5. Plate-fin heat exchanger (Sherman and Chen 2008).

5.2.4   Printed Circuit Heat Exchanger

The printed circuit heat exchanger (PCHE) is a relatively new concept that has been commercially manufactured by Heatric™ since 1985. PCHEs are robust heat exchangers that combine compactness, low pressure drop, high effectiveness, and the ability to operate with a very large pressure differential between hot and cold sides (Heatric™ Homepage 2011). These heat exchangers are especially well suited to applications where compactness is important. The Heatric™ heat exchanger falls within the category of compact heat exchangers because of its high surface area density ($2,500 \ m^2/m^3$) (Hesselgreaves 2001).

As the name implies, PCHEs are manufactured by the same technique used to produce standard printed circuit boards for electronic equipment. In the first step of the manufacturing process, the fluid passages are photochemically etched into the metal plate as shown in Figure 5-6. Normally, only one side of each plate is etched to produce channels. The etched plates are thereafter joined by diffusion welding, resulting in extremely strong all-metal heat exchanger cores as shown in Figure 5-7. Plates for primary and intermediate fluids are stacked alternately and formed into a module as shown in Figure 5-8. Modules may be used individually or joined with others to achieve the needed energy transfer capacity between fluids.
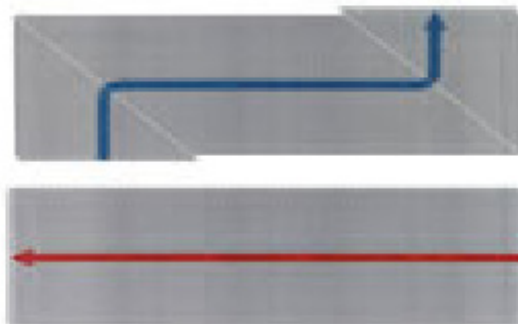
Figure 5-6. First step—plate passages (Heatric™ Homepage 2011).

The diffusion welding process produces grain growth across the weld joint, thereby producing a uniform metallurgical structure that is nearly as strong as the unwelded parent metal. Diffusion welding increases the expected lifetime of the heat exchanger such that it exceeds that of heat exchangers based on a brazed structure (Dewson and Thonon 2003).
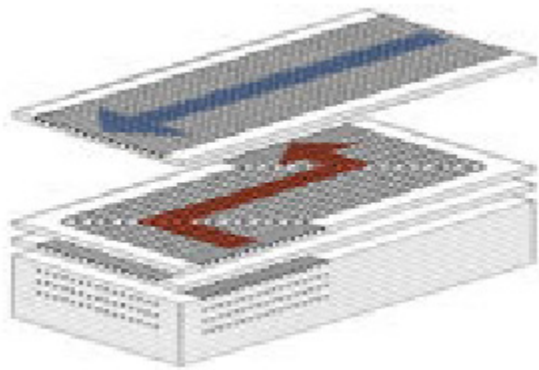
Figure 5-7. Second step—diffusion bonding of plates (Heatric™ Homepage 2011).
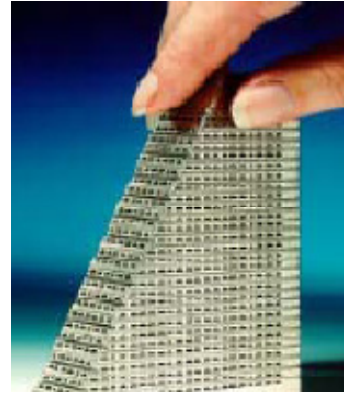
Figure 5-8. Diffusion-bonded PCHE section (Heatric™ Homepage 2011).

Bonding the stack of etched plates into a block comprises the third step. The heat exchanger core is completed by fusion welding as many of these blocks together as the thermal duty (flow capacity) of the heat exchanger requires (see Figure 5-9).

The flow passages typically have a semi-circular cross section as shown in Figure 5-10, and may also be radially corrugated as needed as shown in Figure 5-11. Their width and depth vary between 1.0 and 2.0 mm and 0.5 and 1.0 mm, respectively (Hesselgreaves 2001).

Figure 5-9. Third step—block composed of diffusion-bonded plates (Heatric™ Homepage 2011).

Several unique characteristics contribute to the superior performance of PCHEs. The most distinctive characteristics are the high allowable pressure and temperature limits in combination with the compactness of the heat exchanger. Specifically, the manufacturing company claims that, as a result of its original design, Heatric™ heat exchangers are able to operate at pressures up to 60 MPa and at temperatures not exceeding 900°C (Heatric™ Homepage 2011). To allow operation under such extreme conditions, the materials commonly employed in a PCHE include stainless steel, titanium, and nickel (Shah and Sekulic 2003). Heatric™ has supplied heat exchangers in the ranges indicated by the shaded area of Figure 5-12.

In addition to a wide operating range, the great potential of the PCHE is illustrated by its enhanced safety features. As a result of its construction, it does not use or contain any gaskets or braze material, substantially reducing the risk of leaks or fluid incompatibility. In particular, the risk of leaks in a Heatric™ heat exchanger is approximately two orders of magnitude lower than for any other heat exchanger, thanks to its continuous passage (Dewson and Thonon 2003).

The flexibility of allowed fluid types is another distinguishing feature of Heatric™ heat exchangers. The versatility is particularly shown in the area of allowed fluid types and flow configurations. PCHEs can be designed for use in gas, liquid metal, and molten salt cooled reactors (Heatric™ Homepage 2011). The design also allows multifluid integration (multistream capacity). The most commonly employed flow configurations include counter flow, cross flow, and co-flow or any combination of these as shown in Figure 5-13.
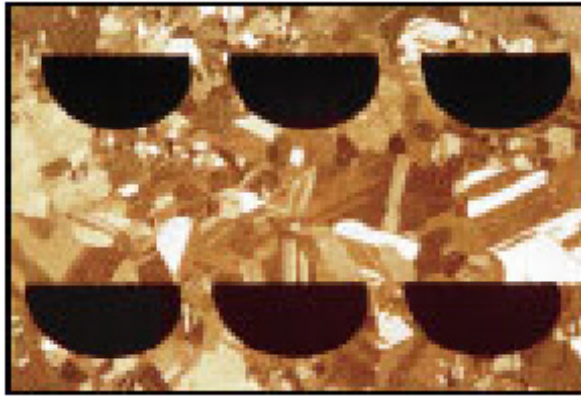
Figure 5-10. Cross sectional view of the semi-circular passages (Heatric™ Homepage 2011).
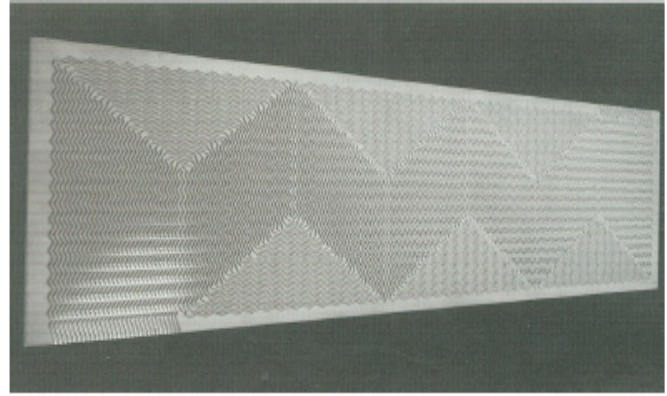
Figure 5-11. Side view of passage shapes (Hesselgreaves 2001).
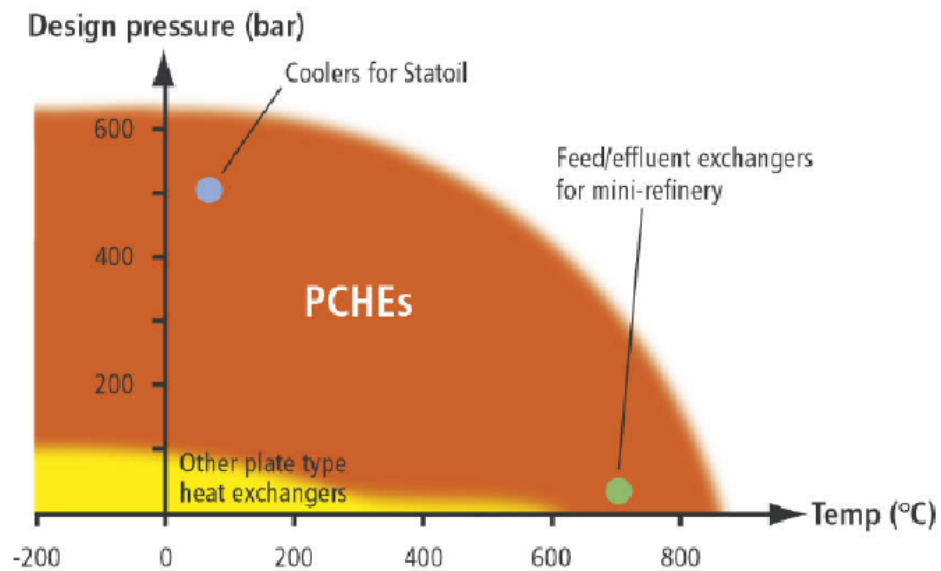
Figure 5-12. Current operating experience of Heatric™ PCHEs (Gezelius 2004).
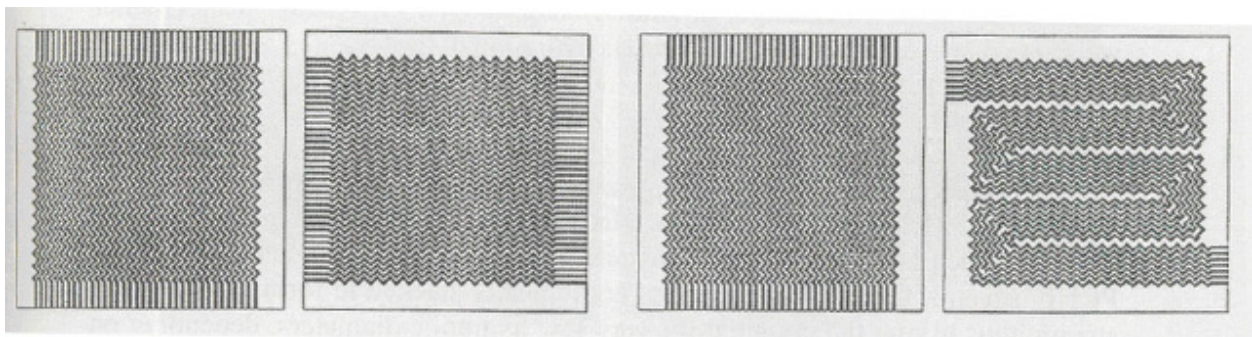
Figure 5-13. Simple cross flow (left) and cross-counterflow (right) configuration (Hesselgreaves 2001).

Lastly, size and pressure drop considerations also favor the PCHE. Because of the compactness provided by its design, the volume of the Heatric™ type heat exchanger is normally between four and six times smaller than that of the standard heat exchanger type designed for the same thermal duty and

pressure drop (Heatric™ Homepage 2011). With respect to mass, the Heatric™ heat exchanger has an average mass-to-duty ratio of 0.2 tons/MW, compared to 13.5 tonnes/MW for a shell-and-tube heat exchanger (Dewson and Thonon 2003). This reduction in size will cut material and handling costs. The actual design does not put any constraints on the heat exchanger with regard to the pressure drop. The flow channels are usually short, which compensates for the narrow passages (Heatric™ Homepage 2011).

Heatric™ has been developing a product to integrate the advantages of the PCHE and a plate and fin heat exchanger (Heatric™ Homepage 2011). This hybrid heat exchanger, shown in Figure 5-14, is called the H^2X. They are formed by alternating a fin layer with an etched plate, which are then diffusion bonded. This heat exchanger offers the high mechanical integrity and high efficiency of diffusion-welded heat exchangers combined with the large passages (lower pressure drop) and lower weight of the plate and fin heat exchanger (Heatric™ Homepage 2011).

5.2.5   Helical Coil Heat Exchanger

Helical coil heat exchangers are shell and tube type heat exchangers that consist of tubes spirally wound into bundles and fitted in a shell as shown in Figure 5-15. The spiral geometry of the tubes results in a higher heat transfer

Figure 5-14. The Heatric™ H²X heat exchanger—PCHE construction on the left side and plate and fin side on the right (Heatric™ Homepage 2011).

rate than that for a straight tube (Shah and Sekulic 2003). Because of the tube bundle geometry, a considerable amount of surface can be accommodated inside the shell. These heat exchangers are used for gas-liquid heat transfer applications, primarily when the operating temperature and/or pressure are very high. Cleaning a helical coil heat exchanger can be very difficult (Shah and Sekulic 2003).

5.2.6   Ceramic Heat Exchanger

The main benefits of ceramic heat exchangers are their ceramic material properties. Silicon carbide (SiC) ceramics are the leading choice for heat exchangers because they are ideally suited for high temperature, corrosive environments. These ceramics are able to operate safely at higher temperatures (~1300ºC) than metallic alloys (Heat Transfer International Homepage 2011). A
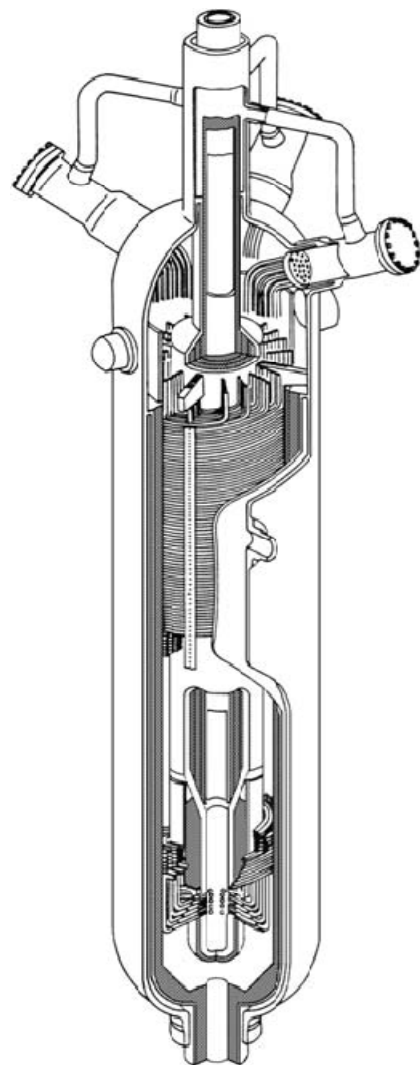
Figure 5-15. A helical-coil heat exchanger (Areva 2008).

shell and tube type ceramic heat exchanger can operate at about 1.3 MPa (Heat Transfer International Homepage 2011). However, leakage between the primary and intermediate fluids can be a significant issue if the pressure difference between the fluids is large. Stress analyses and material properties studies indicated that siliconized SiC is an attractive ceramic material for fabrication of pressurized heat exchangers (Taborek et al. 1983).

SiC ceramics are also highly inert chemically and have a low coefficient of thermal expansion. However, SiC can be susceptible to oxidation at high temperatures. Individual tubes can be easily replaced in the Heat Transfer International design (Heat Transfer International Homepage 2011). Particulate build-up can be removed and cleaning can be performed without process interruption (Heat Transfer International Homepage 2011).

The mechanical properties of SiC material are dependent on factors such as porosity and the impurity concentration (Snead et al. 2007). Under some conditions of high-temperature exposure, the helium permeability of SiC ceramics can increase by at least three orders of magnitude with a pressure difference of 520 kPa across the tube walls (Taborek 1983). An area that requires further work is the fabrication of joint between ceramics and metallic piping systems.

Some of the potential applications of ceramic heat exchangers considered for advanced energy systems include gas turbines in various configurations and coal gasifiers (Taborek 1983).

5.3   Summary

The key to high efficiency is a highly effective heat exchanger, so an efficiently designed SHX is critical for effective use of the energy generated in an AHTR. The potential options for the SHX were described in this section. The heat exchanger options will be examined to determine the best fit for an AHTR application. Based on past industrial experience, the shell and tube (helical coiled) type heat exchanger is the design that presents the least risk for a 20 MW(t) test reactor. Use of a proven technology in a demonstration reactor allows the development team to focus on the reactor island, fuel performance, etc. If this reactor type is to be commercially deployed, other heat exchanger designs such as compact heat exchangers should continue to be evaluated for future AHTR designs with 3,400 MW(t) reactors to improve efficiency and commercial viability. Analysis results of potential designs for commercial deployment will be presented in future deliverables.

6.   HEAT EXCHANGER EVALUATION AND SELECTION METHOD

6.1   Introduction

A variety of heat exchangers are available in industry, including shell-and-tube, plate-and-frame, brazed-plate, plate-and-fin, PCHE, bayonet, etc. Heat exchanger design and selection involves many trade-offs associated with geometrical and operational variables.

Two steps were performed in this study to select the best heat exchanger:

1. Screening the candidate heat exchanger types based on the operating parameters.

2. Evaluating the matrix for selecting the AHTR heat exchanger.

Candidate heat exchangers were selected based on operating parameters; mainly, temperature and pressure. More detailed comparisons were then carried out among the candidate designs using an evaluation matrix. Further multicriteria decision analysis (MCDA) will be used to select the optimum heat exchanger for a given application.

6.2   Initial Screening of Heat Exchanger Type Based on Operating Parameters

To evaluate and select the SHX for an AHTR, the following base assumptions and requirements were followed:

- ROT: 700°C

- Application Type: Power Conversion System (3,400 MW(t))*

  - Helium Brayton ($\eta = 40.3\%$)

  - Steam Rankine ($\eta = 41.9\%$)

  - Supercritical CO_2 Modified Brayton ($\eta = 43.7\%$)

  - Supercritical Rankine ($\eta = 44.0\%$)

- Pressure:

  - SHX primary: 0.1 MPa

  - SHX secondary:

    – Helium Brayton: 7.11 MPa

    – Steam Rankine: 17.7 MPa

    – Supercritical CO_2 Modified Brayton: 24.99 MPa

    – Supercritical Rankine: 21.66 MPa

- Coolant   :

  - SHX primary: FLiNaK

  - SHX secondary:

    – Helium Brayton: Helium

    – Steam Rankine: Water (Steam)

    – Supercritical CO_2 Modified Brayton: Supercritical CO_2

    – Supercritical Rankine: Water (Steam)

The type of power conversion system has not yet been determined in this study; it will be finalized in the next phase of the feasibility study. Once the type of power conversion system is decided, the assumptions, performance and requirements will be narrowed down.

Table 6-1 summarizes general operating conditions and principal features for various heat exchanger types (Shah, 2003) in the current industry. This table summarizes the following:

- Heat exchanger type: Sixteen heat exchanger types are listed in this table.

- Compactness: Compactness indicates (surface area)/ (heat exchanger core volume). If compactness is high, the heat exchanger can be smaller.

- System Type: System type indicates what fluid phases are generally used for a certain heat exchanger type in the industry.

- Material: Material indicates what material has been used and experienced for a certain type of heat exchanger in the current industry.

- Temperature Range: Temperature range indicates the applicable temperature ranges of a certain type of heat exchanger.

- Maximum Pressure: Pressure indicates the applicable pressure ranges of a certain type of heat exchanger.

- Cleaning Method: Cleaning method indicates if the heat exchanger can be cleaned physically or chemically.

- Multistream Capability: Multistream capability indicates if it can connect several independent flow loops in a single heat exchanger.

- Multipass Capability: Multipass capability indicates if it can split flow into several paths in the heat exchanger.

According to Table 6-1, only a few heat exchanger types can meet the minimum requirements with sufficient margin because of the severe requirements of an AHTR. Currently, the available heat exchanger types are as follows:

- Shell-and-tube

- PCHE.

The shell-and-tube heat exchanger is the most typical type of heat exchanger. These heat exchangers are generally built of circular tubes and have considerable flexibility in design. They can be designed for high pressures relative to the environment and high-pressure differences between the fluids. PCHE is a plate type heat exchanger. The plates are chemically etched and then diffusion-welded. Fluid inlet/outlet headers are then welded on. Details on the heat exchanger types are presented in Section 5.

Table 6-1. Principal features of several types of heat exchangers (Shah 2003).

Heat Exchanger Type	Compactness (m²/m³)	System Types	Material	Temperature Range (C)[a]	Maximum Pressure (bar)[b]	Cleaning Method	Multistream Capability[c]	Multipass Capability[d]
Shell and Tube	~100	Liquid/Liquid, Gas/Liquid, 2Phase	s/s, Ti, Incoloy, Hastelloy, graphite, polymer	~ +900	~ 300	Mechanical, Chemical	No	Yes
Plate-and-frame (gaskets)	~200	Liquid/Liquid, Gas/Liquid, 2Phase	s/s, Ti, Incoloy, Hastelloy, graphite, polymer	-35 ~ +200	25	Mechanical	Yes	Yes
Partially welded plate	~200	Liquid/Liquid, Gas/Liquid, 2Phase	s/s, Ti, Incoloy, Hastelloy	-35 ~ +200	25	Mechanical, Chemical	No	Yes
Fully welded plate (Alfa Rex)	~200	Liquid/Liquid, Gas/Liquid, 2Phase	s/s, Ti, Ni alloys	-50 ~ + 350	40	Chemical	No	Yes
Brazed plate	~200	Liquid/Liquid, 2Phase	s/s	-195 ~ +220	30	Chemical	No	No
Bavex plate	200 to 300	Gas/Gas, Liquid/Liquid, 2Phase	s/s, Ni, Cu, Ti, special steels	-200 ~ +900	60	Mechanical, Chemical	Yes	Yes
Platular plate	200	Gas/Gas, Liquid/Liquid, 2Phase	s/s, Hastelloy, Ni alloys	~700	40	Mechanical	Yes	Yes
Compabloc plate	~300	Liquid/Liquid	s/s, Ti, Incoloy	~300	32	Mechanical	Not usually	Yes
Packinox plate	~300	Gas/Gas, Liquid/Liquid, 2Phase	s/s, Ti, Hastelloy, Inconel	-200 ~ +700	300	Mechanical	Yes	Yes
Spiral	~200	Liquid/Liquid, 2Phase	s/s, Ti, Incoloy, Hastelloy	~400	25	Mechanical	No	No
Brazed plate fin	800 to 1500	Gas/Gas, Liquid/Liquid, 2Phase	Al, s/s, Ni alloy	~ 650	90	Chemical	Yes	Yes
Diffusion bonded plate fin	700 to 800	Gas/Gas, Liquid/Liquid, 2Phase	Ti, s/s	~ 500	> 200	Chemical	Yes	Yes
Printed circuit	200 to 5000	Gas/Gas, Liquid/Liquid, 2Phase	Ti, s/s	-200 ~ +900	> 400	Chemical	Yes	Yes
Polymer (e.g. channel plate)	450	Gas/Liquid	PVDF, PP	~ 150	6	Water Wash	No	No
Plate and shell	—	Liquid/Liquid	s/s, Ti	~ 350	70	Mechanical, Chemical	Yes	Yes

s/s   Stainless steel.

a.   Heat exchanger operational temperature ranges.

b.   Heat exchanger maximum applicable pressure.

c.   Capability to connect several independent flow loops in a single heat exchanger.

d.   Capability to split flow into several paths in the heat exchanger.

6.3 Evaluation Method and Plan for Selection of AHTR Heat Exchanger

This section describes the method for the AHTR heat exchanger evaluation and selection based on MCDA.

6.3.1 Evaluation Method: Analytical Hierarchy Process

The previous sections describe major alternatives for the SHX. This section describes how these criteria and the alternatives are evaluated using an analytical hierarchy process (AHP) to evaluate the candidate heat exchangers. AHP is a structured technique developed for multicriteria decision-making problems, currently among the most widely used MCDA techniques. It helps decision makers find the best option that suits their goals and understanding of the problem. The AHP was first developed at Wharton School of Business in the 1970s by Thomas L. Saaty. It is based on mathematics and psychology (Saaty 1980), and has been extensively studied and refined since then. It provides a comprehensive and rational framework for structuring a decision problem, representing and quantifying its elements, relating those elements to overall goals, and evaluating alternative solutions.

AHP allows for the application of data, experience, insight, and intuition in a logical way. AHP enables decision-makers to derive ratio scale priorities or weights as opposed to arbitrarily assigning values. It therefore supports decision-makers by enabling them to structure complexity, exercise judgment, and incorporate both objective and subjective considerations in the decision process.

In the AHP method, weights and scores are done by structuring complexity as a hierarchy and by deriving ratio scale measures through pair-wise relative comparisons. The pair-wise comparison process can be performed using words, numbers, or graphical bars, and typically incorporates redundancy, which results in a reduction of measurement error as well as producing a measure of consistency of the comparison judgments. This method is based on the fact that humans are much more capable of making relative rather than absolute judgments. The use of redundancy permits accurate priorities to be derived from verbal judgments even though the words are not very accurate. Therefore, the weights or priorities are not arbitrary assigned in the AHP method.

The AHP involves the mathematical synthesis of numerous judgments about the decision problem at hand. It is not uncommon for these judgments to number in the dozens or even the hundreds. While the math is pretty straight forward, it is far more common to use one of several computerized methods for entering and synthesizing the judgments.

The procedure for using the AHP can be summarized as (Satty 1996, Forman 2001, Howell 2007, Bhushnan 2004):

1. Problem identification and description.

2. Setting up final goal and objective.

3. Selecting alternatives.

4. Identifying and listing criteria.

5. Modeling the problem as a hierarchy containing the decision goal, alternatives for reaching it, and criteria for evaluating the alternatives.

6. Establish priorities among the elements of the hierarchy by making a series of judgment based on pair-wise comparisons of the elements. For example, when comparing potential real estate purchases, the investors might say they prefer location over price and price over timing.

7. Synthesize these judgments to yield a set of overall priorities for the hierarchy. This would combine the investors' judgments about location, price, and timing for properties A, B, C, and D into overall priorities for each property.

8. Check the consistency of the judgments.

9. Come to a final decision based on the results of this process.

6.3.2   Goal, Alternatives, and Criteria for AHTR Heat Exchanger Selection

This section describes a goal, alternatives, and criteria for selecting an AHTR heat exchanger.

6.3.2.1   Goal

The final goal of this study is to evaluate and select the best heat exchanger type for an AHTR SHX.

6.3.2.2   Alternatives

From the screening process described in the previous section, the two heat exchanger types identified to be the possible SHX options that meet the base requirements are shell and tube and PCHE.

6.3.2.3   Criteria

Table 7-2 summarizes the criteria for an AHTR SHX evaluation and selection. The details are explained below.

Thermal Performance

Thermal performance is the primary criterion in selecting a heat exchanger since effective heat transfer is its main purpose. Thermal performance consists of high heat transfer performance, effectiveness and fouling. These three subcriteria are defined as follows:

- *Heat transfer performance* in the heat exchanger is greatly affected by the heat exchanger type because they have such diverse channel geometries and configurations. Smaller channels generally have a better heat transfer coefficient with the same flow-rates as larger ones, but there are more frictional losses.

- *The effectiveness* of the heat exchanger is generally a very important design parameter because the system must minimize losses of useful thermal energy when heat is transferred. Higher effectiveness means that the heat exchanger design is closer to the ideal. Typical values for the effectiveness are 0.7 to 0.9 for conventional shell-and-tube design, and 0.9 to 0.98 for the compact heat exchanger design.

- *Fouling* of a heat exchanger is an important factor because it significantly degrades thermal performance, especially for liquid coolants. Fouling drives an oversized heat exchanger design. Cleaning strategies are also needed for specific applications.

Structural Performance

Structural performance is one of the most important criteria for an SHX heat exchanger so it can be safely operated at high temperatures and wide pressures differences throughout a long plant lifetime. Heat exchanger integrity can be categorized primarily by how it operates under steady-state and transient conditions. An AHTR is mainly exposed to mechanical and thermal stress. Vibration is also an important SHX criterion because it could degrade the integrity of the heat exchanger. Thus, an SHX that is less prone to vibration instabilities is preferred. Since an SHX will be operated over a long lifetime at high temperature, important issues that should be considered are creep, fatigue, and creep-fatigue.

Validating the effects of system pressure and temperature on the integrity of joints (diffusion welding, brazing, and fusion welding) in a molten salt environment under steady-state and transient conditions is necessary and would enable a better selection of the SHX. Joints are subjected to static and dynamic loading while the heat exchanger is operating; the one with better performance will be ranked higher. Brazed heat exchangers are appropriate at lower temperatures, but there are potential mechanical integrity problems with temperature cycling at higher temperatures (Tatara 1997). The heat exchanger with a proven joining technique will be preferred when compared with an unproven technique.

The materials being considered for the SHX (Alloys 617, 230, 800H and N) all spontaneously form chromium-rich oxide scales that will present problems in making diffusion welds. The diffusion welding process needs to be further developed and bonding process parameters and controls identified. The technical literature addresses microstructure and mechanical properties, but not the parameters used to perform the bonding. Techniques such as mating surface pickling, nickel plating, or a nickel foil interlayer will have to be investigated. Mechanical testing of the diffusion welded joints will be needed to identify promising joining parameters, such as temperature, applied pressure, and hold time for optimization. In addition to optimizing process parameters and inspection of diffusion bonds, other specific concerns that must be addressed are:

- Microstructural stability during the high temperature exposure associated with diffusion welding

- Production of large components is limited by the size of the fabrication equipment used.

Creep and creep-fatigue will be influenced by peak stresses because of the stress concentration effects of the coolant channels. Creep fatigue combined with the high temperature environmental degradation caused by the influence of an AHTR environment makes the creep-fatigue characterization very complicated. Creep and creep-fatigue data at these high temperatures will be needed for the selected material in order to develop a creep-fatigue interaction diagram.

Structural performance consists of mechanical stress, thermal stress, and vibration. These subcriteria in an AHTR are described as follows:

- *Mechanical stress* should be considered in evaluating and selecting the SHX because it is exposed to large pressure difference at high temperature between the primary and the intermediate sides, depending on the integrated systems. Mechanical stress in a heat exchanger is also significantly affected by channel/tube configuration, size, and geometry. Joining methods are very important in the mechanical integrity of the heat exchanger. The heat exchanger type should be able to withstand the mechanical stress in the given environment.

- *Thermal stress* should be considered because large temperature gradients exist in the heat exchanger. Thermal stress is affected by heat exchanger configurations and geometries. Therefore, the thermal stress should be minimized in the heat exchanger design.

- *Vibration* is one of the major failure mechanisms of the heat exchanger tube or channel. It is highly affected by heat exchanger geometry and configuration. Therefore, the vibration should be minimized in the heat exchanger design.

Material Performance

Corrosion is an important criterion for an AHTR heat exchanger because of the environmental degradation caused by the fluoride salt at high temperatures. A factor in the lifetime of a heat exchanger will be its resistance to corrosion in an AHTR environment. Corrosion resistance will be a function of the materials of construction as well as the thickness of various sections. Design features of the heat exchanger and the material of construction will also impact corrosion. Corrosion is resisted by using special alloys in construction. If the selected material cannot effectively prevent corrosion, a better or a

preferred option will be for the heat exchanger to have thicker walls (more forgiving) and more corrosion allowance incorporated into its design when compared with other heat exchangers. The subcriteria are:

- Geometry

- Corrosion allowance in design (uniform corrosion)

- Localized corrosion/environmental cracking

- Fluid compatibility.

Technology Readiness

Technology readiness should also be considered in selecting an AHTR heat exchanger. A technology may look promising in industrial applications but still need to be demonstrated under AHTR operation and environmental conditions. The subcriteria selected for determining technology readiness are material, fabrication method, and American Society of Mechanical Engineers (ASME) Boiler and Pressure Vessel (BPV) Code status. These subcriteria are describes as follows:

- *Material* is a major issue in manufacturing an AHTR SHX because of its severe environment (high temperatures and high corrosives). The technology readiness of manufacturing materials should therefore be considered when evaluating the heat exchanger.

- The *fabrication method* should be evaluated for the selected candidate material, since some heat exchanger types such as PCHE have unique fabrication methods like diffusion welding.

- The *ASME BPV Code* should be considered in the heat exchanger evaluation process because the material used in the manufacture of a heat exchanger must be supported by the ASME BPV code (Section 3 deals with primary pressure boundaries applicable to nuclear service, Section 8 deals with intermediate processes applicable to SHXs).

- In a nuclear energy system, a proven technology based on *industrial experience* is always recommended because of its experience and low uncertainty.

System Integration

The main role of the SHX in an AHTR is to integrate the nuclear reactor with the power conversion system or with a process heat application plant. Integration should therefore be considered. The applicable subcriteria are size and adaptability, which are described as follows:

- The *Size* of the heat exchanger is important to the integration of the heat exchanger with the systems. Smaller size is generally preferred.

- *Adaptability* is the ease of integrating the SHX with various applications. This adaptability will depend on what system will be integrated with the heat exchanger.

Tritium Permeation

Tritium is mainly generated in an AHTR core by ternary fission and various neutron reactions. Tritium is a major concern because it easily permeates high temperature metallic surfaces. Since this tritium is a radioactive isotope, it eventually radioactively contaminates the industrial system and products, although tritium separation and capture is relatively easier in a nonhydrogenous liquid coolant. For mitigating tritium permeation, less heat transfer surface area and larger heat exchanger thickness are preferred in the design. The subcriteria for tritium permeation are material and geometry, which are described as follows:

- The types of tube or channel *material* in the heat exchanger is significantly affected by tritium permeation. It is also highly affected by existing oxide-layers and applied coatings.

- *Geometrical parameters* such as heat transfer area and wall thickness effect total tritium permeation through the heat transfer surface of the heat exchanger. Tritium permeation is proportional to the heat transfer area and inversely proportional to the wall thickness.

Inspection

Inspection should be easily accomplished to determine the state of the equipment. Compact heat exchangers, being small units, will not be easy to inspect. A heat exchanger designed so that joints can be examined and cracks and crack growth identified more easily over its operational lifetime is preferred. Nondestructive evaluation (such as eddy current testing, ultrasonic testing, radiography, and pressure leak testing) may be used to evaluate the structural integrity of heat exchanger components. It is not possible to offer more insight because of the lack of historical inspection and operation data for the compact heat exchangers being considered.

Maintenance

The ease of maintenance, such as cleaning, repair, and serviceability, is an important characteristic for a successful AHTR heat exchanger. All heat exchangers should be chemically cleanable, which is more effective and efficient than dismantling and physically cleaning them. The heat exchanger should also have provision for replacing any components subject to corrosion, unless it is more economical to replace the whole unit (Shah 2003). Thus, a heat exchanger with these capabilities is preferred. The subcriteria for maintenance are cleaning, waste, and repairing, which are described as follows:

- *Cleaning* of the heat exchanger should done regularly to remove fouling on the channel/tube inside. Generally, it can be cleaned physically, chemically, or by both methods, depending on the heat exchange type.

- *Waste* discharged when cleaning and repairing heat exchangers should be considered in the evaluation.

- *Repairing* a tube rupture or some other problems in the heat exchanger should be easy.

Initial Cost

In one respect, the life-cycle cost for a given heat exchanger can serve as a single criterion for comparison. The costs of development, design, fabrication, installation, and maintenance can be included in the life-cycle cost. However, at this point in the project, the heat exchanger concepts are not sufficiently developed to provide accurate cost information on which to base these comparisons. Therefore, the cost comparisons will be qualitatively addressed. The cost could include fabrication, material, and installation costs, which can be characterized as follows:

- *Fabrication costs* are complicated by designs that might cost more to fabricate than simpler designs. In order to increase the surface area density of the heat exchanger, the fluid channel diameter (or effective diameter) is reduced, which generally increases the net fabrication cost. The fabrication method has to be acceptable and meet all the requirements imposed by ASME. The heat exchanger designs are still in the development phase, so fabrication cost values are rough estimates. The equivalent (same thermal duty) heat exchanger will be compared based on the net fabrication cost; the one with the highest value for a specific thermal load in kW (quantitatively measured as Heat Load (Q) in kW per dollar ($) spent) per money spent will be ranked higher than the others.

- *Materials* used in the construction of the heat exchanger are based on size; more material will be required for larger heat exchangers, increasing the cost.

- *Installation* costs could potentially be higher for conventional heat exchanger designs when compared with compact designs.

Operability

It is currently not possible to supply details on the operability of compact heat exchangers because operation data in a molten salt environment with high temperature conditions are not available. The subcriteria for the operability are reliability and operating and maintenance.

Table 6-2. Criteria for AHTR heat exchanger selection.

Criteria	Subcriteria
Thermal Performance	High Heat Transfer Performance (heat transfer/pumping power)
	High Effectiveness
	Fouling
Structural Performance (Evaluated by ASME B&PV Design rules)	Mechanical Stress
	Thermal Stress
	Vibration
Material Performance	Geometry (heat exchanger wall thickness)
	Corrosion Allowance in Design (uniform corrosion)
	Localized Corrosion/Environmental Cracking
	Fluid Compatibility
Technology Readiness	Material
	Fabrication Method
	ASME B&PV Code Status
	Industrial Experience
System Integration	Size
	Adaptability
Tritium Permeation	Material
	Geometry (total heat transfer area + wall thickness)
Inspection	Ease of Inspection (geometry) and field access
Maintenance	Cleaning
	Waste
	Repairing
Initial Cost [a]	Material
	Fabrication
	Installation
Operability	Reliability
	Operating & Maintenance

6.3.3 Modeling AHTR Heat Exchanger Selection

The AHP hierarchy for selecting an AHTR heat exchanger is shown in Figure 6-1, which is developed based on criteria in Table 6-2 and alternatives in Section 6.3.2.
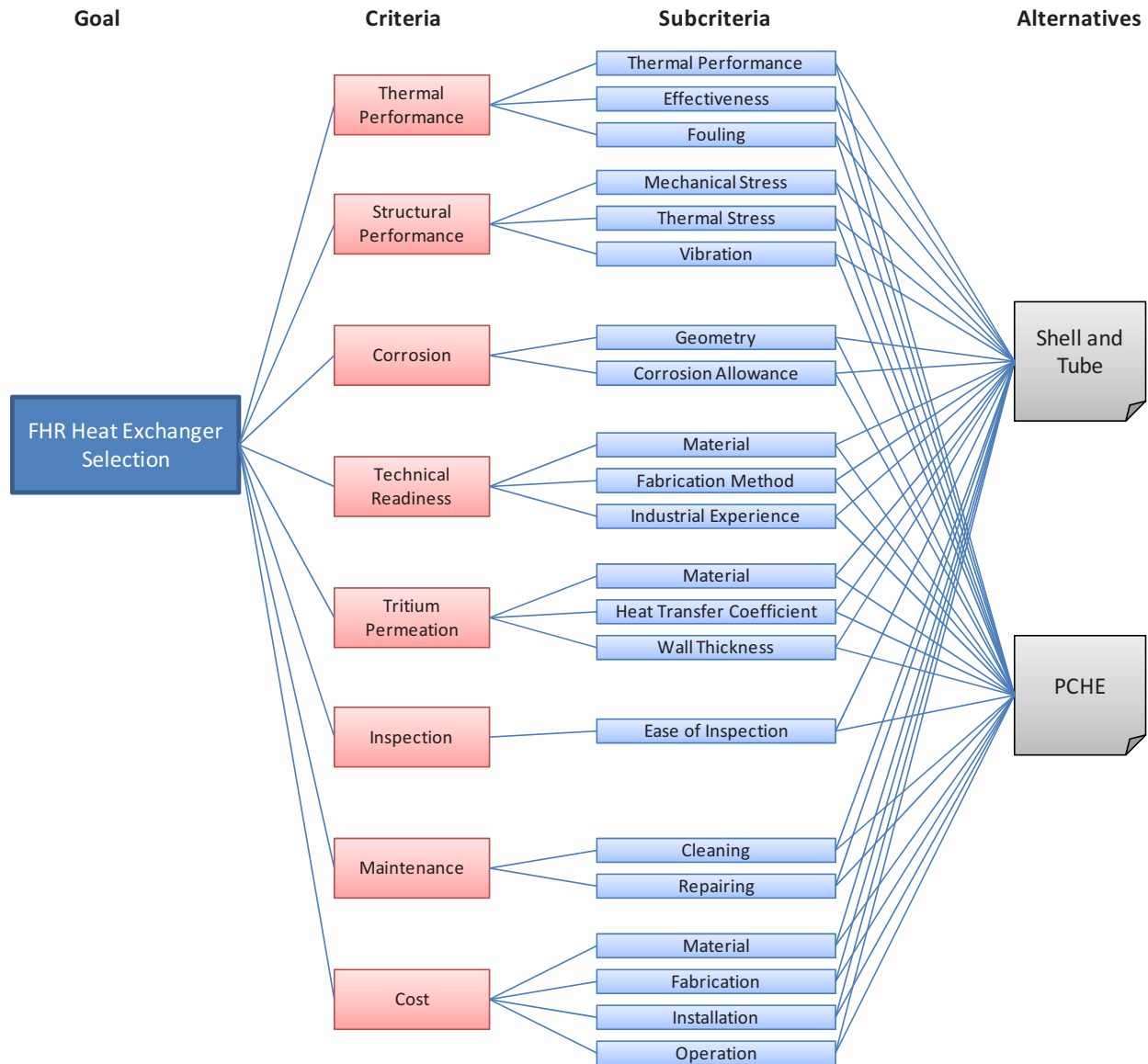
Figure 6-1. Decision hierarchy for AHTR heat exchanger selection.

6.3.4   Pair-wise Comparisons

Once the hierarchy has been constructed in the AHP, participants analyze it through a series of pair-wise comparisons that derive numerical scales of measurement for the nodes. The criteria are pair-wise compared with the goal for importance. The alternatives are pair-wise compared against each of the criteria for preference. The comparisons are processed mathematically, and priorities are derived for each node. Table 6-3 shows the fundamental scale for pair-wise comparison recommended in the AHP (Forman 2001).

Table 6-3. Fundamental scale for pair-wise comparison in AHP (Forman 2001).

The Fundamental Scale for Pairwise Comparisons		
Intensity of Importance	Definition	Explanation
1	Equal importance	Two elements contribute equally to the objective
3	Moderate importance	Experience and judgment slightly favor one element over another
5	Strong importance	Experience and judgment strongly favor one element over another
7	Very strong importance	One element is favored very strongly over another; its dominance is demonstrated in practice
9	Extreme importance	The evidence favoring one element over another is of the highest possible order of affirmation
Intensities of 2, 4, 6, and 8 can be used to express intermediate values. Intensities 1.1, 1.2, 1.3, etc. can be used for elements that are very close in importance.		

6.3.5   AHP Software (for Evaluation of Model): MakeItRational

This study uses MakeItRational software to evaluate and select an AHTR heat exchanger. MakeItRational is well-known multicriteria decision making software. This Web-based software is based on the AHP method and uses pair-wise comparisons for weighting and rating preferences. It provides group decision evaluations and also sensitivity analysis results. Figure 6-2 is a screen shot of this software. Currently, all the goals, alternatives, criteria, and subcriteria are implemented into the software with the hierarchy structure shown in Figure 6-1. This setup will be finally used to evaluate and select an AHTR heat exchanger in the next stage with feasibility studies.
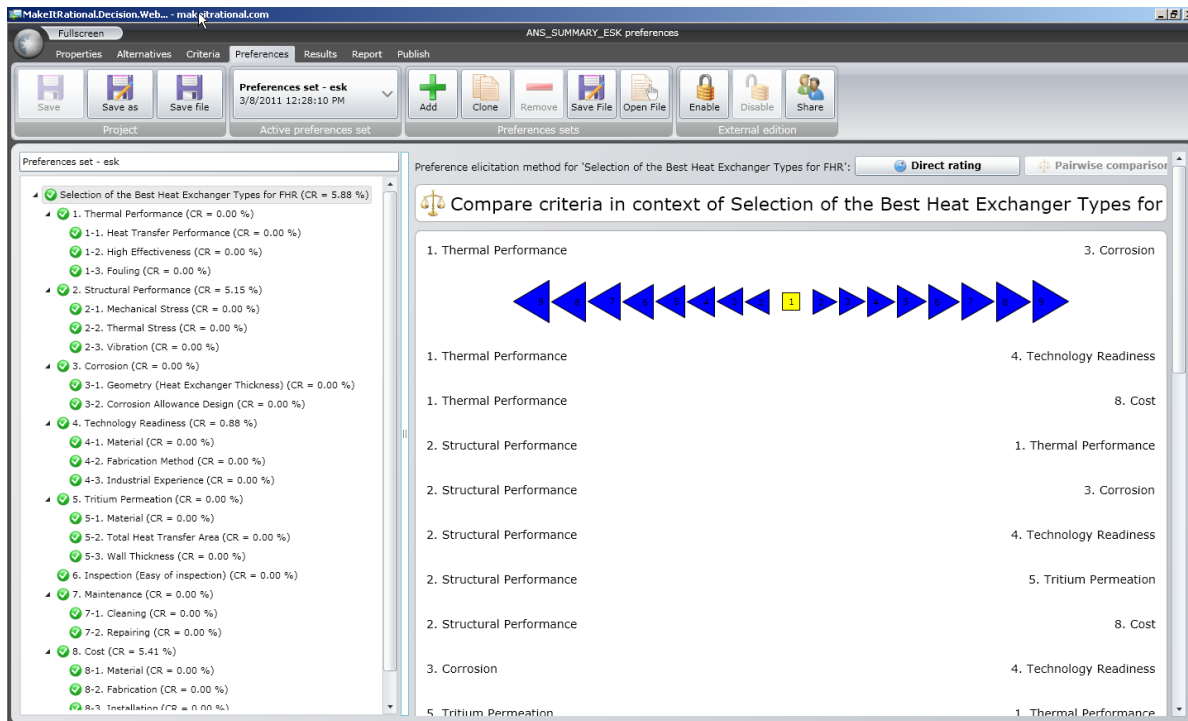
Figure 6-2. Screenshot of MakeItRational.

6.3.6   Plan for AHTR Heat Exchanger Evaluation and Selection

Currently, the basic setup for selecting an AHTR heat exchanger has been established with evaluation goals, alternatives, and criteria as shown in the previous sections. However, without sufficient information and knowledge, it is difficult to make a right decision. The current priority is therefore to collect information to help decision making.

Feasibility studies will be conducted in the next term of this study to provide sufficient information for the evaluation and decision making process. Once sufficient information is collected, it will be distributed and shared among the members who will participate in making the final decision. Currently, eight members with different background and expertise have been identified to participate in this process.

Development of the integration methodology is an ongoing task and will be covered in the later reports as the work progresses.

7. SUMMARY AND CONCLUSION

The primary purpose of this study is to aid in the development and selection of the required heat exchanger for power production and process heat application for an AHTR. An AHTR currently has an expected ROT of 704°C, which may increase with later designs. Design and demonstration of the SHX is vital to providing high temperatures to power production or process heat applications. To design an SHX for an AHTR, various aspects need to be considered. Of primary importance is how the heat from the reactor will be used. The heat from the reactor is anticipated to be used for power generation and process heat applications.

The molten salt coolants considered for use in the intermediate coolant loop are LiF-NaF-KF (FLiNaK), $KF-ZrF_4$, and $KCl-MgCl_2$. The potential power conversion cycles identified are supercritical Rankine steam cycle, supercritical CO_2 cycle, subcritical Rankine steam cycle, and a helium Brayton cycle. The results of the analysis of the different cycles showed the following:

- The supercritical Rankine steam cycle has the highest power cycle efficiency (44.0%) and is also a current commercial technology. The cycle has the disadvantage of having the highest turbine inlet pressure (24.99 MPa).

- The supercritical CO_2 cycle has a power cycle efficiency (43.7 to 43.9%) that is nearly the same as the supercritical Rankine steam cycle. It also has a maximum pipe diameter that is less than the other power cycles. The cycle also has the advantage of very few components. The disadvantage of the cycle is the high turbine inlet pressure (21.66 MPa). This cycle is in small-scale testing and not available commercially.

- The subcritical Rankine steam cycle is currently used in commercial power plants. The power cycle efficiency of 41.9 to 42.0% is reasonable.

- The helium Brayton cycle has the advantage of adjustable pressures to reduce the pressure difference across the IHX. Brayton cycles have been developed for future gas reactors, however commercial cycles are not available.

- Using FLiNaK as the intermediate coolant results in the smallest heat exchanger size; however, the difference is not large enough to justify its selection based on that feature.

- The binary salts $KF-ZrF_4$ and $KCl-MgCl_2$ provide identical results with respect to the IHX design.

The potential options explored for use as an SHX are shell and tube, plate, plate and fin, printed circuit, helical coil, and ceramic. A shell and tube (helical coiled) heat exchanger is a recommended for a demonstration reactor because of its reliability while the reactor design is tested. For future AHTR commercial demonstrations, other heat exchangers should be evaluated to improve the commercial viability of the reactor type.

Potential industrial applications were evaluated considering a maximum available temperature of 650°C for use by the process heat applications. This assumes the reactor outlet temperature is approximately 700°C and conservatively requires 50°C differential temperature to transfer the reactor's heat through the primary and intermediate loops. The current AHTR design could provide process heat for the following applications in the near term:

- Power production cycles (steam Rankine cycles, helium Brayton cycle, SCO_2 cycle)

- Oil shale (in situ)

- Oil shale (ex situ)

- Oil sands.

The basic setup for the selection of the SHX has been established with evaluation goals, alternatives, and criteria. Feasibility studies will be conducted to provide sufficient information for the evaluation and decision making process. Development of the integration methodology is an ongoing task.

8.   REFERENCES

Anderson, M., et al., 2010, "University of Wisconsin-Madison Molten Salt Program- Experiments and Lessons Learned," March 2010.

Baade, William F., Uday N. Parekh, and Venkat S. Raman (Air Products and Chemicals, Inc.), 2001, "Hydrogen," *Kirk-Othmer Encyclopedia of Chemical Technology*, John Wiley & Sons.

Bejan, A., Tsatsaronis, G., Moran, M., Thermal Design and Optimization, John Wiley & Sons, 1996.

Bhushan, Navneet, and Kanwal Rai, 2004, *Strategic Decision Making: Applying the Analytic Hierarchy Process*, London: Springer-Verlag. ISBN 1-8523375-6-7.

Bonilla, C. F., 1958, "Comparisons of Coolants," Section 9-3, Chapter 6.5, *Nuclear Engineering Handbook*, Ed. H. Etherington, McGraw-Hill, NY.

Dewson, S. J., and B. Thonon, 2003, "The Development of High Efficiency Heat Exchangers for Helium Gas Cooled Reactors," Report No. 3213, *International Conference on Advanced Nuclear Power Plants (ICAP)*, Cordoba, Spain.

Dostal, V., M. J. Driscoll, and P. Heizlar, 2004, A *Supercritical Carbon Dioxide Cycle for Next Generation Nuclear Plants, MIT-ANP-TR-100200.* Boston: Massachusetts Institute of Technology.

Elshout, Ray, 2010, "Hydrogen Production By Steam Reforming," *Chemical Engineering*, May 2010, pp. 34–38.

Fisher, D. L., and R. L. Sindelar, 2008, "Compact Heat Exchanger Manufacturing Technology Evaluation," *Savannah River Nuclear Solutions,* SRNS-STI-2008-00014, Savannah River Site, Aiken, South Carolina.

Forman, Ernest H., Saul I. Gass, 2001-07, "The analytical hierarchy process—an exposition," *Operations Research*, Vol. 49, Issue 4, pp. 469–487.

Grimes, W. R., E. G. Bohlmann, A. S. Meyer, and J. M. Dale, 1972, "Fuel can Coolant Chemistry," Chapter 5 in M. W. Rosenthal, P. N. Haubenreich, and R. B. Briggs, *The Development Status of Molten-Salt Breeder Reactors*, Oak Ridge National Laboratory Report ORNL-4812.

Hallowell, David L., 2005, "Analytical Hierarchy Process (AHP) – Getting Oriented," *SixSigma.com.* Retrieved 2007-08-21.

Hesselgreaves, J. E., 2001, *Compact Heat Exchangers, Selection, Design and Operation*, First edition, Pergamon.

Holcomb, D. E., S. M. Cetiner, G. F. Flanagan, F. J. Pertz, and G. L. Yoder, 2009, *An Analysis of Testing Requirements for Fluoride Salt-Cooled High Temperature Reactor Components*, *ORNL/TM-2009/297*, November 2009.

Ingersoll, D. T et al., 2004, *Status of Preconceptual Design of the Advanced High Temperature Reactor (AHTR)*, Oak Ridge National Laboratory Report ORNL/TM-2004/104.

Ingersoll, D. T., C. W. Forsberg, and P. E. MacDonald, 2007, *Trade Studies on the Liquid-Salt-Cooled Very High-Temperature Reactor: Fiscal Year 2006 Progress Report*, Oak Ridge National Laboratory Report ORNL/TM-2006/140.

Kitto, J. B., and S. C. Stultz, 2005, "Thermodynamics of Steam," *Steam: Its Generation and Use, Edition 41* (p. 16). Barberton, Ohio, The Babcock and Wilcox Company.

Latzko, D. G. H., 1970, "Sodium-Cooled Fast Reactor Engineering," Proceeding of a Symposium on Progress in Sodium-Cooled Fast Reactor Engineering held by the IAEA in Monaco, IAEA-SM—130/20.

LeBlanc, D., 2010a, "Molten Salt Reactors: A New Beginning for an Old Idea," *Nuclear Engineering and Design*, Vol. 240, pp. 1644–1656.

LeBlanc, D., 2010b, "Too Good to Leave on the Shelf," available at http://memagazine.asme.org/Articles/2010/May/Too_Good_Leave_Shelf.cfm Accessed on Aug 27th 2010.

O. Benes, C. Cabet, S. Delpech, P. Hosnedl, V. Ignatiev, R. Konings, D. Lecarpentier, O. Matal, E. Merle-Lucotte, C. Renault, J. Uhlir (2009) "Assessment of Liquid Salts for Innovative Applications," available at ftp://ftp.cordis.europa.eu/pub/fp6-euratom/docs/alisia-deliverable-d50-v4_en.pdf, accessed on September 7th 2010

Renault, C., M. Hron, R. Konings, and D. E. Holcomb. 2009, "The Molten Salt Reactor (MSR) in Generation IV: Overview and Perspectives," *GIF Symposium-Paris (France), September 9 and 10, 2009*.

Saaty, T. L., 1996, *The Analytic Hierarchy Process*, New York, N.Y., McGraw Hill, 1980, reprinted by RWS Publication, Pittsburgh.

Sabharwall, P., M. Ebner, M. Sohal, P. Sharpe, M. Anderson, K. Sridharan, J. Ambrosek, L. Olson, and P. Brooks, 2010a, *Molten Salts for High Temperature Reactors: University of Wisconsin Molten Salt Corrosion and Flow Loop Experiments – Issues Identified and Path Forward*, Idaho National Laboratory report INL/EXT-10-18090.

Sabharwall, P., M. Patterson, V. Utgikar, and F. Gunnerson, 2010b, "Phase change heat transfer device for process heat applications," *Nuclear Engineering and Design*, In Press.

Sabharwall, P., 2009, *Engineering Design Elements of a Two-Phase Thermosyphon to Transfer NGNP Thermal Energy to a Hydrogen Plant*," Idaho National Laboratory report INL/EXT-09-15383.

Sabharwall, P., and F. Gunnerson, 2009, "Engineering Design Elements of a Two-Phase Thermosyphon to Transfer NGNP Thermal Energy to a Hydrogen Plant," *Nuclear Engineering and Design*, Vol. 239, Issue 11, pp. 2293–2301.

Sabharwall, P., and E. S. Kim, 2011, "Fluoride High Temperature Reactor Integration with Industrial Process Applications," *Idaho National Laboratory,* TEV-1160

Sanders, J. P., *A review of possible choices for secondary coolants for molten salt reactors*, ORNL CF-71-8-10, Oak Ridge National Laboratory, Oak Ridge, TN, 1971.

Saltelli, A. et al., Global Sensitivity Analysis, John Wiley & Sons, ISBN 978-0-470-05997-5, 2008.

Shah, R. K., and S. P. Sekulic, 2003, *Fundamentals of Heat Exchanger Design*, John Wiley and Sons, 2003.

Shah, R. K., 2003, *Fundamentals of Heat Exchanger Design*, John Wiley and Sons.

Sherman, S. R., and Y. Chen, 2008, *Heat Exchanger Testing Requirements and Facility Needs for the NHI/NGNP Project*, WSRC-STI-2008-00152, April 2008.

Snead, L. L., T. Nozawa, Y. Katoh, T. S. Byun, S. Kondo, and D. A. Petti, 2007, "Handbook of SiC Properties for Fuel Performance Modeling," *Journal of Nuclear Materials,* Vol. 371, pp. 329–377.

Sohal, M., M. Ebner, P. Sabharwall, and P. Sharpe, March 2010, *Engineering Database of Liquid Salt Thermophysical and Thermochemical Properties*, Idaho National Laboratory report INL/EXT-10-18297.

Sohal, M. S., M. Ebner, P. Sabharwall, and P. Sharpe, 2010, *Engineering Database of Liquid Salt Thermophysical and Thermochemical Properties*, Idaho National Laboratory report INL/EXT-10-18297.

Taborek, J., G. F. Hewitt, and N. Afgan, 1983, *Heat Exchangers Theory and Practice*, Hemisphere Publishing Corporation.

Tatara, R., 1997, "Heat Exchangers: An Overview of Maintenance and Operations," *Duke Engineering and Services*, EPRI.

Van Wylen, G., and R. Sonntag, 1973, Chapter 9: "Some Power and Refrigeration Cycles." In G. Van Wylen, and R. Sonntag, *Fundamentals of Classical Thermodynamics* (pp. 302–322; 340–352). New York: John Wiley and Sons, Inc.

Vinegar, H., 2006, "Shell's In-situ Conversion Process," *26th Oil Shale Symposium, Golden, Colorado, October 16–18, 2006.*

Welty, J.R., Wicks, C.E., Wilson, R.E., Fundamentals of Momentum, Heat, and Mass Transfer, John Wiley & Sons, 1984.

Williams, D. F., 2006, "Assessment of Candidate Molten Salt Coolants for the NGNP/NHI Heat-Transfer Loop," Oak Ridge National Laboratory Report ORNL/TM-2006/69.

Williams, D. F., L. M. Toch, and K. T. Clarno, *Assessment of Candidates Molten Salt Coolants for the Advanced High Temperature Reactor*, ORNL/TM-2006/12, 2006a.

Appendix A

Development of Figures of Merit for Coolant Thermal-Hydraulic Performance

Appendix A—Development of Figures of Merit for Coolant Thermal-Hydraulic Performance

A-1. INTRODUCTION

If the properties of one coolant are all superior to those of another coolant, the selection of the coolant becomes straight forward. However, each coolant generally has both superior and inferior properties. It is therefore useful to compare some key parameters that determine coolant thermal performance in the system of interest. This section discusses only coolant thermal-hydraulic characteristics; the other characteristics are discussed in later sections.

Figures of merits (FOMs) were used in evaluating the thermal performance of the coolants. Bonilla (1958) provided the FOMs based on minimal pumping power for a given coolant temperature rise as

$$FOM = \mu^{0.2} / \left(\rho^2 C_P^{2.8} \right),$$ (A-1)

where

μ = viscosity (Pa-s),

ρ = density (kg/m^3),

C_p = heat capacity (J/kg K).

Sanders (1971) proposed the following FOM based on the heat exchanger surface area:

$$FOM = \mu^{0.2} / \left(\rho^{0.3} C_p^{0.6} k^{0.6} \right).$$ (A-2)

Williams (2006) used the above FOMs for comparing heat transfer performance of the molten salt coolants for a Next Generation Nuclear Plant/Nuclear Hydrogen Initiative heat transfer loop.

The above two parameters are very useful for comparing overall coolant heat transfer performance at the early stages of research. However, they are still not complete for evaluating all the important thermal performance parameters in the system of interest. Figure A-1 shows the general thermal-hydraulic requirements for the intermediate coolant in an AHTR system.
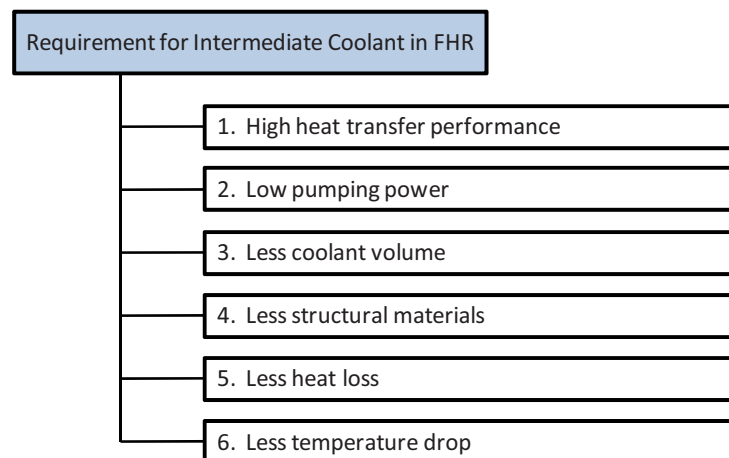
Figure A-1. General thermal-hydraulic requirements for the intermediate coolant in AHTR systems.

The following are general thermal-hydraulic requirements for the coolant in an AHTR:

- *High heat transfer performance*: Coolant should transfer heat efficiently. Good heat transfer performance leads to efficient heat transfer between the primary and the intermediate loops.

- *Low pumping power*: Coolant should require low pumping power to minimize efficiency loss and economic loss.

- *Less coolant volume*: Small volume of coolant is preferred for economic reasons.

- *Less structural materials for containing coolant*: Small amount of structural materials for the coolant containment is preferred for economic reasons.

- *Less heat loss*: Heat loss of the coolant should be minimized when transferring heat long distances for a more efficient system.

- *Less temperature drop*: The coolant temperature drop should be minimized when transferring heat to long distances for a more efficient system.

The above requirements are associated with the thermal-hydraulic properties including thermal conductivity, density, heat capacity, and viscosity. This study developed five different FOMs that can represent each requirement.

Figure A-2 shows the basic configuration of the general intermediate heat transfer loop. Heat (Q) is transferred to the coolant system through heat exchangers, increasing coolant temperature. This coolant is driven by pumps or circulators to transport the heat to several areas for use in electricity generation, chemical processes, etc. Therefore, the operating temperature and pressure of this system are generally determined and optimized by how the energy is used. However, detailed heat transfer performance, system size, and major component specifications are significantly affected by types of coolants.
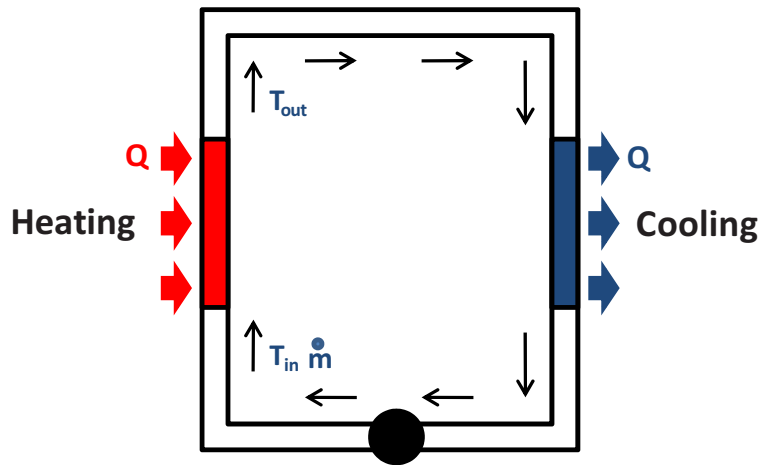
Figure A-2. General configuration of intermediate heat transfer loop.

A-2. HEAT TRANSFER PERFORMANCE FACTOR: FOM FOR HEAT TRANSFER PERFORMANCE (FOM$_{HT}$)

The major role of any coolant is heat transfer. Therefore, heat transfer performance is one of the most important factors to consider in coolant options. Heat transfer performance of the coolants can be compared by calculating the heat transfer at the same pumping power for the given geometry. If a certain coolant has the highest heat transfer coefficient, the coolant can be considered as having the best heat transfer performance.

51

The FOM for the heat transfer performance can be derived as Equation A-3. Figure A-3 shows a circular pipe with diameter, D and length, L. In this derivation, the pumping power was assumed to be the same for the different fluids. The pumping power is expressed as

$$P_{pump} = \frac{\Delta P \cdot G}{\eta} \tag{A-3}$$

where

P_{pump} = pumping power (W)

ΔP = pressure drop (Pa)

G = volumetric flow rate

η = pump efficiency.
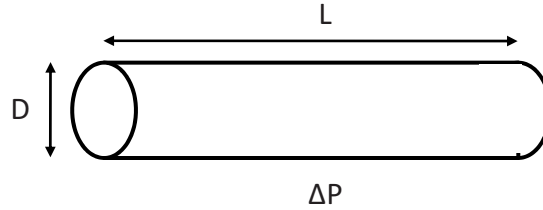
Figure A-3. Geometry and input parameters for FOM development (heat transfer performance).

The cooling system is generally operated in the turbulent flow regime. Therefore, ignoring change of elevation, the pressure drop is expressed by (Welty et al. 1984):

$$\Delta P = f \cdot \frac{1}{2} \rho \cdot U^2 \cdot \frac{L}{D} \tag{A-4}$$

where

f = friction factor (constant for the high Reynolds number)

ρ = density

L = channel length

D = channel diameter

U = flow velocity.

The friction factor (f) can be calculated by the Blasius formula for a smooth pipe as (Welty et al. 1984)

$$f = 0.316 \cdot \mathrm{Re}^{-0.25} \tag{A-5}$$

where

$$\mathrm{Re} = \frac{\rho \cdot U \cdot D}{\mu}. \tag{A-6}$$

The volumetric flow rate can be expressed by

$$\overline{Q} = U \cdot A = U \cdot \left(\frac{\pi}{4} D^2 \right)$$ (A-7)

where

A = channel cross-sectional area.

By inserting Eqs. (A-4), (A-5), (A-6), and (A-7) in Eq. (A-3), the following expression can be obtained:

$$P_{pump} = \frac{\left(f \cdot \frac{1}{2} \rho \cdot U^2 \cdot \frac{L}{D} \right) \cdot U \cdot \left(\frac{\pi}{4} D^2 \right)}{\eta} = \frac{\left(0.316 \cdot \left(\frac{\rho \cdot U \cdot D}{\mu} \right)^{-0.25} \cdot \frac{\pi}{8} \rho \cdot U^3 \cdot L \cdot D \right)}{\eta}$$

$$= \frac{\left(\frac{0.316 \cdot \pi}{8} \rho^{0.75} \cdot U^{2.75} \cdot L \cdot D^{0.75} \cdot \mu^{0.25} \right)}{\eta}.$$ (A-8)

Therefore, the flow velocity can be derived by

$$U = \left(\frac{\eta \cdot P_{pump}}{\left(\frac{0.316 \cdot \pi}{8} L \cdot D^{0.75} \right)} \right)^{0.36} \cdot (\rho)^{-0.27} \cdot (\mu)^{-0.09} = C_1 \cdot (\rho)^{-0.27} \cdot (\mu)^{-0.09}.$$ (A-9)

For the given conditions, the variable C_1 can be considered as constant. Therefore, the flow velocity is determined by only coolant density and viscosity.

General convective heat transfer is expressed as (Welty et al., 1984)

$$Q = h \cdot S \cdot \Delta T$$ (A-10)

where

Q = heat

h = convective heat transfer coefficient

S = heat transfer surface area

ΔT = temperature differences between bulk fluid and wall.

In the given condition, surface area (S) and temperature difference (ΔT) are fixed. Therefore, the heat transfer is proportional to the heat transfer coefficient (h). The heat transfer coefficient for the turbulent flow is generally expressed by the Dittus-Boelter correlation (Welty et al., 1984)

$$h = \frac{k}{D} \cdot Nu = \frac{k}{D} \cdot \left(0.023 \, Re^{0.8} \, Pr^{0.4} \right)$$ (A-11)

where

k = thermal conductivity

Nu = Nusselt number

Re = Reynolds number

Pr = Prandtl number.

The Prandtl number (Pr) is defined as

$$Pr = \frac{C_p \cdot \mu}{k} .$$

(A-12)

By inserting Eqs. (A-6) and (A-12) in Eq. (A-11), the heat transfer coefficient (h) can be written as

$$h = \frac{k}{D} \cdot \left(0.023 \left(\frac{\rho \cdot U \cdot D}{\mu} \right)^{0.8} \left(\frac{C_p \cdot \mu}{k} \right)^{0.4} \right).$$

(A-13)

The velocity in Eq. (A-13) can be replaced by Eq. (A-9) as

$$h = \frac{k}{D} \cdot \left(0.023 \left(\frac{\rho \cdot D}{\mu} \right)^{0.8} \cdot \left(C_1 \cdot (\rho)^{-0.27} \cdot (\mu)^{-0.09} \right)^{0.8} \cdot \left(\frac{C_p \cdot \mu}{k} \right)^{0.4} \right)$$

(A-14)

therefore,

$$h = \left(\frac{0.023 \cdot (C_1)^{0.8}}{D^{0.2}} \right) \cdot (k)^{0.6} \cdot (\rho)^{0.58} \cdot (C_p)^{0.4} \cdot (\mu)^{-0.47} .$$

(A-15)

In this derivation, C_1 is a constant and channel diameter (D) is a fixed parameter. Therefore,

$$h \sim (k)^{0.6} \cdot (\rho)^{0.58} \cdot (C_p)^{0.4} \cdot (\mu)^{-0.47} .$$

(A-16)

The FOM for the heat transfer performance is defined by normalization as

$$FOM_{ht} = \frac{h}{h_0}$$

(A-17)

where

h = heat transfer coefficient for a certain coolant

h_0 = heat transfer coefficient for a reference coolant.

Therefore,

$$FOM_{ht} = \frac{(k)^{0.6} \cdot (\rho)^{0.58} \cdot (C_p)^{0.4} \cdot (\mu)^{-0.47}}{R_{ht,0}}$$

(A-18)

and

$$R_{ht,0} = (k_0)^{0.6} \cdot (\rho_0)^{0.58} \cdot (C_{p,0})^{0.4} \cdot (\mu_0)^{-0.47} . \tag{A-19}$$

According to Eq. (A-16), the coolant shows better heat transfer performance if it has higher thermal conductivity, density, and heat capacity and lower viscosity. The sensitivity of each property for the heat transfer performance factor (FOM_{ht}) can be calculated by normalized form as follows:

$$S_{k,ht} = \frac{\partial FOM_{ht} / FOM_{ht}}{\partial k / k} = 0.6 \tag{A-20}$$

$$S_{\rho,ht} = \frac{\partial FOM_{ht} / FOM_{ht}}{\partial \rho / \rho} = 0.58 \tag{A-21}$$

$$S_{C_p,ht} = \frac{\partial FOM_{ht} / FOM_{ht}}{\partial C_p / C_p} = 0.4 \tag{A-22}$$

$$S_{\mu,ht} = \frac{\partial FOM_{ht} / FOM_{ht}}{\partial \mu / \mu} = -0.47 . \tag{A-23}$$

The above results show that thermal conductivity is the most sensitive property affecting heat transfer performance, followed by coolant density, viscosity, and heat capacity, respectively.

A-3. PUMPING FACTOR: FOM FOR PUMPING POWER (FOM_P)

To operate a heat transfer loop, less pumping power is highly preferred for the coolant. This study proposes the same figure of merit provided by Bonilla (1958), in the normalized form, which is based on minimal pumping power for a given coolant temperature rise as

$$FOM_p = \frac{\mu^{0.2} / (\rho^2 \cdot C_P^{2.8})}{R_{p,0}} \tag{A-24}$$

where:

$$R_{p,0} = \mu_0^{0.2} / (\rho_0^2 \cdot C_{P,0}^{2.8}) \text{ (for the reference coolant)}. \tag{A-25}$$

According to Eq. (A-25), the coolant needs less pumping power if it has higher density, higher heat capacity, and lower viscosity. The sensitivity of each property for the required pumping power factor (FOM_p) can be calculated by normalized form as follows:

$$S_{k,p} = \frac{\partial FOM_p / FOM_p}{\partial k / k} = 0.0 \tag{A-26}$$

$$S_{\rho,0} = \frac{\partial FOM_p / FOM_p}{\partial \rho / \rho} = -2 \tag{A-27}$$

$$S_{C_p,p} = \frac{\partial FOM_p / FOM_p}{\partial C_p / C_p} = -2.8 \tag{A-28}$$

$$S_{\mu,p} = \frac{\partial FOM_p / FOM_p}{\partial \mu / \mu} = 0.2 .$$

(A-29)

The above results show that heat capacity is the most important property affecting required pumping power, followed by coolant density and viscosity, respectively. Relatively, the viscosity effect is small because the friction loss in the coolant is dominated by turbulent mixing not by viscous friction. Thermal conductivity does not affect the required pumping power.

A-4. COOLANT VOLUME FACTOR: FOM FOR COOLANT VOLUME (FOM$_{CV}$)

Since each coolant has different thermal properties, the volumes required for the coolant loops are also different, depending on the coolant types. Smaller coolant volume is usually preferred for economic reasons. The volume of the coolant is generally determined based on the given heat transfer duty and the pumping power (or friction loss). Therefore, the volumes of the coolants in the heat transfer loop can be compared by calculating the channel diameter for the same heat duty, pumping power, and pipe length.

Heat transfer in the heat transfer loop is expressed by (Welty et al. 1984)

$$Q = \dot{m} \cdot C_p \cdot \Delta T = \left(\frac{\pi}{4} D^2 \cdot \rho \cdot U \right) \cdot C_p \cdot \Delta T .$$

(A-30)

Therefore, the velocity (U) can be expressed by

$$U = \frac{Q}{\left(\frac{\pi}{4} D^2 \cdot \Delta T \right) \cdot C_p \cdot \rho} = \left(\frac{Q}{\left(\frac{\pi}{4} D^2 \cdot \Delta T \right)} \right) \cdot C_p^{-1} \cdot \rho^{-1} .$$

(A-31)

The pumping power is expressed as

$$P_{pump} = \frac{\left(f \cdot \frac{1}{2} \rho \cdot U^2 \cdot \frac{L}{D} \right) \cdot U \cdot \left(\frac{\pi}{4} D^2 \right)}{\eta} = \frac{\left(\frac{0.316 \cdot \pi}{8} \rho^{0.75} \cdot L \cdot D^{0.75} \cdot \mu^{0.25} \right)}{\eta} \cdot U^{2.75}$$

(A-32)

Therefore,

$$P_{pump} = \frac{\left(\frac{0.316 \cdot \pi}{8} \rho^{0.75} \cdot L \cdot D^{0.75} \cdot \mu^{0.25} \right)}{\eta} \cdot \left(\left(\frac{Q}{\left(\frac{\pi}{4} D^2 \cdot \Delta T \right)} \right) \cdot C_p^{-1} \cdot \rho^{-1} \right)^{2.75}$$

$$= \frac{Q^{2.75} \cdot \left(\frac{0.316 \cdot \pi}{8} L \right)}{\eta \cdot \left(\frac{\pi}{4} \Delta T \right)^{2.75}} \cdot (\rho)^{-2} \cdot (C_p)^{-2.75} \cdot (D)^{-4.75} \cdot (\mu)^{0.25} .$$

(A-33)

56

Therefore, the channel diameter (D) can be calculated as

$$D = \left(\frac{Q^{2.75} \cdot \left(\frac{0.316 \cdot \pi}{8} L \right)}{P_{pump} \cdot \eta \cdot \left(\frac{\pi}{4} \Delta T \right)^{2.75}} \right)^{0.21} \cdot (\rho)^{-0.42} \cdot (C_p)^{-0.58} \cdot (\mu)^{0.05} . \tag{A-34}$$

Thus, the volume of the coolant is

$$V = \frac{\pi}{4} D^2 L = \frac{\pi}{4} L \cdot \left(\frac{Q^{2.75} \cdot \left(\frac{0.316 \cdot \pi}{8} L \right)}{P_{pump} \cdot \eta \cdot \left(\frac{\pi}{4} \Delta T \right)^{2.75}} \right)^{0.42} \cdot (\rho)^{-0.84} \cdot (C_p)^{-1.16} \cdot (\mu)^{0.1} . \tag{A-35}$$

The FOM for the coolant volume is here defined by normalization as

$$FOM_{cv} = \frac{V}{V_0} \tag{A-36}$$

where:

V = volume required for a certain coolant

V_0 = volume required for a reference coolant.

Therefore,

$$FOM_{cv} = \frac{(\rho)^{-0.84} \cdot (C_p)^{-1.16} \cdot (\mu)^{0.1}}{R_{cv,0}} \tag{A-37}$$

where

$$R_{cv,0} = (\rho_0)^{-0.84} \cdot (C_{p,0})^{-1.16} \cdot (\mu_0)^{0.1} . \tag{A-38}$$

According to Eq. (A-37), the coolant needs higher density and higher heat capacity to have smaller volume. This is because more heat can be stored and transferred per unit volume with a higher density and heat capacity. The sensitivity of each property for the required coolant volume factor (FOM_{cv}) can be calculated by normalized form as follows:

$$S_{k,cv} = \frac{\partial FOM_{cv} / FOM_{cv}}{\partial k / k} = 0.0 \tag{A-39}$$

$$S_{\rho,cv} = \frac{\partial FOM_{cv} / FOM_{cv}}{\partial \rho / \rho} = -0.84 \tag{A-40}$$

$$S_{C_p,cv} = \frac{\partial FOM_{cv} / FOM_{cv}}{\partial C_p / C_p} = -1.16 \tag{A-41}$$

57

$$S_{\mu,cv} = \frac{\partial FOM_{cv} / FOM_{cv}}{\partial \mu / \mu} = 0.1 .$$

<div align="right">(A-42)</div>

The above results show that heat capacity is the most important property affecting required coolant volume, followed by coolant density and viscosity, respectively.

A-5. PIPE MATERIAL VOLUME FACTOR: FOM FOR COOLANT CONTAINMENT VOLUME (FOM$_{CCV}$)

Depending on flow conditions (temperature and pressure), the heat transfer structure requires different pipe sizes and thickness. A larger pipe size and thickness requires more volume of structural materials leading to increased cost. In comparing required pipe material volumes for the coolant and the operating conditions, pipe size and thickness were calculated for the same heat duty and pumping power.

Pipe diameter was already estimated in Eq. (A-34) for the given heat duty and pumping power as

$$D = \left(\frac{Q^{2.75} \cdot \left(\frac{0.316 \cdot \pi}{8} L \right)}{P_{pump} \cdot \eta \cdot \left(\frac{\pi}{4} \Delta T \right)^{2.75}} \right)^{0.21} \cdot (\rho)^{-0.42} \cdot (C_p)^{-0.58} \cdot (\mu)^{0.05} .$$

<div align="right">(A-43)</div>

In the heat transfer loop, the pipe thickness is determined based on the mechanical stress. Mechanical stresses in the thin-walled cylindrical shaped pipe (the vessel must have a wall thickness of no more than about 1/20 (Bejan et al. 1996)) are estimated as follows:

$$\sigma_\theta = \frac{P \cdot r}{t} \text{ (hoop stress)}$$

<div align="right">(A-44)</div>

$$\sigma_z = \frac{P \cdot D^2}{(D+2t)^2 - D^2} \text{ (axial stress)}$$

<div align="right">(A-45)</div>

$$\sigma_r = -\frac{P}{2} \text{ (radial stress)}$$

<div align="right">(A-46)</div>

where:

P = internal pressure

r = pipe radius

D = average pipe diameter

t = pipe thickness.

Generally, under only internal pressure, the values of axial stress and radial stress are less than hoop stress. Thus, hoop stress becomes the limiting factor for determining pipe thickness. For the same material that has the same stress criteria, the thickness of the pipe can be calculated by Eq. (A-44) as

$$t = \frac{P \cdot D}{2 \cdot \sigma_\theta} = \left(\frac{1}{2 \cdot \sigma_\theta} \cdot \left(\frac{Q^{2.75} \cdot \left(\frac{0.316 \cdot \pi}{8} L \right)}{P_{pump} \cdot \eta \cdot \left(\frac{\pi}{4} \Delta T \right)^{2.75}} \right) \right)^{0.21} \cdot (P) \cdot (\rho)^{-0.42} \cdot (C_p)^{-0.58} \cdot (\mu)^{0.05} .$$

(A-47)

The volume of the pipe materials per unit length can be estimated for the thin walled pipe as

$$V_p = \pi \cdot D \cdot t \cdot 1 = \pi \cdot \left(\frac{P}{2 \cdot \sigma_\theta} \right) \cdot D^2 .$$

(A-48)

Therefore,

$$V_p = \left(\pi \cdot \left(\frac{1}{2 \cdot \sigma_\theta} \right) \cdot \left(\frac{Q^{2.75} \cdot \left(\frac{0.316 \cdot \pi}{8} L \right)}{P_{pump} \cdot \eta \cdot \left(\frac{\pi}{4} \Delta T \right)^{2.75}} \right) \right)^{0.42} \cdot (P) \cdot (\rho)^{-0.84} \cdot (c_p)^{-1.16} \cdot (\mu)^{0.1}$$

(A-49)

The FOM for the coolant volume is here defined by normalization as

$$FOM_{ccv} = \frac{V_p}{V_{p,0}}$$

(A-50)

where:

V_p = volume required for a pipe materials

$V_{p,0}$ = volume required for the reference pipe materials.

Therefore,

$$FOM_{ccv} = \frac{(P) \cdot (\rho)^{-0.84} \cdot (C_p)^{-1.16} \cdot (\mu)^{0.1}}{R_{ccv,0}}$$

(A-51)

where

$$R_{ccv,0} = (P_o) \cdot (\rho_0)^{-0.84} \cdot (C_{p,0})^{-1.16} \cdot (\mu_0)^{0.1} .$$

(A-52)

According to Eq. (A-51), the coolant needs higher density, higher heat capacity, and lower operating pressure to have smaller material volume. The sensitivity of each property for the required material volume factor (FOM_{ccv}) can be calculated by

$$S_{k,ccv} = \frac{\partial FOM_{ccv} / FOM_{ccv}}{\partial k / k} = 0.0$$

(A-53)

$$S_{\rho,ccv} = \frac{\partial FOM_{ccv} / FOM_{ccv}}{\partial \rho / \rho} = -0.84$$

(A-54)

$$S_{C_p.ccv} = \frac{\partial FOM_{ccv} / FOM_{ccv}}{\partial C_p / C_p} = -1.16 \qquad \text{(A-55)}$$

$$S_{\mu,ccv} = \frac{\partial FOM_{ccv} / FOM_{ccv}}{\partial \mu / \mu} = 0.1 \qquad \text{(A-56)}$$

$$S_{P,ccv} = \frac{\partial FOM_{ccv} / FOM_{ccv}}{\partial P / P} = 1.0 . \qquad \text{(A-57)}$$

The above results show that heat capacity is the most important property affecting required material volume, followed by coolant pressure and density, respectively. Effects of viscosity and thermal conductivity are negligible.

A-6. HEAT LOSS FACTOR: FOM FOR HEAT LOSS (FOM$_{HL}$)

There are times when a heat transfer loop is required to transfer heat over very long distances. Heat loss should thus be minimized to keep high system efficiency. The heat loss for different coolants can be compared for the same heat duty and pumping power as shown in the above sections. The overall heat transfer in the heat transfer loop can be expressed by (Welty et al. 1984)

$$Q = \dot{m} \cdot C_p \cdot \Delta T = \left(\rho \cdot U \cdot \frac{\pi}{4} D^2 \right) \cdot C_p \cdot \Delta T . \qquad \text{(A-58)}$$

Therefore, the velocity of the coolant can be expressed by

$$U = \frac{Q}{\left(\frac{\pi}{4} \cdot D^2 \cdot \Delta T \right) \cdot \rho \cdot C_p} . \qquad \text{(A-59)}$$

The heat loss at a certain location can be defined by

$$dQ = h \cdot (\pi \cdot D \cdot dx) \cdot (T - T_w) . \qquad \text{(A-60)}$$

Where:

   dQ =   heat loss at the surface

   T =   coolant temperature

   T_w =   pipe inner wall temperature.

Therefore,

$$q_{loss} = \frac{dQ}{dx} = h \cdot (\pi \cdot D) \cdot (T - T_w) . \qquad \text{(A-61)}$$

By substituting Eq. (A-13) in Eq. (A-61),

$$q_{loss} = \frac{k}{D} \cdot \left(0.023 \left(\frac{\rho \cdot U \cdot D}{\mu} \right)^{0.8} \left(\frac{C_p \cdot \mu}{k} \right)^{0.4} \right) \cdot (\pi \cdot D) \cdot (T - T_w)$$

$$= \left(0.023\pi \cdot (T - T_w)\right) \cdot k^{0.6} \cdot C_p^{\ 0.4} \cdot \rho^{0.8} \cdot \mu^{-0.4} \cdot U^{0.8} \cdot D^{0.8}. \tag{A-62}$$

Inserting Eq. (A-59) into Eq. (A-62) obtains

$$q_{loss} = \left(0.023\pi \cdot (T - T_w)\right) \cdot k^{0.6} \cdot C_p^{\ 0.4} \cdot \rho^{0.8} \cdot \mu^{-0.4} \cdot \left(\frac{Q}{\left(\frac{\pi}{4} \cdot D^2 \cdot \Delta T\right) \cdot \rho \cdot C_p}\right)^{0.8} \cdot D^{0.8}$$

$$= \left((0.023\pi \cdot (T - T_w)) \cdot \left(\frac{Q}{\left(\frac{\pi}{4} \cdot \Delta T\right)}\right)^{0.8}\right) \cdot k^{0.6} \cdot C_p^{\ -0.4} \cdot \mu^{-0.4} \cdot D^{-0.8}. \tag{A-63}$$

For the same heat duty and pumping power, Eq. (A-43) can be replaced with D in Eq. (A-63) as

$$q_{loss} = \left((0.023\pi \cdot (T - T_w)) \cdot \left(\frac{Q}{\left(\frac{\pi}{4} \cdot \Delta T\right)}\right)^{0.8} \cdot \left(\frac{Q^{2.75} \cdot \left(\frac{0.316 \cdot \pi}{8} L\right)}{P_{pump} \cdot \eta \cdot \left(\frac{\pi}{4} \Delta T\right)^{2.75}}\right)^{-0.17}\right) \cdot (k)^{0.6} \cdot (\mu)^{-0.44} \cdot (\rho)^{0.34} \cdot (C_p)^{0.06}$$

$$= C_2 \cdot (k)^{0.6} \cdot (\mu)^{-0.44} \cdot (\rho)^{0.34} \cdot (C_p)^{0.06}. \tag{A-64}$$

The FOM for the heat loss is here defined by normalization as

$$FOM_{hl} = \frac{q_{loss}}{q_{loss,0}} \tag{A-65}$$

where:

q_{loss} =   heat loss for a certain coolant,

$q_{loss,0}$ =   heat loss for a reference coolant.

Therefore,

$$FOM_{hl} = \frac{(k)^{0.6} \cdot (\mu)^{-0.44} \cdot (\rho)^{0.34} \cdot (C_p)^{0.06}}{R_{hl,0}} \tag{A-66}$$

where

$$R_{hl,0} = (k_0)^{0.6} \cdot (\mu_0)^{-0.44} \cdot (\rho_0)^{0.34} \cdot (C_{p,0})^{0.06}. \tag{A-67}$$

According to Eq. (A-66), the coolant heat loss increases with thermal conductivity and decreases with heat capacity, density, and viscosity. The sensitivity of each property for the heat loss factor (FOM_{hl}) can be calculated in normalized form as

$$S_{k,hl} = \frac{\partial FOM_{hl} / FOM_{hl}}{\partial k / k} = 0.6 \tag{A-68}$$

$$S_{\rho,hl} = \frac{\partial FOM_{hl} / FOM_{hl}}{\partial \rho / \rho} = 0.34 \tag{A-69}$$

$$S_{C_p,hl} = \frac{\partial FOM_{hl} / FOM_{hl}}{\partial C_p / C_p} = 0.06 \tag{A-70}$$

$$S_{\mu,hl} = \frac{\partial FOM_{hl} / FOM_{hl}}{\partial \mu / \mu} = -0.44 \; . \tag{A-71}$$

The above results show that thermal conductivity is the most important property affecting heat loss of coolant followed by viscosity and coolant density, respectively. The effect of heat capacity is negligible.

A-7. TEMPERATURE DROP FACTOR: FOM FOR TEMPERATURE DROP (FOM$_{DT}$)

A heat transfer loop is required to transfer heat a very long distance with little temperature drop in order to minimize efficiency loss. The temperature drop of the coolants can be compared at the same heat duty and pumping power as shown in the above section. The temperature drop of the coolant originates from heat loss. Therefore, starting from Eq. (A-61) and rearranging as follows:

$$q_{loss} = \frac{dQ}{dx} = \dot{m} \cdot C_p \cdot \frac{dT}{dx} = h \cdot (\pi \cdot D) \cdot (T - T_w). \tag{A-72}$$

Therefore,

$$\frac{dT}{dx} = \frac{h \cdot (\pi \cdot D) \cdot (T - T_w)}{\dot{m} \cdot C_p} = \frac{h \cdot (\pi \cdot D) \cdot (T - T_w)}{Q / \Delta T}. \tag{A-73}$$

where,

$$\dot{m} \cdot C_p = \frac{Q}{\Delta T} \; . \tag{A-74}$$

For the same heat duty and operating conditions, Eq. (A-74) is fixed. Therefore, the temperature drop equation (Eq. (A-74)) has the same form as the heat loss equation (Eq. (A-61)) except it is constant.

The figure of merit (FOM) for the temperature drop is here defined by normalization as

$$FOM_{dt} = \frac{(dT / dx)}{(dT / dx)_0}. \tag{A-75}$$

where

    dT/dx = temperature drop per unit length for a certain coolant,

    $(dT/dT)_0$ = temperature drop per unit length for the reference coolant.

Therefore,

$$FOM_{dt} = \frac{(k)^{0.6} \cdot (\mu)^{-0.44} \cdot (\rho)^{0.34} \cdot (C_p)^{0.06}}{R_{dt,0}} \ . \tag{A-76}$$

where

$$R_{dt,0} = (k_0)^{0.6} \cdot (\mu_0)^{-0.44} \cdot (\rho_0)^{0.34} \cdot (C_{p,0})^{0.06} \ . \tag{A-77}$$

According to Eq. (A-77), the coolant temperature drop increases with thermal conductivity and decreases with heat capacity, density, and viscosity. The sensitivity of each property for the temperature drop factor (FOM_{dt}) can be calculated by normalized form as

$$S_{k,dt} = \frac{\partial FOM_{dt} / FOM_{dt}}{\partial k / k} = 0.6 \tag{A-78}$$

$$S_{\rho,dt} = \frac{\partial FOM_{dt} / FOM_{dt}}{\partial \rho / \rho} = 0.34 \tag{A-79}$$

$$S_{C_p,dt} = \frac{\partial FOM_{dt} / FOM_{dt}}{\partial C_p / C_p} = 0.06 \tag{A-80}$$

$$S_{\mu,dt} = \frac{\partial FOM_{dt} / FOM_{dt}}{\partial \mu / \mu} = -0.44 \ . \tag{A-81}$$

The above results show that thermal conductivity is the most important property affecting temperature drop, followed by viscosity and coolant density, respectively. The effect of heat capacity is negligible.

A-8. SUMMARY OF FOMS FOR HEAT TRANSFER COOLANT

Table A-1 summarizes all of the FOMs derived and proposed for the intermediate heat transfer coolants. This table lists six FOMs and sensitivities for various coolant properties. Based on the FOMs summarized, heat transfer performance, pumping power, coolant volume, pipe material volume, coolant heat loss, and coolant temperature drop can be compared easily and quantitatively for the same heat duty and pumping power requirements. Sensitivity with a plus sign (+) indicates that the FOM increases with the properties while one with a minus (-) sign indicates that the FOM decreases with the properties. The values of the sensitivities show how much the FOMs are affected by the properties. If the sensitivity is higher, the FOM is more significantly affected by that property. From this table, the effects of properties on the thermal-hydraulic performance of the coolants can be interpreted as follows:

- Increasing thermal conductivity can increase heat transfer performance by an order of 0.6, but it also increases the heat loss and temperature drop of the coolant at the same rate.

- Increasing coolant density can increase heat transfer performance and reduce coolant volume by orders of 0.58 and 0.84 respectively, but it also decreases pumping power by an order of 2.

- Increasing heat capacity can increase heat transfer performance and significantly reduce coolant/material volume by orders of 0.4 and 1.16, respectively, while increases of heat loss and temperature drop are negligible (order = 0.06). It also decreases pumping power by an order of 2.8.

- Increasing viscosity increases pumping power slightly (0.2) and significantly reduces heat transfer performance (0.47), but it also slightly increases coolant volume by 0.1.

Table A-1. Summary of FOMs for heat transfer coolant.

Figure of Merits	Sensitivity of Properties				
	S_k	S_ρ	S_{Cp}	S_μ	S_P
Heat transfer performance factor (FOM_{ht}): $$FOM_{ht} = \frac{(k)^{0.6} \cdot (\rho)^{0.58} \cdot (C_p)^{0.4} \cdot (\mu)^{-0.47}}{R_{ht,0}}$$	0.6	0.58	0.4	-0.47	0.0
Pumping factor (FOM_p): $$FOM_p = \frac{\rho^{-2} \cdot C_P^{-2.8} \cdot \mu^{0.2}}{R_{p,0}}$$	0.0	-2	-2.8	0.2	0.0
Coolant volume factor (FOM_{cv}): $$FOM_{cv} = \frac{(\rho)^{-0.84} \cdot (C_p)^{-1.16} \cdot (\mu)^{0.1}}{R_{cv,0}}$$	0.0	-0.84	-1.16	0.1	0.0
Material Volume factor (FOM_{ccv}): $$FOM_{ccv} = \frac{(P) \cdot (\rho)^{-0.84} \cdot (C_p)^{-1.16} \cdot (\mu)^{0.1}}{R_{ccv,0}}$$	0.0	-0.84	-1.16	0.1	1.0
Heat loss factor (FOM_{hl}): $$FOM_{hl} = \frac{(k)^{0.6} \cdot (\rho)^{0.34} \cdot (C_p)^{0.06} \cdot (\mu)^{-0.44}}{R_{hl,0}}$$	0.6	0.34	0.06	-0.44	0.0
Temperature drop factor (FOM_{dt}): $$FOM_{dt} = \frac{(k)^{0.6} \cdot (\rho)^{0.34} \cdot (C_p)^{0.06} \cdot (\mu)^{-0.44}}{R_{dt,0}}$$	0.6	0.34	0.06	-0.44	0.0

Appendix B

Comparisons of Fluoride High Temperature Reactor Coolant Properties and Selection Process

Appendix B—Comparisons of Fluoride High Temperature Reactor Coolant Properties and Selection Process

B-1. INTRODUCTION

A coolant comparison study is an essential part of an advanced high temperature reactor (AHTR) heat exchanger study because major heat exchanger designs, performance, and issues are closely related to the coolant characteristics. Figure B-1 shows the basic outline of an AHTR heat exchanger coolant study. This study basically consists of three steps:

1. The coolant options for the primary and the intermediate loops of the heat exchangers are identified. Since the heat exchangers in an AHTR are used for various purposes, there are many heat exchanger coolant options.

2. Based on the requirements, the potential candidates for coolants are identified.

3. The key parameters associated with the coolants are reviewed and are further compared. The key parameters include thermal/physical properties, corrosion characteristics, and material cost.

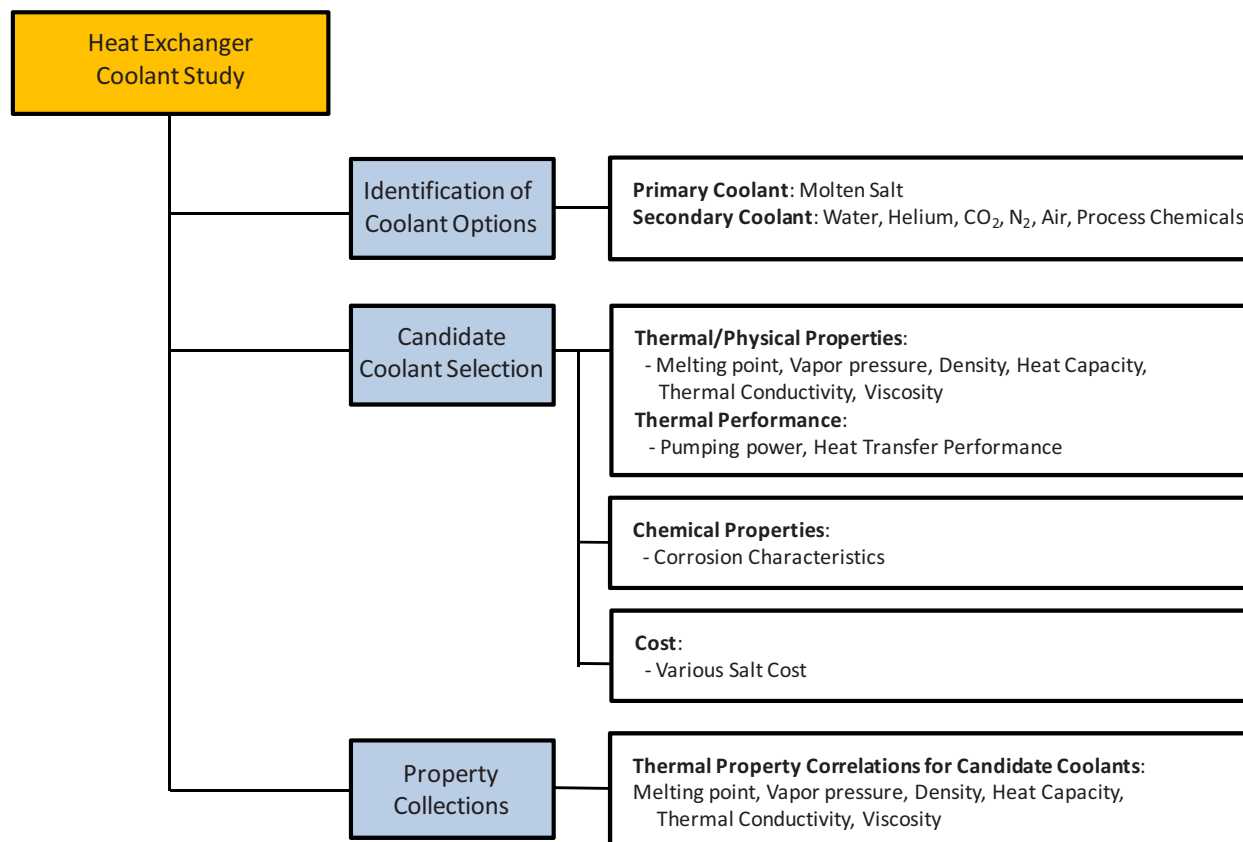

Figure B-1. AHTR heat exchanger coolant study.

B-2. AHTR COOLANT TYPES

The primary coolant in an AHTR's heat exchangers is fluoride molten salt, while the intermediate coolants, depending on the application, could be: fluoride/chloride/nitride molten salts, helium, CO_2, N_2, air, water, or process chemicals. Many recently published technical reports have reviewed various molten

salt coolant properties (Williams et al. 2006a, Williams et al. 2006b, and Sohal et al. 2010). According to Williams' (2006b), the following 11 molten salts are recommended as candidate coolants for heat transfer loops, and are listed with the mol% and basic properties in Table B-1:

- LiF-NaF-KF   (46-11.5-42.5)
- NaF-ZrF$_4$ (59.5-40.5)
- KF-ZrF$_4$ (58-42)
- LiF-NaF-ZrF$_4$ (26-37-37)
- LiCl-KCl   (59.5-40.5)
- LiCl-RbCl   (58-42)
- NaCl-MgCl$_2$ (63-37)
- KCl-MgCl$_2$ (68-32)
- NaF-NaBF$_4$ (8-92)
- KF-KBF$_4$ (25-75)
- RbF-RbF$_4$ (31-69).

Table B-1. Summary of the candidate molten salt properties for heat transfer loop (Williams et al. 2006b).

Salt [a]	Formula weight (g/mol)	Melting point (°C)	900°C vapor pressure (mm Hg)	Heat-transfer properties at 700°C			
				ρ, density (g/cm^3)	$\rho*Cp$, volumetric heat capacity (cal/cm^3-°C)	μ, viscosity (cP)	k, thermal conductivity (W/m-K)
LiF-NaF-KF	41.3	454	~0.7	2.02	0.91	2.9	0.92
NaF-ZrF$_4$	92.7	500	5	3.14	0.88	5.1	0.49
KF-ZrF$_4$	103.9	390	1.2	2.80	0.70	< 5.1	0.45
LiF-NaF-ZrF$_4$	84.2	436	~5	2.92	0.86	6.9	0.53
LiCl-KCl	55.5	355	5.8	1.52	0.435	1.15	0.42
LiCl-RbCl	75.4	313	--	1.88	0.40	1.30	0.36
NaCl-MgCl$_2$	73.7	445	< 2.5	1.68	0.44	1.36	0.50
KCl-MgCl$_2$	81.4	426	< 2.0	1.66	0.46	1.40	0.40
NaF-NaBF$_4$	104.4	385	9500	1.75	0.63	0.90	0.40
KF-KBF$_4$	109.0	460	100	1.70	0.53	0.90	0.38
RbF-RbF$_4$	151.3	442	< 100	2.21	0.48	0.90	0.28

This study uses information provided by Williams et al. (2006b) and Sohal et Al. (2010), but focuses on heat exchanger design and performance.

B-3. KEY PARAMETERS FOR AN AHTR HEAT EXCHANGER COOLANT THERMAL PERFORMANCE

Some of the key thermal parameters considered in choosing an AHTR heat exchanger coolant (molten salt) can be summarized as follows:

- *Melting Point*: The melting point of molten salt is an important consideration when used as a coolant in a heat transport loop because of potential freezing issues. The typical coolant melting point is required to be as low as possible, preferably less than 525°C for an AHTR (Williams et al. 2006a).

- *Vapor Pressure:* Lower vapor pressure is preferred for the heat transport loop or heat exchangers to avoid cavitations and coolant boiling issues.

- *Density*: Greater density is generally preferred because it increases the heat transport capability. However, if the coolant is too dense, it can cause undesirable hydrostatic heads and place extra demands on pumping equipment. A highly dense gradient by temperature enhances natural circulation capability in accident conditions.

- *Heating Capacity*: A high heating capacity is preferred in the heat transport loop and heat exchangers because it increases heat transport performance and requires less mass flow to transport the same amount of heat, thus reducing pumping power. Fluoride salts have a relatively large heating capacity compared with other coolants. The product of density and heat capacity (volumetric heat capacity) is ~4.18E6 J/m^3 (1 cal/cm^3) for fluoride salts, which is similar to water.

- *Thermal Conductivity*: Higher thermal conductivity is preferred because it provides better heat transfer performance.

- *Viscosity*: A lower viscosity is preferred because it results in less friction loss for the same traveling distance.

B-4. COMPARISONS OF COOLANT THERMAL-HYDRAULIC PERFORMANCE

Selecting a coolant with superior properties to the other coolants is straight forward. However, coolants generally have some good properties and some less desirable properties. It is therefore useful to compare some of the key parameters that determine coolant thermal performance in systems of interest. This section discusses coolant thermal-hydraulic characteristics; other characteristics are discussed later.

Some figures of merit (FOMs) were used to evaluate general thermal performance of the coolants. Bonilla (1958) provided the FOMs based on minimal pumping power for a given coolant temperature rise as

$$FOM = \mu^{0.2} / \left(\rho^2 C_P^{2.8} \right) \qquad \text{(B-1)}$$

where:

μ = viscosity (Pa-s)

ρ = density (kg/m^3)

C_p = heat capacity (J/kg K).

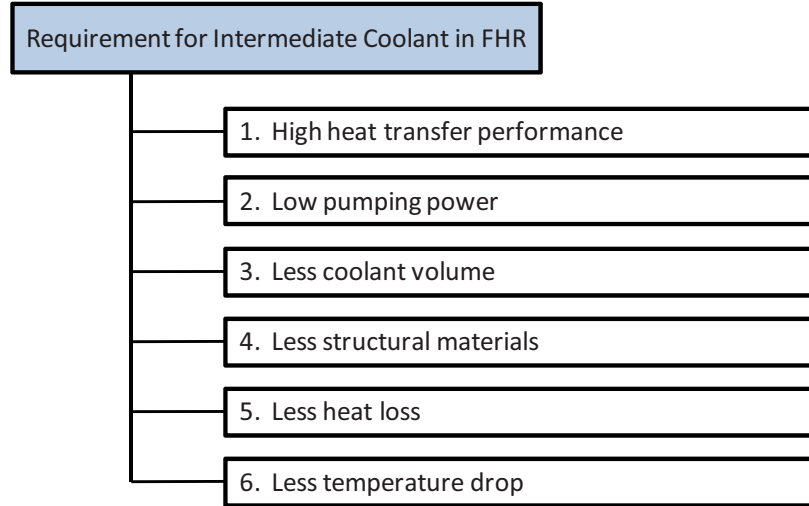Sanders (1971) proposed the following FOM based on the heat exchanger surface area:

$$FOM = \mu^{0.2} / \left(\rho^{0.3} C_p^{0.6} k^{0.6} \right). \qquad \text{(B-2)}$$

where:

k =   thermal conductivity (W/m K)

Williams (2006) used the above FOMs to compare the heat transfer performance of molten salt coolants for an NGNP Nuclear Hydrogen Initiative heat transfer loop.

The above two parameters are very useful for comparing overall coolant heat transfer performance at the early stages of research. However, they are still not complete for evaluating all the important thermal performance parameters in the system of interest. Figure B-2 shows the general thermal-hydraulic requirements for the intermediate coolant in an AHTR system.

Requirement for Intermediate Coolant in FHR

1. High heat transfer performance

2. Low pumping power

3. Less coolant volume

4. Less structural materials

5. Less heat loss

6. Less temperature drop

Figure B-2. General thermal-hydraulic requirements for the intermediate coolant in an AHTR system.

Based on Figure B-2, the following are general thermal-hydraulic requirements for coolants in an AHTR:

- *Increased heat capability*: Increased heat capability leads to more efficient heat transfer between the primary and intermediate loops.

- *Low pumping power*: Coolant that requires lower pumping power minimizes economic losses and maximizes efficiency.

- *Less coolant volume*: Lower coolant volumes are more economic.

- *Less structural materials for containing coolant*: Less structural material for containing the coolant is more economical.

- *Less heat loss*: Minimizing heat loss when transferring heat long distances is more efficient.

- *Less temperature drop*: Minimized coolant temperature drop when transferring heat long distances is more efficient.

With the six requirements mentioned above, six FOMs were developed in this study (See Appendix A for detail analysis). The following summarizes the FOMs and their physical meanings:

- *Heat Transfer Performance Factor (FOM$_{ht}$)*: This FOM represents the heat transfer performance of the coolant. It measures the heat transfer rate per unit pumping power for a given geometry.

- *Pumping Factor (FOM$_p$)*: This FOM represents the pumping power of the coolant. It measures the pumping power required to transport the same energy for a given coolant.

- *Coolant Volume Factor (FOM$_{cv}$)*: This FOM represents the volume of the coolant. It measures the coolant volume required for transferring heat with the same heat and pumping power.

- *Material Volume Factor (FOM$_{ccv}$)*: This FOM represents the volume of the structural materials. It measures the volume of the coolant structural materials required for transferring heat with the same heat duty and pumping power under given operating conditions (temperature and pressure).

- *Heat Loss Factor (FOM$_{hl}$)*: This FOM represents the heat loss of the coolant. It measures the heat loss of the coolant when it is transported to same distance with the same heat duty and pumping power.

- *Temperature Drop Factor (FOM$_{dt}$)*: This FOM represents the heat loss of the coolant. It measures the temperature drop of the coolant when it is transported to the same distance with the same heat duty and pumping power.

Table B-2 summarizes all the FOMs derived and proposed for the intermediate high temperature loop coolants. Based on the FOMs summarized, heat transfer performance, pumping power, coolant volume, pipe material volume, coolant heat loss, and coolant temperature drop can be compared easily and quantitatively for the same heat duty and pumping power requirements. A plus sign (+) of a sensitivity indicates that the FOM increases with the properties, while a minus sign (-) indicates that the FOM decreases with the properties. This table also shows the sensitivity of the FOMs in terms of various fluid properties. The sensitivities of the FOMs were estimated by (Saltelli et al. 2008)

$$S_\varphi = \frac{\partial FOM \, / \, FOM}{\partial \varphi \, / \, \varphi} \tag{B-3}$$

where, φ is a variable for a given *FOM*.

The numbers of the sensitivities show how much the FOMs are affected by each property. If the number is higher, the FOM sensitivity is more significantly affected by that property. From this table, the effects of properties on the thermal-hydraulic performance of the coolants can be interpreted as follows:

- Increasing thermal conductivity can increase heat transfer performance by a power of 0.6, but it also increases heat loss and temperature drop of the coolant at the same rate.

- Increasing coolant density can increase heat transfer performance and reduce coolant volume by powers of 0.58 and 0.84, respectively, but it also decreases pumping power by a power of 2.

- Increasing heat capacity can increase heat transfer performance and significantly reduce coolant/material volume by powers of 0.4 and 1.16, respectively, with decreases of pumping power, but the increases in heat loss and temperature drop are negligible (= 0.06).

- Increasing viscosity increases pumping power and coolant volume with significant reductions in heat transfer performance.

Table B-3 shows the reference values for the FOMs that will be used in this study. These reference values are estimated based on water at 25°C and 0.1 MPa. Therefore, the estimated FOMs indicate coolant performance of a certain coolant relative to water at 25°C and 1 atm (0.1 MPa). Water was used for comparison purposes because it is one of the most common coolants with wide application.

71

Table B-2. Summary of FOMs for heat transfer coolant (see Appendix A for details).

Figures of Merit	Sensitivity of Properties				
	S_k	S_ρ	S_{Cp}	S_μ	S_P
Heat transfer performance factor (FOM_{ht}): $FOM_{ht} = \dfrac{(k)^{0.6} \cdot (\rho)^{0.58} \cdot (C_p)^{0.4} \cdot (\mu)^{-0.47}}{R_{ht,0}}$	0.6	0.58	0.4	-0.47	0.0
Pumping factor (FOM_p): $FOM_p = \dfrac{\rho^{-2} \cdot C_P^{-2.8} \cdot \mu^{0.2}}{R_{p,0}}$	0.0	-2	-2.8	0.2	0.0
Coolant volume factor (FOM_{cv}): $FOM_{cv} = \dfrac{(\rho)^{-0.84} \cdot (C_p)^{-1.16} \cdot (\mu)^{0.1}}{R_{cv,0}}$	0.0	-0.84	-1.16	0.1	0.0
Material Volume factor (FOM_{ccv}): $FOM_{ccv} = \dfrac{(P) \cdot (\rho)^{-0.84} \cdot (C_p)^{-1.16} \cdot (\mu)^{0.1}}{R_{ccv,0}}$	0.0	-0.84	-1.16	0.1	1.0
Heat loss factor (FOM_{hl}): $FOM_{hl} = \dfrac{(k)^{0.6} \cdot (\rho)^{0.34} \cdot (C_p)^{0.06} \cdot (\mu)^{-0.44}}{R_{hl,0}}$	0.6	0.34	0.06	-0.44	0.0
Temperature drop factor (FOM_{dt}): $FOM_{dt} = \dfrac{(k)^{0.6} \cdot (\rho)^{0.34} \cdot (C_p)^{0.06} \cdot (\mu)^{-0.44}}{R_{dt,0}}$	0.6	0.34	0.06	-0.44	0.0

Table B-3. Summary of reference values in FOMs (water at 25°C, 1 atm).

	k [W/m K]	ρ [kg/m³]	C_p [J/kg K]	μ [Pa s]	P [Pa]	Reference Values
$R_{ht,0}$	0.61	997.05	4181	0.00089	1.0 E+05	3.11E+04
$R_{p,0}$	0.61	997.05	4181	0.00089	1.0 E+05	1.79E-17
$R_{cv,0}$	0.61	997.05	4181	0.00089	1.0 E+05	1.08E-07
$R_{ccv,0}$	0.61	997.05	4181	0.00089	1.0 E+05	1.08E-07
$R_{hl,0}$	0.61	997.05	4181	0.00089	1.0 E+05	2.82E+02
$R_{dt,0}$	0.61	997.05	4181	0.00089	1.0 E+05	2.82E+02
* Definitions of $R_{ht,0}$, $R_{p,0}$, $R_{cv,0}$, $R_{ccv,0}$, $R_{hl,0}$, and $R_{dt,0}$ are referred to Eqs. (A-19), (A-25), (A-38), (A-52), and (A-67).						

Table B-4 shows the comparisons of thermal-hydraulic characteristics of molten-salt coolants based on estimated FOMs. All of the FOMs were estimated based on a temperature of 700°C. The following summarizes the results:

- FOM_{th}: FOM_{th} physically represents the heat transfer rate per unit pumping power for a given geometry. Therefore, a higher FOM_{th} is preferred for better heat transfer performance. According to the comparisons, LiF-NaF-KF shows the highest value (=0.8), then NaF-NaBF$_4$ (=0.71), followed by KF-KBF$_4$ (=0.64) (See Figure B-3).

- *FOM_p*: Lower FOM_p is preferred because it requires less pumping power for transferring the same amount of heat. According to the comparisons, LiF-NaF-KF shows the lowest values (=2.82), then NaF-ZrF$_4$ (=5.02), followed by LiF-NaF-ZrF$_4$ (=5.36) (See Figure B-4).

- *FOM_cv*: Lower FOM_{cv} is preferred because it requires less coolant volume to provide the same amount of heat transfer performance under the same pumping power. According to the comparisons, LiF-NaF-KF shows the lowest value (=1.57), then NaF-ZrF$_4$ (=1.98), followed by NaF-NaBF$_4$ (=2.04) (See Figure B-5).

- *FOM_ccv*: Lower FOM_{ccv} is preferred because it requires less structural material volume for both heat transfer pipes and components. According to the comparisons, LiF-NaF-KF shows the lowest values (=1.57), then NaF-ZrF$_4$ (=1.98), followed by NaF-NaBF$_4$ (=2.04) (See Figure B-6).

- *FOM_hl*: Lower FOM_{hl} is preferred because it requires less insulation for preventing heat loss. According to the comparisons, LiF-NaF-ZrF$_4$ shows the lowest value (=0.50), then KF-ZrF$_4$ (=0.51), followed by NaF-ZrF$_4$ (=0.56) (See Figure B-7).

- *FOM_dt*: Lower FOM_{dt} is preferred because more thermal energy can be transferred long distances without much of a temperature drop. According to the comparisons, LiF-NaF-ZrF4 shows the lowest value (=0.50), then KF-ZrF$_4$ (=0.51), followed by NaF-ZrF$_4$ (=0.56) (See Figure B-8).

Overall, LiF-NaF-KF is considered as the best heat transfer coolant among the molten salt coolants used in this analysis. It shows the best performance in heat transfer, pumping power, coolant volume, and structural material volume. However, it shows the worst performance for heat loss and temperature drop. These two factors are generally lower priorities because they can be easily addressed by thickening or adding multiple insulation layers. Figures B-3 to B-8 show the results. The blue color in each figure represents the preferred material in terms of the FOMs compared (see Appendix A for a detailed study).

Table B-4. Comparisons of FOMs for the various molten salt coolants.

| Coolant	Melting Point (°C)	K (W/m K)	ρ (kg/m3)	Cp (J/kg K)	μ (Pa s)	P (atm)	FOM$_{th}$	FOM$_p$	FOM$_{cv}$	FOM$_{ccv}$	FOM$_{hl}$	FOM$_{dt}$
Water (25°C)	0	0.61	997.05	4181	0.00089	1	1.00	1.00	1.00	1.00	1.00	1.00
LiF–NaF–KF	454	0.92	2020	1886	0.0029	1	0.80	2.87	1.57	1.57	0.92	0.92
NaF–ZrF$_4$	500	0.49	3140	1173	0.0051	1	0.45	5.02	1.98	1.98	0.56	0.56
KF–ZrF$_4$	390	0.45	2800	1046	0.0051	1	0.38	8.69	2.49	2.49	0.51	0.51
LiF–NaF–ZrF$_4$	436	0.53	2920	1233	0.0069	1	0.40	5.36	2.05	2.05	0.50	0.50
LiCl-KCl	355	0.42	1520	1198	0.00115	1	0.55	14.99	3.07	3.07	0.76	0.76
LiCl-RbCl	313	0.36	1880	890	0.0013	1	0.47	23.03	3.66	3.66	0.70	0.70
NaCl-MgCl$_2$	445	0.5	1680	1096	0.00136	1	0.58	16.26	3.18	3.18	0.81	0.81
KCl-MgCl$_2$	426	0.4	1660	1160	0.0014	1	0.50	14.30	3.02	3.02	0.70	0.70
NaF-NaBF$_4$	385	0.4	1750	1507	0.0009	1	0.71	5.66	2.04	2.04	0.88	0.88
KF-KBF$_4$	460	0.38	1700	1305	0.0009	1	0.64	8.98	2.47	2.47	0.84	0.84
RbF-RbF$_4$	442	0.28	2210	909	0.0009	1	0.54	14.61	3.01	3.01	0.75	0.75
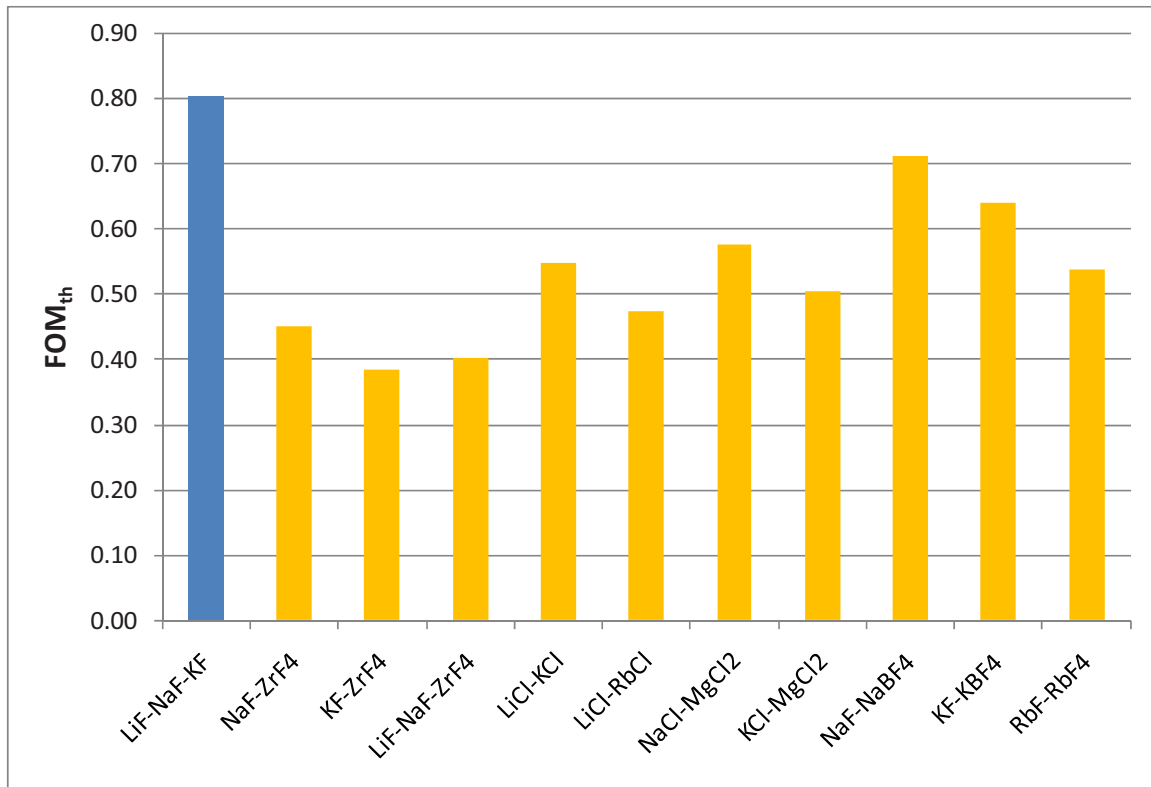
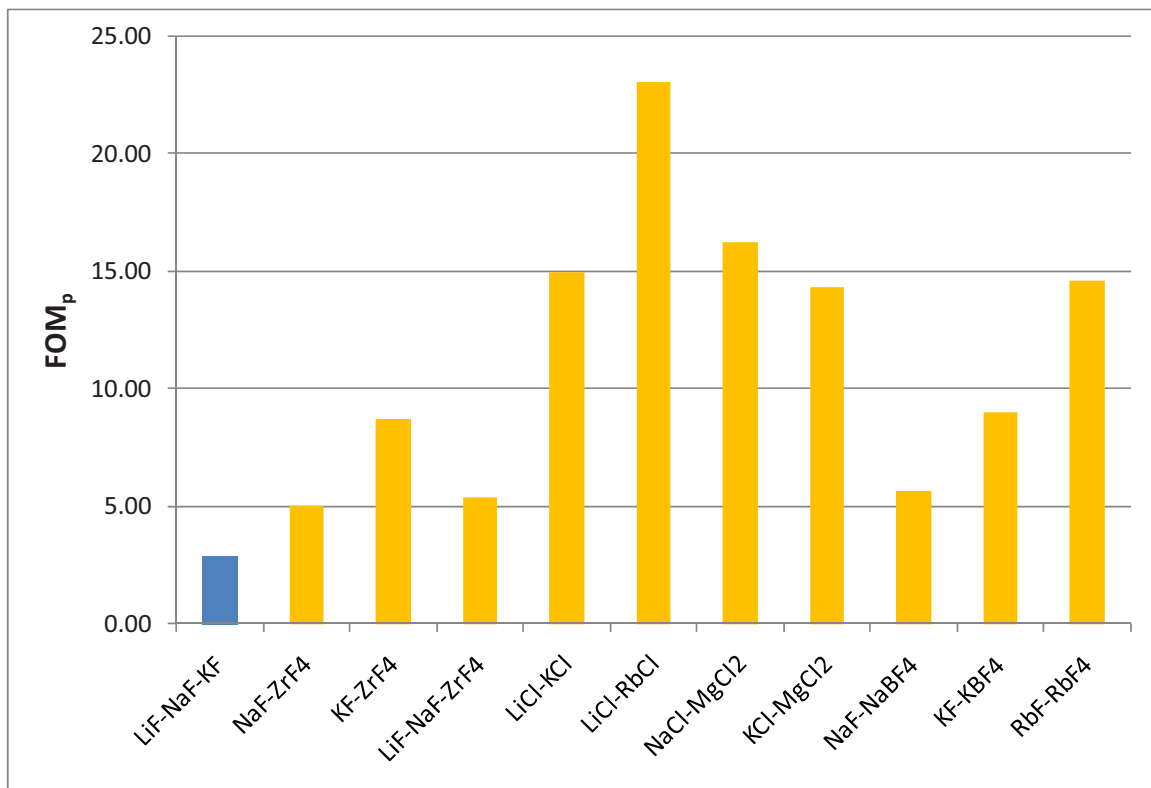Figure B-3. Comparisons of FOM$_{th}$ for molten salt coolants.

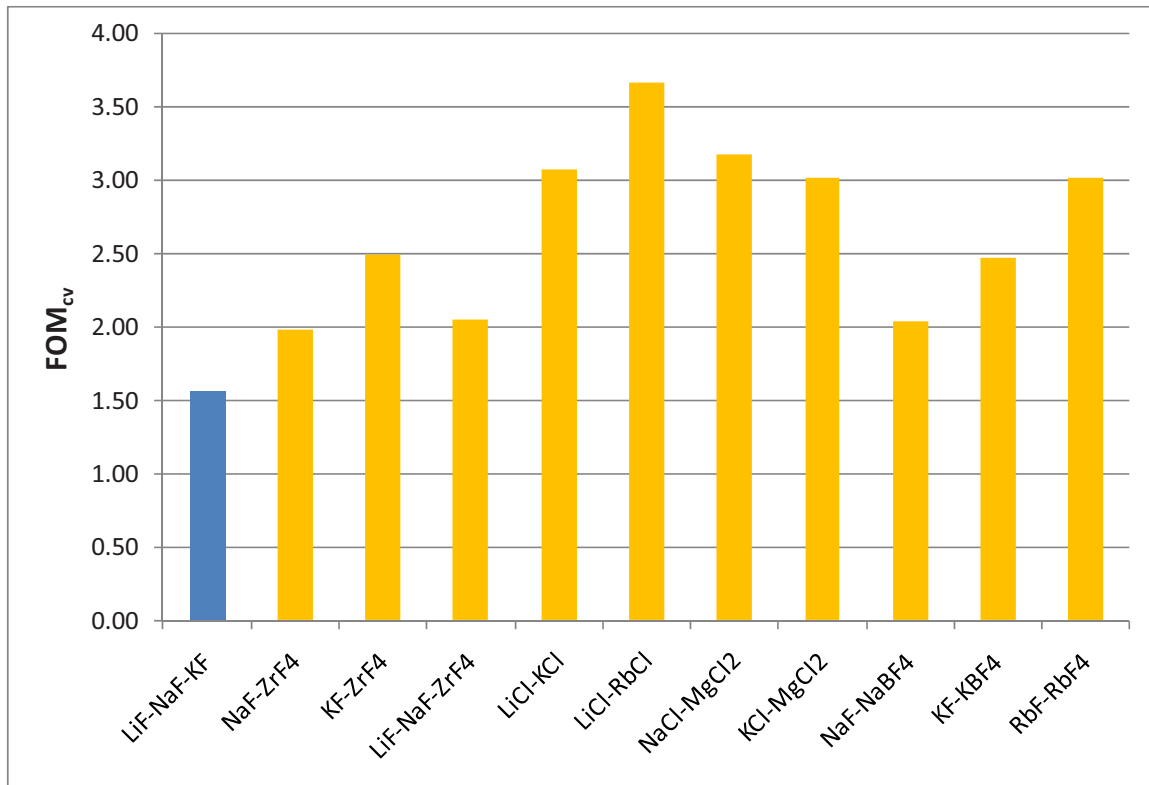Figure B-4. Comparisons of FOM$_p$ for molten salt coolants.

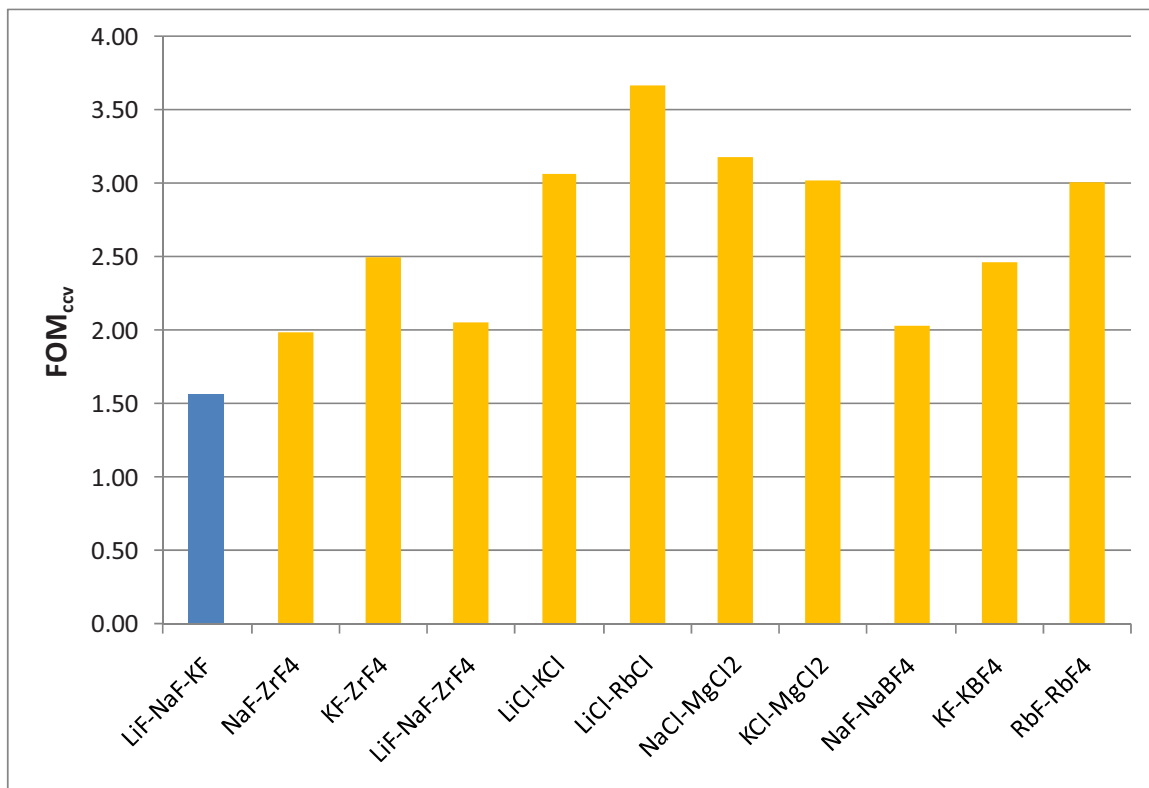**Figure B-5. Comparisons of FOM$_{cv}$ for molten salt coolants.**

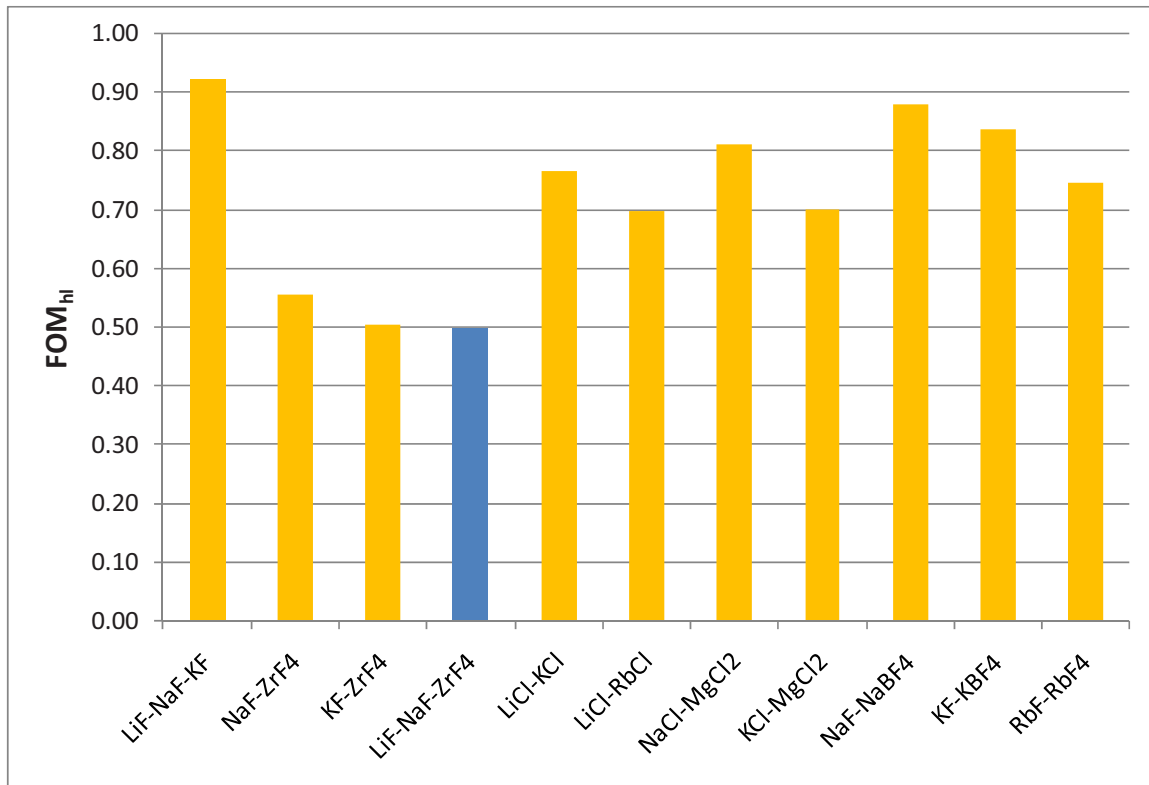**Figure B-6. Comparisons of FOM$_{ccv}$ for molten salt coolants.**

Figure B-7. Comparisons of FOM$_{hl}$ for molten salt coolants.
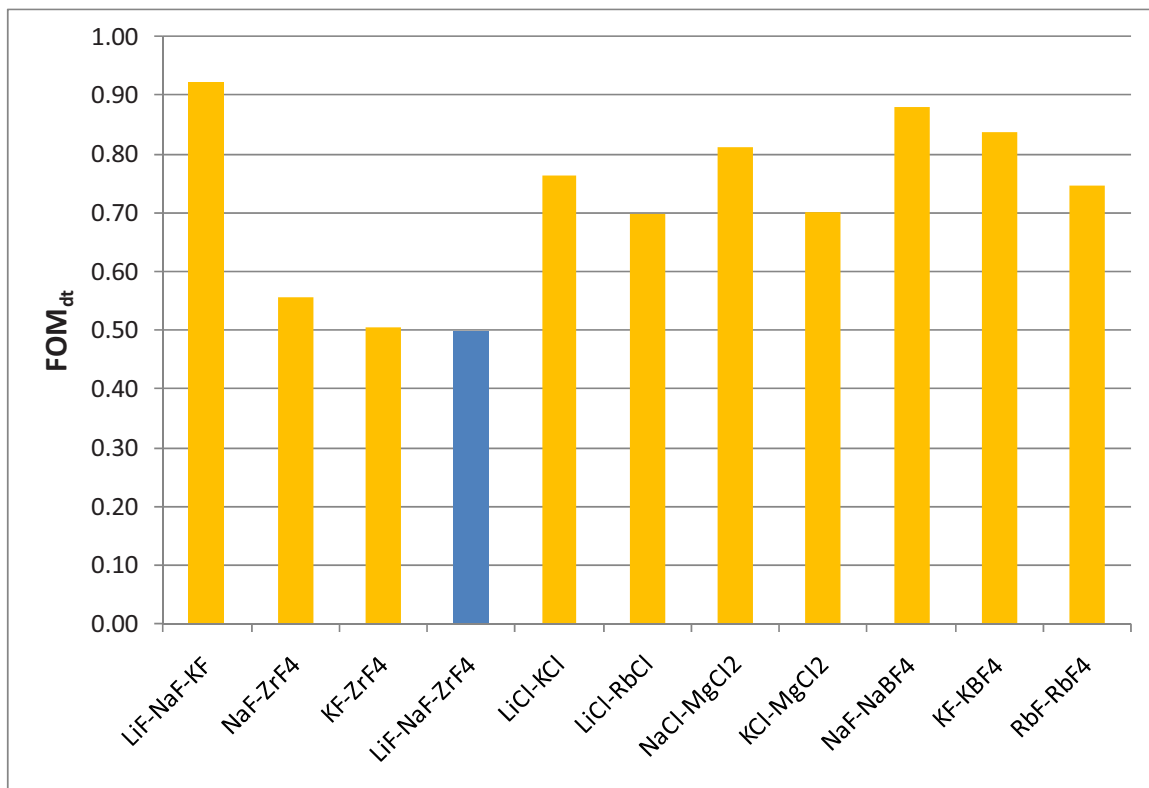

Figure B-8. Comparisons of FOM$_{dt}$ for molten salt coolants.

B-5. COOLANT COST (COST OF SALTS)

The cost is an important factor for selecting the intermediate coolant. This cost was relatively estimated based on the data summarized by Williams (2006). The total cost of the coolants required in the intermediate heat transfer loop can be simply expressed by

$$C_t = V_c \cdot c_c \qquad \text{(B-4)}$$

where:

C_t = total coolant cost ($)

V_c = total coolant volume (m^3)

c_c = raw material cost/volume ($/m^3$).

However, in Eq. (B-4), the total volume cannot be determined before the final design of the system, so the relative volumes of the coolants in this study were taken into considerations based on the coolant volume factor (FOM_{cv}). The expression used for coolant cost comparisons is

$$R_{C_t} = FOM_{cv} \cdot c_c \qquad \text{(B-5)}$$

where:

R_{Ct} = relative total coolant cost ($/m^3$)

FOM_{cv} = coolant volume factor

c_c = raw material cost/volume ($/m^3$).

The cost data for the raw material cost/volume was obtained from the report by Williams (2006). In this estimation, not all the candidate coolants were taken into considerations because of a lack of available information. Table B-5 summarizes the raw material cost data and relative total cost estimations. According to the comparisons, $KCl\text{-}MgCl_2$ shows the lowest cost followed by $NaCl\text{-}MgCl_2$; all other molten salt costs are about two orders of magnitude higher than these two coolants. The most expensive coolant in this estimation is $KF\text{-}ZrF_4$. Among the fluoride based salts, $KF\text{-}KBF_4$ showed the lowest cost, followed by $NaF\text{-}NaBF_4$ and $LiF\text{-}NaF\text{-}KF$, respectively.

Table B-5. Raw material costs for various salt mixtures and relative total cost estimations.

Coolant	Cost/volume ($/L)	Cost/Volume ($/m^3$)	FOM_{cv}	R_{ct} ($/m^3$)
LiF-NaF-KF	15.79	15790	1.57	24724
NaF-ZrF$_4$	12.63	12630	1.98	25053
KF-ZrF$_4$	13.58	13580	2.49	33862
LiF-NaF-ZrF$_4$	—	—	—	—
LiCl-KCl	7.71	7710	3.07	23656
LiCl-RbCl	—	—	—	—
NaCl-MgCl$_2$	0.42	420	3.18	1335
KCl-MgCl$_2$	0.35	350	3.02	1055
NaF-NaBF$_4$	8.55	8550	2.04	17426
KF-KBF$_4$	6.26	6260	2.47	15447

B-6. COOLANT CHEMICAL CONSIDERATIONS

Coolant chemistry is an essential factor for the molten salt coolant selection. However, it is a very complex mechanism affected by various factors, and therefore it is practical to be quantified for precise comparisons at this stage. According to previous reports that present a review and discussions on the molten salt coolant corrosion (Williams 2006, Williams et al. 2006, and Sohal et al. 2010), the most important chemical factor in coolant selection is to maintain the corrosion level at an acceptably low level that will allow fabrication of components that meet design life requirements.

The corrosion data for various molten salt coolants are limited, as are reliable comparisons of corrosion resistance of various alloys to them. The evidence for selecting a coolant based on corrosion is not adequate at present (Williams et al. 2006). So coolant salt selection factors for corrosion discussed in this section are briefly summarized based on the previous study. The four factors discussed by Williams et al. (2006) for the coolant selection are:

- Oxidation state of corrosion product

- Temperature dependence of dissolved chromium concentration

- Polythermal corrosion test loops with coolant salts

- Redox control factors.

According to the literature survey, corrosion of FLiNaK (LiF-NaF-KF) is among the worst in various perspectives (Williams 2006, Williams et al. 2006, and Sohal et al. 2010). In addition, none of the redox-control strategies have been developed to the extent that can be relied on for coolant salt selection. However, for a lower-temperature system (<750°C), Hastelloy N appears to be fully capable of being used as a containment alloy, even without the need for a redox strategy.

William et al. (2006) also suggested the following approaches for resolving molten salt corrosion issues:

- Using low-chromium/chromium-free alloys or suitable clad systems as a container (structural materials)

- Selecting a salt that should support the minimum level of corrosion in the absence of a highly reducing environment (ZrF_4 salts, BeF_2 salts)

- Selecting a salt with a large redox window that can be maintained in a highly reducing state (FLiNaK, BeF_2 salts).

Finally, ZrF_4 salts without strong reductants, or FLiNaK with strong reductants and a redox buffer, were recommended as a promising approach because of high expenses and difficulty in developing beryllium-containing salt.